Published in final edited form as:
Chem Rev. 2014 April 9; 114(7): 3466–3494. doi:10.1021/cr400400p.

Hydrogen Tunneling in Enzymes and Biomimetic Models

Joshua P. Layfield and **Sharon Hammes-Schiffer**
Department of Chemistry, 600 South Mathews Avenue, University of Illinois at Urbana-Champaign, Urbana, IL 61801

Sharon Hammes-Schiffer: shs3@illinois.edu

1. Introduction

Hydrogen transfer reactions play an important role throughout chemistry and biology. In general, hydrogen transfer reactions encompass proton and hydride transfer, which are associated with the transfer of a positively or negatively charged species, respectively, and proton-coupled electron transfer (PCET), which corresponds to the net transfer of one electron and one proton in the simplest case. Such PCET reactions can occur by either a sequential mechanism, in which the proton or electron transfers first, or a concerted mechanism, in which the electron and proton transfer in a single kinetic step with no stable intermediate. Furthermore, concerted PCET reactions can be subdivided into hydrogen atom transfer (HAT), which corresponds to the transfer of an electron and proton between the same donor and acceptor (i.e., the transfer of a predominantly neutral species), and electron-proton transfer (EPT), which corresponds to the transfer of an electron and proton between different donors and acceptors, possibly even in different directions. In all of these types of hydrogen transfer reactions, hydrogen tunneling could potentially play a significant role.

The majority of experimental evidence for hydrogen tunneling is related to the kinetic isotope effects (KIEs), as defined by ratios of the rate constants k_H, k_D, and k_T for hydrogen, deuterium, and tritium transfer, respectively. In particular, a large hydrogen/deuterium KIE (i.e., k_H/k_D greater than ~7) is considered to implicate hydrogen tunneling.[1] Another indicator of tunneling is the Swain-Schaad exponent, defined as $\ln(k_H/k_T)/\ln(k_D/k_T)$. A Swain-Schaad exponent greater than 3.3 is considered to be a manifestation of tunneling because it exceeds the upper limit obtained semiclassically in the absence of tunneling.[2–5] In addition, the temperature dependence of the KIEs has also been interpreted in the context of hydrogen tunneling. Specifically, the degree of curvature in the Arrhenius plots is isotope dependent for systems exhibiting hydrogen tunneling. Thus, fitting the temperature dependence of the rate constants for hydrogen, deuterium, and tritium transfer in the experimentally accessible temperature range often leads to slopes that deviate from the expected trend for the activation energies and to Arrhenius prefactors that do not converge toward a single point.[1] These types of behaviors for secondary KIEs, in which an isotopic substitution at the non-transferred position reduces the rate constant, have also been interpreted as supportive evidence of hydrogen tunneling.

Given the experimental evidence of hydrogen tunneling in condensed phase systems, a variety of theoretical and computational methods have been developed to investigate this phenomenon. The simplest approach is the Bell tunneling correction, which is based on a one-dimensional inverted parabolic model and is included as a prefactor to the transition state theory rate constant.[6] This type of treatment has been shown to be inadequate to describe the vast body of available experimental data. The most rigorous treatment of

Correspondence to: Sharon Hammes-Schiffer, shs3@illinois.edu.

tunneling would be the fully quantum mechanical description of all electrons and all nuclei, solving a mixed nuclear-electronic Schrödinger equation that includes all non-Born-Oppenheimer effects, but such an approach is impractical for chemical systems of interest. Even when the Born-Oppenheimer separation between electrons and nuclei is invoked, the fully quantum mechanical treatment, in which all nuclei move quantum mechanically on a potential energy surface that is generated on-the-fly with *ab initio* electronic structure methods, is not computationally practical. As a result, approximate methods have been developed to allow the investigation of hydrogen tunneling reactions in solution and enzymes.

The objective of this review is to summarize the theoretical treatments and simulation methods that have been developed to study hydrogen tunneling processes and to present illustrative examples of hydrogen tunneling in specific enzymatic and biomimetic systems. The ideas and concepts in this review have originated with assorted authors in various fields. Although we have made a substantial effort to provide the historical context and cite the key papers, our presentation could not be exhaustive and may have overlooked some connections and relations. Moreover, for certain peripheral topics, we do not provide an in-depth discussion but instead refer the reader to the relevant papers in the literature.

In Section 2 of this review, we discuss the theoretical concepts and fundamental physical principles underlying hydrogen tunneling processes. Within this section, we characterize proton and hydride transfer, HAT, and EPT reactions in terms of electronic and vibrational nonadiabaticity[7] and explain how to differentiate these types of reactions using electronic structure and/or semiclassical methods. We present rate constant expressions for each type of reaction and discuss the approximations involved in the derivations of these expressions and the regimes in which they are valid. We also examine the physical meaning of the parameters within these rate constant expressions and the relation of these parameters to the experimentally observed rate constants and KIEs. In particular, the proton donor-acceptor motion is shown to be highly significant, and the impact of the equilibrium proton donor-acceptor distance and associated effective frequency on the rate constant is clarified.[8–11] Analysis of these analytical rate constant expressions provides insight into the fundamental physical principles underlying these types of reactions and enables the modeling of experimentally studied systems.

Section 3 presents the various simulation methods that have been developed to study hydrogen tunneling in condensed phase systems. The potential energy surface can be obtained with an empirical valence bond (EVB) method,[12] in which the system is represented as a linear combination of valence bond states, or a quantum mechanical/molecular mechanical (QM/MM) method, in which the chemically relevant portion of the system is treated quantum mechanically while the remainder of the system is treated with a molecular mechanical force field. The nuclear quantum effects can be incorporated using a grid-based method,[13–15] where the transferring hydrogen nucleus is represented as a three-dimensional wavefunction calculated on a grid, or with Feynman path integral methods,[16] where the transferring hydrogen nucleus is represented as a ring of beads.[17–18] More sophisticated path integral formulations that include dynamical effects and, in some cases, the quantum effects of additional nuclei have also been implemented.[19–21] Another successful approach that is discussed in this section is the ensemble-averaged variational transition state theory with multidimensional tunneling method.[22] The final portion of this section focuses on the simulation of EPT processes by calculating the input quantities for the analytical rate constant expressions or the correlation functions for the dynamical rate constant expressions.[11] Nonadiabatic molecular dynamics methods can be utilized to study photoinduced EPT processes that involve nonequilibrium dynamical effects.

In Section 4, we discuss hydrogen tunneling in enzymatic reactions, focusing on liver alcohol dehydrogenase (LADH) and soybean lipoxygenase (SLO). LADH catalyzes proton and hydride transfer reactions, whereas SLO catalyzes a PCET reaction that is thought to occur via an EPT mechanism. The LADH-catalyzed hydride transfer reaction has been studied with a wide range of simulation methods that all indicate a significant degree of hydrogen tunneling,[13–14,23–33] although this degree of hydrogen tunneling is similar in aqueous solution and the enzyme and therefore is not catalytically relevant.[25] Dynamical barrier recrossings were found to be insignificant for this enzymatic reaction.[14,23–24] Equilibrium conformational sampling was found to play an important role in generating configurations conducive to the chemical reaction,[13–15,34–36] but no convincing evidence of direct dynamical coupling between protein modes and the chemical reaction has been obtained. For the SLO-catalyzed PCET reaction, the experimentally observed hydrogen/deuterium KIE of ~80 at room temperature, as well as the weak temperature dependence of the KIE, implicate a significant degree of hydrogen tunneling.[37] This reaction has also been studied with a variety of simulation methods that differ in the assumptions about the degree of electron-proton nonadiabaticity but agree on the significance of hydrogen tunneling for this system.[38–44] The nonadiabatic studies suggest that the large KIE arises from the relatively small overlap between the reactant and product vibrational wavefunctions, while the weak temperature dependence is explained in terms of the effective frequency of the proton donor-acceptor mode.[43–44]

Section 5 examines biomimetic systems, focusing on redox-active tyrosines designed to mimic systems such as photosystem II (PSII) and class 1 ribonuclease reductase (RNR), as well as hydrogen oxidation and production catalysts designed to mimic hydrogenase enzymes. All of the systems in this section are thought to occur via the EPT mechanism and have been studied both experimentally and theoretically. The theoretical studies are based on the nonadiabatic EPT formalism[11] and support the important role of hydrogen tunneling. In these types of biomimetic systems, the EPT reaction is induced either electrochemically or photochemically, providing more well-controlled experimental conditions than is possible for enzymatic systems. Thus, these types of biomimetic systems provide an opportunity to elucidate the fundamental principles underlying EPT reactions and to improve the theoretical and computational methods by direct comparison to experimental data. For example, the impact of altering the driving force or the proton donor-acceptor distance in redox-active tyrosines has been investigated through the synthesis and characterization of various substituted phenol-amine compounds[45–47] and tyrosine-bound ruthenium complexes.[48–53] In terms of molecular electrocatalysts designed to mimic hydrogenase enzymes, we focus on the nickel-based complexes with pendant amines that have been shown to effectively oxidize and/or produce hydrogen.[54–60] The PCET reaction involving proton transfer between the pendant amine and the nickel center and electron transfer between the nickel complex and the electrode has been studied with the nonadiabatic EPT formalism.[61–62] An important objective of such theoretical studies is to help guide the design of more effective molecular catalysts for hydrogen production in an effort to develop environmentally friendly and renewable alternative energy sources.

The final section of this review provides brief concluding remarks that emphasize the importance of understanding the limitations and capabilities of the theoretical and computational methods used to study hydrogen tunneling processes. In addition, the interplay between theoretical and experimental studies is critical for the further development of these methods, as well as enhancing our basic understanding of these types of processes. The insights gained from such integrated studies will have implications for a broad range of fields, including protein design and the development of alternative energy conversion devices.

2. Theoretical concepts of hydrogen tunneling

2.1 Proton and hydride transfer

In this subsection, we discuss proton and hydride transfer reactions, which are described as the transfer of a positively or negatively charged hydrogen species. First we present the basic concepts used to describe proton and hydride transfer reactions, defining the terminology for electronic and vibrational adiabaticity and nonadiabaticity.[7] Then we present analytical rate constant expressions in various well-defined limits.

2.1.1 Basic concepts—Proton and hydride transfer reactions are typically electronically adiabatic in that they occur on the electronic ground state and do not involve excited electronic states. In a valence bond framework, the two diabatic electronic states for a proton transfer reaction are:

$$\begin{array}{l}(a)\ \mathrm{D_p{-}H^+ \cdots\cdots A_p} \\ (b)\ \mathrm{D_p \cdots\cdots {}^+H{-}A_p}\end{array} \quad (1)$$

This notation for the valence bond states represents the general case of proton transfer from a donor to an acceptor and does not imply specific overall charges for the donor and acceptor species. The adiabatic electronic states are linear combinations of these two diabatic electronic states, and the electronic coupling between these two diabatic electronic states is usually so strong that the large energy splitting between the ground and excited adiabatic electronic states prohibits population of the excited state.[8–9,63] Typically the ground electronic state corresponds to a double well potential along the proton coordinate. In theoretical descriptions of proton transfer, often the hydrogen is depicted as moving in a one-dimensional double-well potential, although the extension to three-dimensional motion is straightforward. In electronically adiabatic reactions, the excited electronic state is usually so high in energy that it is not even shown. The physical interpretation of this limit is that the electrons respond instantaneously to the proton motion.

These types of proton and hydride transfer reactions can be either vibrationally adiabatic or nonadiabatic, where the vibrationally adiabatic case indicates that the system remains in the vibrational ground state without involvement of the excited vibrational states.[7] Figure 1 depicts the impact of changes in the proton donor-acceptor distance on the proton potential energy curves. Changes in the proton donor-acceptor distance typically alter the height and width of the barrier of the double-well proton potential. Figure 2 depicts the impact of fluctuations of the environment, namely the solvent and/or protein. For simplicity, we denote this environmental reaction coordinate as the collective solvent coordinate, although the protein motion is also included. The collective solvent coordinate, which is also denoted an energy gap reaction coordinate, is often defined as the difference in energy between the two diabatic states in Eq. (1) interacting with the solvent. Solvent fluctuations typically alter the relative energies of the two minima in the double-well potential. The separation between the proton donor-acceptor mode and the collective solvent coordinate is somewhat artificial but assists in the analysis of the fundamental physical principles.

As mentioned above, Figure 1 depicts the proton potentials and adiabatic proton vibrational states as the proton donor-acceptor distance changes. For simplicity, the proton potentials are symmetric in this figure. When the proton donor-acceptor distance is small enough, the proton moves in a single-well potential. As this distance increases, a barrier appears, and the barrier height increases as the donor-acceptor distance increases. At relatively small distances, the proton vibrational ground state is above the barrier (left curve in Fig. 1). As the proton donor-acceptor distance increases, the barrier height and width increase. At

relatively large distances, the lowest two proton vibrational states are below the barrier (middle and right curves in Fig. 1). In these situations, the tunneling splitting is defined as the difference between the lowest two proton vibrational states in the symmetric configuration. Typically the tunneling splitting decreases dramatically as the proton donor-acceptor distance increases.

Figure 2a depicts the changes in the proton potentials and adiabatic proton vibrational states in response to fluctuations of the environment. If the tunneling splitting is large (middle potential of Fig. 1), the proton remains in its ground vibrational state. In this case, the environmental fluctuations lead to proton transfer that is adiabatic but also involves hydrogen tunneling in the sense that the proton has not surmounted the barrier, and the proton vibrational wavefunction reflects significant probability in the classically forbidden barrier region. If the tunneling splitting is small (right potential of Fig. 1), nonadiabatic transitions to the excited vibrational state may occur, and the proton may not transfer due to this particular fluctuation (i.e., the proton may remain localized in the donor well but in an excited vibrational state). In this case, the proton transfer is nonadiabatic, with the probability of tunneling depending on the tunneling splitting. Another possible situation is that the ground vibrational state is above the barrier for the symmetric configuration (left potential of Fig. 1). Such a reaction will most likely be vibrationally adiabatic in that the proton will remain in the ground vibrational state. In this case, the proton will transfer due to the solvent fluctuation, but the process does not involve hydrogen tunneling, although zero point energy effects may be significant.

Proton and hydride transfer reactions can be described in either the adiabatic or diabatic representation for the proton vibrational states. Figure 2a depicts the adiabatic proton vibrational states, which are solutions of the time-independent Schrödinger equation for the proton moving in the entire proton potential. Figure 2b depicts the diabatic proton vibrational states, which are solutions of the Schrödinger equation for the proton moving in only the donor or acceptor well (blue and red states, respectively, in Fig. 2b). Note that the adiabatic and diabatic states are similar for asymmetric double well proton potentials but differ qualitatively for symmetric double well potentials. In particular, for the symmetric double well potential, the adiabatic proton vibrational states become delocalized over both wells, with a symmetric and antisymmetric wavefunction for the ground and first excited state, respectively, while the diabatic proton vibrational states remain localized in either the donor or acceptor well.

The free energy curves associated with the lowest two proton vibrational states are depicted along the collective solvent coordinate in the adiabatic and diabatic representations in Figure 3. The solid black curves depict the adiabatic representation. In the context of Figure 2a, the solid black curves in Figure 3 correspond to the energies of the adiabatic proton vibrational states along this reaction coordinate, and the tunneling splitting Δ corresponds to the minimum energy difference between the adiabatic proton vibrational states in Figure 3 and this difference for the symmetric (middle) proton potential in Figure 2a. In the context of Figure 2b, the dashed blue and red curves in Figure 3 depict the diabatic representation, where each diabatic state corresponds to the proton localized in the donor or acceptor well, respectively. The coupling C between the diabatic proton vibrational states at the solvent configuration for which they are degenerate (i.e., when the dashed curves cross in Figure 3, corresponding to the middle proton potential in Figure 2b) is associated with the tunneling splitting, $\Delta = 2C$, between the adiabatic proton vibrational states. The coupling C determines the tunneling probability between the diabatic proton vibrational states. Rate constant expressions have been derived for proton and hydride transfer reactions in the vibrationally adiabatic and nonadiabatic limits. The remainder of this subsection discusses the analytical rate constants derived for these limits.

2.1.2 Vibrationally adiabatic rate constant—When the reaction is vibrationally adiabatic, the rate constant can be calculated in the framework of transition state theory (TST). Hynes and coworkers derived an expression for the TST rate constant for the specific case of a collective solvent coordinate with relatively large solvent reorganization energy (i.e., strong interaction between the proton transfer reaction and the polar solvent). One of the limiting forms of this expression is:[64–66]

$$k^{\mathrm{TST}}=\frac{\omega_S}{2\pi}\exp\left(-\frac{\Delta G^{\ddagger}}{k_{\mathrm{B}}T}\right) \quad (2)$$

where $\Delta G^{\ddagger}$ is the free energy barrier along the collective solvent coordinate and ω_S is the harmonic frequency of oscillation of the solvent coordinate in the reactant well. Expressions have been derived for the free energy barrier in various limits of the proton donor-acceptor motion.[64–65] TST neglects the dynamical recrossings of the dividing surface, but this expression can be extended to include such recrossings by including a prefactor κ, the transmission coefficient. In this case, the rate constant is expressed as:

$$k=\kappa k^{\mathrm{TST}}, \quad (3)$$

where $0 < \kappa \leq 1$ accounts for dynamical recrossings of the dividing surface.[67–69]

In a more general sense, reactive flux theory can be used to calculate the TST rate constant and transmission coefficient for any reaction coordinate, including the collective solvent coordinate. These computational approaches will be discussed in Section 3.

2.1.3 Vibrationally nonadiabatic rate constant—In the vibrationally nonadiabatic limit, the rate constant expression can be derived using Fermi's golden rule in conjunction with linear response theory in the vibrationally diabatic representation. Hynes and coworkers derived rate constant expressions for vibrationally nonadiabatic proton transfer using a dynamical treatment based on the time integral of the time correlation function of the probability flux associated with the proton tunneling reaction.[8–9,70] This formalism requires strong enough coupling between the proton transfer reaction and the solvent (i.e., a large enough solvent reorganization energy) to ensure convergence of integrals that arise in the derivation. As discussed above, the diabatic proton vibrational states are depicted in Figure 2b, with the corresponding free energy curves indicated by the dashed lines in Figure 3 for a symmetric system. The coupling C between the diabatic proton vibrational states determines the tunneling probability between these diabatic states and depends strongly on the proton donor-acceptor distance. Figure 4 depicts the diabatic free energy curves along the collective solvent coordinate. Note that Figure 4 corresponds to an asymmetric system, in contrast to Figures 1–3.

The rate constant expression for fixed proton donor-acceptor distance is:[8–9,70]

$$k^{\mathrm{PT}}=\frac{C^2}{\hbar}\sqrt{\frac{\pi}{\lambda_{\mathrm{s}}k_{\mathrm{B}}T}}\exp\left(-\frac{\left(\Delta G^0+\lambda_{\mathrm{s}}\right)^2}{4\lambda_{\mathrm{s}}k_{\mathrm{B}}T}\right), \quad (4)$$

where the solvent reorganization energy λ_{s} and reaction free energy ΔG^0 are defined in Figure 4. Although this rate constant has a similar form as the TST rate constant when the free energy barrier is expressed as

$$\Delta G^{\ddagger}=\frac{\left(\Delta G^{0}+\lambda_{\mathrm{s}}\right)^{2}}{4\lambda_{\mathrm{s}}}, \quad (5)$$

the physical interpretation is fundamentally different. The physical interpretation of Eq. (4) is that the exponential term is associated with the probability of sampling a solvent configuration suitable for proton transfer (i.e., a virtually symmetric proton potential with degenerate diabatic proton vibrational states), and the prefactor C^2 is associated with the probability of proton tunneling at this configuration. As discussed in Ref. 71, however, Eq. (4) can be viewed as a TST rate constant in the sense that the system is assumed to be in equilibrium along the reaction coordinate.

The motion of the proton donor-acceptor distance, represented by the coordinate *R*, can also be included in this rate constant expression. The proton donor-acceptor mode is assumed to be harmonic with effective mass *M* and vibrational frequency Ω. In the derivations, the coupling is assumed to decrease exponentially with *R*:[8–9,72–74]

$$C(R)=C(\overline{R})\exp\left[-\alpha(R-\overline{R})\right], \quad (6)$$

where $\overline{R}$ is the equilibrium proton donor-acceptor distance and α is a parameter that can be determined computationally. In the limit of moderate to high temperatures relative to the frequency of the proton donor-acceptor mode, assuming the same equilibrium proton donor-acceptor distance in the reactant and product states, the rate constant expression is[8–9,70]

$$k^{\mathrm{PT}}=\frac{\left\langle C^{2}\right\rangle}{\hbar}\sqrt{\frac{\pi}{\left(\lambda_{\mathrm{s}}+\tilde{\lambda}_{\alpha}\right)k_{\mathrm{B}}T}}\exp\left(-\frac{\left(\Delta G^{0}+\lambda_{\mathrm{s}}+\lambda_{\alpha}\right)}{4\left(\lambda_{\mathrm{s}}+\tilde{\lambda}_{\alpha}\right)k_{\mathrm{B}}T}\right) \quad (7)$$

$$\lambda_{\alpha}=\frac{\hbar^{2}\alpha^{2}}{2M} \quad (8)$$

$$\tilde{\lambda}_{\alpha}=\lambda_{\alpha}\frac{\hbar\Omega}{2k_{\mathrm{B}}T}\coth\left(\frac{\hbar\Omega}{2k_{\mathrm{B}}T}\right)\approx\lambda_{\alpha} \quad (9)$$

$$\left\langle C^{2}\right\rangle=C^{2}(\overline{R})\exp\left[\frac{2\lambda_{\alpha}}{\hbar\Omega}\coth\left(\frac{\hbar\Omega}{2k_{\mathrm{B}}T}\right)\right]\approx C^{2}(\overline{R})\exp\left[\frac{2k_{\mathrm{B}}T\alpha^{2}}{M\Omega^{2}}\right]. \quad (10)$$

In Eqs. (9) and (10), the approximation in the second part corresponds to the high-temperature limit in which coth(*x*) =1/*x* for small *x*. When this approximation is not invoked, the rate constant in Eq. (7) involves two different reorganization energies in the numerator and denominator of the exponential (i.e., λ_α and $\tilde{\lambda}_\alpha$), representing a departure from the usual global linear coupling model in Marcus theory.[75] The free energy barrier associated with Eq. (7) is defined analogously to Eq. (5) but includes reorganization energy contributions from both the solvent and the proton donor-acceptor mode (i.e., $\lambda_{\mathrm{s}} + \lambda_{\alpha}$). Eq. (7) includes only the ground reactant and product proton vibrational states. The inclusion of excited proton vibrational states is straightforward and involves summing over the rate constants associated with all pairs of reactant and product states, weighting each pair by the Boltzmann probability for the reactant state.[70]

In this limit, the rate constant is the same as the expression in Eq. (4) for fixed *R* except that the reorganization energy is replaced by ($\lambda_s + \lambda_\alpha$) and the coupling is multiplied by the factor $\exp\left[\frac{2k_B T\alpha^2}{M\Omega^2}\right]$. The term λ_s appearing in the free energy barrier represents an energetic contribution to the barrier due to thermal activation of the proton donor-acceptor mode. The factor $\exp\left[\frac{2k_B T\alpha^2}{M\Omega^2}\right]$ in the average coupling arises from the dependence of the tunneling probability on the proton donor-acceptor mode. In particular, the tunneling probability increases as the dependence of the coupling on *R* increases (i.e., as α increases) and as the force constant associated with the proton donor-acceptor mode decreases (i.e., as $M\Omega^2$ decreases) to enable the sampling of a wider range of distances. This factor vanishes if the dependence of the coupling on the proton donor-acceptor distance *R* is very weak or if the proton donor-acceptor mode is very stiff. These additional terms significantly impact the kinetic isotope effects (KIEs) because α is isotopically sensitive. Thus, the isotopic dependence of this rate constant is determined by both λ_α, which is contained in the free energy barrier, and the prefactor associated with the coupling. These additional terms also impact the temperature dependence of the rate constant and KIE.

Since these reactions are electronically adiabatic, the coupling *C* corresponds to half of the tunneling splitting associated with the electronically adiabatic proton potential energy curve. This potential energy curve, *V*(*x*), is calculated for a fixed configuration of the environment invoking the Born-Oppenheimer approximation, where the electrons respond instantaneously to the motion of the proton along the *x* coordinate. Moreover, this potential is generated at a configuration of heavy nuclei for which the two diabatic proton vibrational states are in resonance (i.e., the configuration at which the proton moves in a virtually symmetric double well potential). The diabatic proton vibrational states for this potential *V*(*x*) are depicted in the middle potential of Figure 2b, where the diabatic proton vibrational states localized in the donor and acceptor wells are clearly in resonance. Interaction between these two degenerate diabatic proton vibrational states according to the coupling *C* leads to the tunneling splitting Δ between the adiabatic proton vibrational states depicted in the middle potential of Figure 2a. For a particular system, the adiabatic proton vibrational states and the associated tunneling splitting Δ can be calculated by numerically solving the one-dimensional nuclear Schrödinger equation for the proton moving in the potential *V*(*x*). As mentioned above, the coupling *C* can be calculated as $C = \Delta/2$.

The coupling *C* can also be calculated for model systems using semiclassical methods. For a proton moving in a potential *V*(*x*) with barrier height $V^\ddagger$, vibrational frequencies ω_D and ω_A in the donor and acceptor wells, respectively, and barrier frequency $\omega^\ddagger$, the coupling between the proton vibrational ground states localized in the donor and acceptor wells is:[74]

$$C \approx \frac{\hbar\sqrt{\omega_D\omega_A}}{2\pi}\exp\left[-\frac{\pi}{\hbar\omega^\ddagger}\left(V^\ddagger - \mathrm{ZPE}\right)\right], \quad (11)$$

where ZPE is the zero-point energy of the proton, i.e., ZPE $\approx \hbar g\omega_D/2$. This expression can be extended to provide the coupling for other pairs of reactant and product proton vibrational states (i.e., excited vibrational states) with energy levels below the barrier by modifying ZPE. The dependence of the coupling on the proton donor-acceptor distance *R* is due mainly to the change in the proton barrier height $V^\ddagger$ with *R*. The approximately linear dependence of $V^\ddagger$ on *R* leads to the exponential dependence of the coupling on *R*, as given in Eq. (6). Note that the frequencies are inversely proportional to the square root of the mass of the transferring species, so both the magnitude of the coupling and the exponential factor α

are isotopically sensitive. The exponential factor a also depends on the specific pair of reactant and product proton vibrational states, but this dependence is relatively weak.

2.2 PCET reactions

The proton and hydride transfer reactions discussed in Section 2.1 were assumed to be electronically adiabatic. In other words, the electrons respond instantaneously to the proton motion for these systems. As a result, the proton was assumed to move on the electronically adiabatic ground state potential energy surface. This approximation is physically reasonable for the majority of proton and hydride transfer reactions. In contrast, proton-coupled electron transfer (PCET) reactions often exhibit electronically nonadiabatic proton transfer, and the electronically excited state can no longer be neglected. In this subsection, we start out by explaining the basic concepts of PCET reactions and discuss the distinction between two types of concerted PCET reactions, namely electron-proton transfer (EPT) and hydrogen atom transfer (HAT), in terms of the electron-proton nonadiabaticity. Then we present the rate constant expressions for EPT reactions, which are electronically nonadiabatic, and discuss expressions for HAT reactions, which are electronically adiabatic. Finally, we summarize the approximations underlying these analytical expressions and clarify the limits of applicability.

2.2.1 Basic concepts—The simplest PCET reaction involves the transfer of one electron and one proton. Extensions to multiple electrons and protons are straightforward[76–77] but will not be discussed here. PCET reactions can occur by either concerted or sequential mechanisms. The rigorous distinction between concerted and sequential mechanisms is challenging because of the quantum mechanical, delocalized nature of the electron and proton and the fast timescales involved. The reaction can be identified as sequential if an intermediate associated with single electron transfer (ET) or single proton transfer (PT) is observed, either experimentally by isolation of the intermediate or theoretically through the location of a minimum on the potential energy surface. This type of distinction is not always possible, however, and may depend on somewhat arbitrary aspects of the experimental capabilities, the specification of a lifetime, and/or the level of theory. Moreover, photoinduced PCET reactions, which are inherently nonequilibrium processes, typically occur on too fast a timescale for thermal equilibration and hence are not conducive to the isolation of a thermally equilibrated intermediate. For the purposes of this review, concerted PCET reactions are defined qualitatively in terms of the absence of a stable intermediate. Sequential PCET reactions can be treated with theories developed for single ET and PT reactions.[78] The remainder of this subsection will focus on concerted PCET reactions.

In the valence bond framework, PCET reactions can be described in terms of four diabatic electronic states:[76]

$$\begin{array}{ll} (1a) & \mathrm{D_e^-}\text{—}\mathrm{D_p}\text{—}\mathrm{H^+}\cdots\cdots\mathrm{A_p}\text{—}\mathrm{A_e} \\ (1b) & \mathrm{D_e^-}\text{—}\mathrm{D_p}\cdots\cdots{}^+\mathrm{H}\text{—}\mathrm{A_p}\text{—}\mathrm{A_e} \\ (2a) & \mathrm{D_e}\text{—}\mathrm{D_p}\text{—}\mathrm{H^+}\cdots\cdots\mathrm{A_p}\text{—}\mathrm{A_e^-} \\ (2b) & \mathrm{D_e}\text{—}\mathrm{D_p}\cdots\cdots{}^+\mathrm{H}\text{—}\mathrm{A_p}\text{—}\mathrm{A_e^-} \end{array} \quad (12)$$

where 1 and 2 denote the ET state, and *a* and *b* denote the PT state. As for the proton transfer reactions described in Section 2.1, the adiabatic electronic states are linear combinations of these four diabatic electronic states, and the coupling between the PT states (i.e., the (*a*) and (*b*) diabatic electronic states) is typically so strong that the associated excited adiabatic electronic states are high enough in energy to be neglected. The coupling between the ET states (i.e., the (1) and (2) diabatic electronic states), however, is typically significantly smaller. Thus, PCET reactions can be described in terms of two diabatic

electronic states, denoted I and II, which correspond to the ground adiabatic electronic states from the 1*a*/1*b* and 2*a*/2*b* combinations, respectively.[11,79]

Including the nuclear quantum effects of the transferring proton, PCET reactions are described in terms of diabatic electron-proton vibronic states.[11,79] In particular, the proton vibrational states are calculated for each diabatic electronic state I and II. The reactant and product vibronic states are products of the diabatic electronic state I and II, respectively, and the associated proton vibrational states. In the limit that the reaction is electronically adiabatic, as discussed in Section 2.1, these diabatic vibronic states are simply diabatic proton vibrational states associated with the electronic ground state. In general, however, these diabatic electron-proton vibronic states involve contributions from the excited electronic state as well.

Figure 5 depicts the free energy curves and proton potentials associated with the ground reactant (I) and product (II) diabatic vibronic states along the collective solvent coordinate. The shapes of the diabatic proton potentials do not change significantly along the collective solvent coordinate because the electrostatic attraction between the electron and proton maintains the asymmetry of the proton potential in each case. For diabatic electronic state I (blue), where the electron is on its donor, the proton donor well is lower in energy, and for diabatic electronic state II (red), where the electron is on its acceptor, the proton acceptor well is lower in energy. In this case, changing the collective solvent coordinate alters the relative energies but not the shapes of the two diabatic proton potentials. At the crossing point of the free energy curves in Figure 5, the ground proton vibrational states are degenerate. Note that these free energy curves correspond to electron-proton vibronic states, which involve contributions from the excited electronic state, while those shown in Figure 4 correspond to proton vibrational states for the ground electronic state.

Alternatively, a more simplistic description of PCET reactions may be utilized. In this simpler approach, the diabatic states 1*b* and 2*a* are assumed to be so much higher in energy that they can be neglected, and the reaction is described in terms of only two diabatic electronic states, 1*a* and 2*b*, in Eq. (12). In this case, states I and II are simply the diabatic electronic states 1*a* and 2*b*. This description leads to the same physical picture shown in Figure 5 except the blue and red proton potentials are each a single well potential without the higher local minimum.

2.2.2 Distinguishing between EPT and HAT—Throughout the literature, concerted PCET reactions have been classified as HAT or EPT. Traditionally, HAT reactions have been defined as a reaction in which the electron and proton transfer between the same donor and acceptor (i.e., between the same orbitals or bonds). In contrast, EPT reactions are typically defined as reactions in which the electron and proton transfer between different donors and acceptors.[80–81] This method of distinguishing between HAT and EPT is not rigorous, however, and provides only qualitative guidance. A more rigorous method for distinguishing HAT and EPT is through the degree of electron-proton nonadiabaticity. Specifically, HAT reactions exhibit electronically adiabatic proton transfer, whereas EPT reactions exhibit electronically nonadiabatic proton transfer.[82–83] In this case, the relevant nonadiabaticity is between the electrons and the transferring proton, thereby denoted *electron-proton nonadiabaticity*.

The degree of electron-proton nonadiabaticity can be determined using a semiclassical formulation that defines an adiabaticity parameter as the ratio of the proton tunneling time and the electronic transition time.[82,84] The proton transfer is electronically adiabatic when the proton tunneling time is much longer than the electronic transition time and is electronically nonadiabatic in the opposite regime.[82] In the electronically adiabatic regime,

the proton moves slowly enough for the electrons to respond instantaneously to its motion, and the system remains in the electronic ground state. In the electronically nonadiabatic regime, the electrons are unable to respond quickly enough to the proton motion to remain in the electronic ground state, leading to the involvement of the excited electronic state.

In this semiclassical formalism,[84] the general vibronic coupling $V_{\mu\nu}^{(\mathrm{sc})}$ is expressed in terms of the adiabatic vibronic coupling $V_{\mu\nu}^{(\mathrm{ad})}$:

$$V_{\mu\nu}^{(\mathrm{sc})}=\kappa V_{\mu\nu}^{(\mathrm{ad})}, \quad (13)$$

where the factor κ is defined as

$$\kappa=\sqrt{2\pi p}\frac{e^{p\ln p-p}}{\Gamma\left(p+1\right)}. \quad (14)$$

Note that this κ is distinct from the transmission coefficient κ described elsewhere in this review. Here $\Gamma(x)$ is the gamma-function, and p is the proton adiabaticity parameter defined as

$$p=\frac{\left|V^{\mathrm{el}}\right|^2}{\hbar\left|\Delta F\right|v_t}, \quad (15)$$

where V^{el} is the electronic coupling between the diabatic electronic states I and II, v_t is the so-called tunneling velocity[84] of the proton at the crossing point of the two proton potential energy curves, and $|\Delta F|$ is the difference between the slopes of the proton potential energy curves at the crossing point. The tunneling velocity is given as $v_t=\sqrt{2\left(V_c-E\right)/m_{\mathrm{p}}}$, where V_c is the energy at which the potential energy curves cross and E is the tunneling energy. In the electronically adiabatic limit, $p\gg1$, $\kappa=1$, and the vibronic coupling simplifies to $V_{\mu\nu}^{(\mathrm{ad})}$, which is equivalent to $C=\Delta/2$ in the context of Section 2.1. In the electronically nonadiabatic limit, $p\ll1$, $\kappa=\sqrt{2\pi p}$, and the vibronic coupling reduces to $V_{\mu\nu}^{(\mathrm{na})}=V^{\mathrm{el}}S_{\mu\nu}$, where $S_{\mu\nu}$ is the overlap between the reactant and product proton vibrational wavefunctions for electron-proton vibronic states μ and ν, respectively. Note that Eq. (15) is identical to the adiabaticity parameter defined in the Landau-Zener model.[85–87]

As mentioned above, the electron-proton nonadiabaticity of a PCET reaction can be characterized in terms of the relative timescales for the proton tunneling and the electronic transition. Within the semiclassical framework,[88–89] the proton tunneling time is $\tau_{\mathrm{p}}\sim V^{\mathrm{el}}/|\Delta F|v_t$, the electronic transition time is $\tau_{\mathrm{e}}\sim\hbar/V^{\mathrm{el}}$, and the adiabaticity parameter is $p=\tau_{\mathrm{p}}/\tau_{\mathrm{e}}$. The proton transfer is electronically adiabatic when the proton tunneling time is much longer than the electronic transition time (i.e., $p\gg1$), and the proton transfer is electronically nonadiabatic when the proton tunneling time is much shorter than the electronic transition time (i.e., $p\ll1$). Typically HAT reactions are in the former limit, whereas EPT reactions are in the latter limit.[82] A related analysis of characteristic lengths and times in the context of heme protein kinetics was discussed in Ref. 87.

The distinction between HAT and PCET mechanisms, which are electronically adiabatic and nonadiabatic, respectively, is illustrated by a comparison between the benzyl/toluene and phenoxyl/phenol self-exchange reactions, as depicted in Figure 6.[82] For the benzyl/toluene

system (Figure 6a), the adiabaticity parameter p is greater than unity, with $\tau_p \approx 4\tau_e$. In this case, the electronic transition time is less than the proton tunneling time, so the electrons can respond instantaneously to the proton motion, allowing the proton to remain on the electronically adiabatic ground state surface. For the phenoxyl/phenol system (Figure 6b), the adiabaticity parameter p is very small, with $\tau_p \approx \tau_e$ 80. In this case, the electronic transition time is significantly greater than the proton tunneling time, so the electrons are not able to rearrange fast enough for the proton to remain in the electronically adiabatic ground state.

These two self-exchange reactions can also be used to illustrate the methods for calculating the vibronic coupling for general PCET reactions in the electronically adiabatic and electronically nonadiabatic limits. For the electronically adiabatic benzyl/toluene reaction, the vibronic coupling is half the tunneling splitting for the electronically adiabatic ground state, where the tunneling splitting is indicated as Δ in Figure 6a. For the electronically nonadiabatic phenoxyl/phenol reaction, the vibronic coupling is the product of the electronic coupling between the diabatic states and the overlap of the associated reactant and product proton vibrational wavefunctions, which are depicted in Figure 6b. For systems in the intermediate regime, the semiclassical expression in Eq. (13) can be used to calculate the vibronic coupling.

In addition to this perspective, the electron-proton nonadiabaticity can also be quantified in terms of the nonadiabatic coupling between the ground and excited state adiabatic electronic wavefunctions with respect to the transferring proton coordinate.[83] This nonadiabatic coupling is a measure of the change in electronic charge distribution associated with the adiabatic electronic states along the proton coordinate. According to this diagnostic, the reaction exhibits negligible charge redistribution in the electronically adiabatic regime and exhibits significant charge redistribution in the electronically nonadiabatic regime. Consistent with the traditional definitions, HAT reactions do not involve significant charge redistribution, corresponding to the transfer of a neutral hydrogen atom a few tenths of an angstrom between the same donor and acceptor. In contrast, EPT reactions involve significant charge redistribution, corresponding to the transfer of an electron and a proton between different donors and acceptors. As a result, the solvent reorganization energy is significantly larger for EPT reactions than for HAT reactions, and HAT reactions tend to be dominated by solute rather than solvent reorganization.

Thus, HAT and EPT reactions are described in qualitatively different ways. Although HAT reactions are electronically adiabatic, typically they are expected to be vibrationally nonadiabatic, although in principle they could also be vibrationally adiabatic. Similar to proton and hydride transfer reactions, HAT reactions are described in terms of the electronically adiabatic ground state, and the coupling between the diabatic proton vibrational states is described by half the tunneling splitting, $C = \Delta/2$, as depicted in Figure 6a and given by the approximate expression in Eq. (11). Moreover, HAT reactions are associated with relatively small solvent reorganization energies and are dominated by solute reorganization. The rate constants for HAT reactions will be discussed in Section 2.2.4. In contrast to HAT reactions, EPT reactions are described in terms of diabatic electron-proton vibronic states that involve the excited electronic state, as depicted in Figure 5. In this electronically nonadiabatic regime, the coupling between the diabatic electron-proton vibronic states is given by[11,79]

$$V_{\mu\nu} = V^{\mathrm{el}} S_{\mu\nu}, \quad (16)$$

as discussed above in the context of the semiclassical formulation. Additionally, EPT reactions are associated with relatively large solvent reorganization energies because of substantial charge redistribution. The proton potential energy curves corresponding to the diabatic electronic states and the associated ground state proton vibrational wavefunctions are depicted in Figure 6b. The rate constant expressions for EPT reactions will be given in Section 2.2.3.

2.2.3 EPT rate constant—Our group has derived rate constant expressions for EPT reactions in various well-defined limits.[8–9,11,76,79,90] These derivations and the resulting rate constant expressions are related to theoretical treatments of proton transfer[8–9,74] and other studies of these types of reactions.[91–92] The expressions were derived in the vibronically nonadiabatic limit using the Fermi golden rule formalism in conjunction with a dynamical treatment based on the time integral of the probability flux time correlation function. In this framework, the EPT reaction is described in terms of nonadiabatic transitions between reactant and product electron-proton vibronic states. These electron-proton vibronic states are generated by calculating the proton vibrational states for each diabatic electronic state (i.e., I and II for the reactant and product states, respectively, in Figure 5). This procedure leads to two sets of stacked parabolas (i.e., an extension of Figure 5 that includes blue and red nested parabolas), where the splittings between the free energy curves are determined by the splittings between the proton vibrational states. The total rate constant is obtained by summing over the rate constants associated with all pairs of reactant and product electron-proton vibronic states, weighting each pair by the Boltzmann probability for the reactant state. Note that an analogous procedure can be performed for the proton and hydride vibrationally nonadiabatic rate constants discussed in Section 2.1, although in this case the summation is over the diabatic proton vibrational states associated with the electronic ground state.

The rate constant for a fixed proton donor-acceptor distance R is:[11,79]

$$k^{\mathrm{EPT}}=\sum_{\mu}P_{\mu}\sum_{\nu}\frac{|V_{\mu\nu}|^2}{\hbar}\sqrt{\frac{\pi}{\lambda_{\mathrm{s}}k_{\mathrm{B}}T}}\exp\left[-\frac{\left(\Delta G^{0}_{\mu\nu}+\lambda_{\mathrm{s}}\right)^2}{4\lambda_{\mathrm{s}}k_{\mathrm{B}}T}\right], \quad (17)$$

where the summations are over reactant and product vibronic states, P_{μ} is the Boltzmann probability for the reactant state μ, $V_{\mu\nu}$ is the vibronic coupling between the reactant and product vibronic states μ and ν, λ_{s} is the solvent reorganization energy for states μ and ν, and $\Delta G^{0}_{\mu\nu}$ is the reaction free energy for states μ and ν. The latter two parameters are defined for electron-proton vibronic states analogously to the definitions shown in Figure 4. The solvent reorganization energy could be different for each pair of vibronic states[11,79] but for simplicity is assumed to be the same in this expression. The free energy of reaction, $\Delta G^{0}_{\mu\nu}$, can be expressed as the sum of the value for the ground states and the difference between the product and reactant energy levels ν and μ relative to their respective ground states.

The motion of the proton donor-acceptor mode can be included using the same procedure as used for proton and hydride transfer. Specifically, the vibronic coupling can be assumed to depend exponentially on the proton donor-acceptor distance R:[90]

$$V_{\mu\nu}=V^{(0)}_{\mu\nu}\exp\left[-\alpha_{\mu\nu}\left(R-\overline{R}\right)\right] \quad (18)$$

where R is the equilibrium value of R and $V_{\mu\nu}^{(0)}$ is the vibronic coupling between states μ and ν at proton donor-acceptor distance R. This form of the coupling is a reasonable approximation in the region of R near its equilibrium value, as illustrated by expanding $\ln[V_{\mu\nu}/V_{\mu\nu}^{(0)}]$ in a Taylor series around $R = R$ and retaining only the linear terms.[93] For simplicity, the equilibrium proton donor-acceptor distance is assumed to be the same for all reactant and product vibronic states, although this assumption can easily be avoided.[11,90] We utilized a dynamical formulation involving time correlation functions to derive EPT rate constant expressions in various regimes. As for proton and hydride transfer, this derivation requires a sufficiently large solvent reorganization energy to be valid. In the limit of moderate to high temperatures relative to the frequency of the proton donor-acceptor mode, the rate constant is:[11,90]

$$k^{\mathrm{EPT}}=\sum_{\mu}P_{\mu}\sum_{\nu}\frac{\left|V_{\mu\nu}^{(0)}\right|^{2}}{\hbar}\exp\left[\frac{2k_{\mathrm{B}}T\alpha_{\mu\nu}^{2}}{M\Omega^{2}}\right]\sqrt{\frac{\pi}{\Lambda_{\mu\nu}k_{\mathrm{B}}T}}\exp\left[-\frac{\left(\Delta G_{\mu\nu}^{0}+\Lambda_{\mu\nu}\right)^{2}}{4\Lambda_{\mu\nu}k_{\mathrm{B}}T}\right], \quad (19)$$

where the total reorganization energy is defined as $\Lambda_{\mu\nu}=\lambda_{\mathrm{s}}+\lambda_{\mu\nu}^{(\alpha)}$ and $\lambda_{\mu\nu}^{(\alpha)}$ is defined as in Eq. (8) for $\alpha = \alpha_{\mu\nu}$.

It is useful to compare this EPT rate constant expression to the proton and hydride transfer rate constants discussed in Section 2.1. Each term in the summations of Eq. (19) is identical to Eq. (7) with the approximations in the subsequent equations except for the form of the coupling. In Eq. (7), which is valid for proton and hydride transfer, the coupling is half the tunneling splitting or given by the approximate expression in Eq. (11), whereas in Eq. (19), which is valid for EPT, the coupling is $V_{\mu\nu}^{(0)}=V^{\mathrm{el}}S_{\mu\nu}^{(0)}$, where $S_{\mu\nu}^{(0)}$ is the overlap between the reactant and product proton vibrational wavefunctions μ and ν at $R = R$. In both cases, the coupling is assumed to decrease exponentially with R according to the exponential factor α, which has been found to be ~20–30 $\mathrm{Å}^{-1}$ for both types of coupling.[10,82] Another important difference between EPT and PT is that the solvent reorganization energy is typically much larger for EPT reactions because the solute charge redistribution is substantially greater for EPT reactions. Specifically, PT reactions typically involve the transfer of a proton over a few tenths of an angstrom, whereas EPT reactions also involve a relatively long-range electron transfer reaction, leading to greater charge redistribution. As a result, for EPT reactions, the total reorganization energy can be approximated as $\Lambda_{\mu\nu}\approx\lambda_{\mathrm{s}}$ because $\lambda_{\mathrm{s}}\gg\lambda_{\mu\nu}^{(\alpha)}$. In this case, the rate constant in Eq. (19) further simplifies to:[11,44]

$$k^{\mathrm{EPT}}=\sum_{\mu}P_{\mu}\sum_{\nu}\frac{\left|V_{\mu\nu}^{(0)}\right|^{2}}{\hbar}\exp\left[\frac{2k_{\mathrm{B}}T\alpha_{\mu\nu}^{2}}{M\Omega^{2}}\right]\sqrt{\frac{\pi}{\lambda_{\mathrm{s}}k_{\mathrm{B}}T}}\exp\left[-\frac{\left(\Delta G_{\mu\nu}^{0}+\lambda_{\mathrm{s}}\right)^{2}}{4\lambda_{\mathrm{s}}k_{\mathrm{B}}T}\right]. \quad (20)$$

Note that the analogous rate constant expressions in the limit of low temperatures relative to the frequency of the proton donor-acceptor mode have also been derived for proton transfer[8] and EPT.[11,90] The reader is referred to these sources for the analytical rate constant expressions in this regime.

Considering only the nonadiabatic transition between the two ground vibronic states, the KIE can be approximated from Eq. (20) as[11,44]

$$\mathrm{KIE} \approx \frac{|S_{\mathrm{H}}|^2}{|S_{\mathrm{D}}|^2} \exp\left\{\frac{2k_{\mathrm{B}}T}{M\Omega^2}\left(\alpha_{\mathrm{H}}^2 - \alpha_{\mathrm{D}}^2\right)\right\}, \quad (21)$$

where S_{H} and S_{D} are the overlaps of the hydrogen and deuterium wavefunctions, respectively, at the equilibrium proton donor-acceptor distance, and a_{H} and a_{D} represent the exponential factors for hydrogen and deuterium, respectively. The deuterium overlap decreases faster than the hydrogen overlap as the proton donor-acceptor distance increases (i.e., $a_{\mathrm{D}} > a_{\mathrm{H}}$) because of the larger mass of deuterium. Thus, the term in the exponential has a negative sign, and the ratio of the squared hydrogen and deuterium vibrational wavefunction overlaps, $|S_{\mathrm{H}}|^2/|S_{\mathrm{D}}|^2$, increases as the equilibrium proton donor-acceptor distance increases. According to this approximate expression, the KIE for the ground reactant/product vibronic states is proportional to this ratio of overlaps. Thus, the KIE is predicted to increase as the proton donor-acceptor distance increases when all other parameters remain fixed and only the ground vibronic states contribute to the overall rate constant. However, this approximate expression also indicates that the KIE tends to increase as the frequency Ω associated with the proton donor-acceptor motion increases. In some cases, increasing the equilibrium proton donor-acceptor distance leads to a decrease in the frequency Ω, so these two factors compete with each other. Moreover, the inclusion of contributions from excited vibronic states leads to a more complicated analysis that does not provide straightforward predictions in terms of the proton donor-acceptor equilibrium distance and associated frequency.

In some cases, the assumption that the vibronic coupling decreases exponentially with the proton donor-acceptor distance may not be valid. Typically this assumption is valid only near the equilibrium proton donor-acceptor distance and will break down for lower proton donor-acceptor frequencies that enable sampling of a wider range of R values.[94] Moreover, this assumption is not valid when the proton vibrational wavefunctions change character in the relevant range of R values (i.e., when a proton vibrational state shifts from being localized on one side to the other, or possibly becomes delocalized, as R changes). In these situations, the rate constant expressions based on this assumption are no longer valid.

An alternative approach for including the effects of the proton donor-acceptor motion is to thermally average the rate constant over a Boltzmann distribution function $P(R)$. Assuming that only the proton vibrational overlap factors depend on R, this formulation leads to:[78,95]

$$\begin{aligned} k^{\mathrm{EPT}} &= \int_0^\infty k^{\mathrm{EPT}}(R) P(R) dR \\ &= \sum_\mu P_\mu \sum_\nu \frac{|V^{\mathrm{el}}|^2}{\hbar} \sqrt{\frac{\pi}{\lambda_{\mathrm{s}} k_{\mathrm{B}} T}} \exp\left[-\frac{\left(\Delta G^0_{\mu\nu} + \lambda_{\mathrm{s}}\right)^2}{4\lambda_{\mathrm{s}} k_{\mathrm{B}} T}\right] \int_0^\infty P(R) [S_{\mu\nu}(R)]^2 dR. \end{aligned} \quad (22)$$

Here $k^{\mathrm{EPT}}(R)$ is the EPT rate constant evaluated at a given R value, and $P(R)$ is the normalized probability distribution function for R at a specified temperature. Typically $P(R)$ is assumed to be the Boltzmann probability for a classical harmonic oscillator representation of the R-mode and is given by the expression

$$P(R) = \sqrt{\frac{M\Omega^2}{2\pi k_{\mathrm{B}} T}} \exp\left[\frac{-M\Omega^2\left(R - \overline{R}\right)^2}{(2k_{\mathrm{B}} T)}\right]. \quad (23)$$

$P(R)$ could also be chosen to be the Boltzmann probability for a quantum mechanical harmonic oscillator to include the quantum effects of the R-mode[95] or a more general form based on the energies calculated as a function of R for a specific system. The advantage of this approach is that it is valid for general forms of the proton vibrational overlap (i.e., it avoids the assumption of exponential dependence on R), but the disadvantage of this approach is that it assumes that the R-mode is separable and always at equilibrium.

The EPT rate constant $k^{EPT}(R)$ typically increases dramatically as R decreases because of increasing overlap between the reactant and product proton vibrational wavefunctions. The probability distribution $P(R)$ has a maximum at the equilibrium proton donor-acceptor distance $\bar{R}$ and a width determined by the frequency Ω of the proton donor-acceptor mode. Figure 7 illustrates that the dominant proton donor-acceptor distance (i.e., the distance that contributes the most to the rate constant in Eq. (22), as indicated by the maximum of the purple curve) is significantly smaller than the equilibrium proton donor-acceptor distance $\bar{R}$ (the maximum of the blue curve). According to this theory, the EPT rate constant is expected to increase as the equilibrium proton donor-acceptor distance and associated frequency decrease (i.e., as the blue curve shifts to smaller R values and broadens). Inclusion of excited vibronic states, however, leads to a more complicated situation.

The thermally averaged rate constant in Eq. (22) is identical to a rate constant expression[92] that has been applied to a variety of chemical and biological systems.[53,96–102] This expression can be interpreted as the product of an exponential term associated with the reorganization of the heavy atoms leading to a configuration conducive to hydrogen tunneling (i.e., degenerate diabatic states) and an integral representing the tunneling probability, often denoted the Franck-Condon term. The contributions to the Franck-Condon term can be further divided into $[S_{\mu\nu}(R)]^2$, which is related to the tunneling probability for a given proton donor-acceptor distance R, and $P(R)$, which is the probability of sampling this value of R based on the relative energy of this configuration.

This expression has been used to interpret the temperature dependence of KIEs for a variety of enzyme reactions.[96–102] The first exponential factor in Eq. (22) associated with the probability of achieving thermally activated tunneling-ready configurations depends on the free energy barrier and temperature but is typically assumed to be isotope independent. Note that when the summations over excited vibronic states are included, this term becomes isotope dependent because the splittings between vibronic states, which contribute to $\Delta G^0_{\mu\nu}$, depend on isotope. Moreover, the populations P_μ of the reactant vibronic states also depend on isotope. The Franck-Condon term, given by the integral in Eq. (22), depends on both isotope and temperature, and this term is often used to explain the temperature dependence or, in some cases, the temperature independence of KIEs. Specifically, the overlap $[S_{\mu\nu}(R)]^2$ depends on isotope (i.e., for two harmonic oscillators, the overlap is exponentially dependent on the mass of the proton), and the Boltzmann probability $P(R)$ depends on temperature according to Eq. (23). As mentioned above, the interpretation of the temperature dependence of KIEs is complicated by the inclusion of excited vibronic states, particularly because the relative contribution from each pair of reactant/product vibronic states is different for hydrogen and deuterium and depends strongly on temperature.

We have shown that the EPT rate constant expressions in Eqs. (20) and (22) become equivalent under certain conditions.[95] Specifically, these two expressions are mathematically equivalent when $P(R)$ is assumed to be the Boltzmann probability for a classical harmonic oscillator representation of the R-mode and the proton vibrational overlap is assumed to depend exponentially on R. We emphasize, however, that the thermally averaged rate constant in Eq. (22) is not equivalent to the PT rate constant expression in Eq.

(7) for two main reasons. First, we cannot assume that $\lambda_s \gg \lambda_{\mu\nu}^{(\alpha)}$ and therefore neglect $\lambda_{\mu\nu}^{(\alpha)}$ for proton transfer reactions because the solvent reorganization energy is relatively small. Second, the form of the coupling is completely different for the two expressions, and the approximation of the coupling as the product of an electronic coupling and the proton vibrational wavefunction overlap is not theoretically justified for an electronically adiabatic proton or hydride transfer reaction. Thus, Eq. (22) should be used only for reactions that involve electronically nonadiabatic proton transfer, as is typical for EPT reactions. Application of this expression to electronically adiabatic proton and hydride transfer reactions, as well as HAT reactions defined as in Sec. 2.2.2, is not theoretically justified.

The effects of intramolecular solute modes (i.e., inner-sphere reorganization) may be significant for EPT reactions, as well as proton and hydride transfer reactions. We have derived rate constant expressions that include these effects following the well-known approaches for electron transfer reactions.[79,103–105] In the high-temperature limit for uncoupled solute modes, the rate constant expressions given above are modified by adding the inner-sphere reorganization energy to the solvent reorganization energy.

2.2.4 HAT rate constant—On the basis of the definition given in Section 2.2.2, HAT reactions are electronically adiabatic and can be described in a similar manner as the proton and hydride transfer reactions discussed in Section 2.1. Such reactions can be described in terms of two diabatic electronic states, analogous to Eq. (1), except that a neutral hydrogen atom is transferred instead of a positively charged proton. In this case, only the proton potentials associated with the electronic ground state, as in Figures 1 and 2, must be considered, and the free energy curves along the collective solvent coordinate are associated with the proton vibrational states of these proton potentials, as in Figures 3 and 4. The coupling between the diabatic proton vibrational states is half the tunneling splitting, $C = \Delta/2$, and this coupling is typically weak enough to ensure that HAT reactions are vibrationally nonadiabatic, although they could be vibrationally adiabatic in some cases.

An important difference between HAT and proton or hydride transfer reactions is that the solute charge redistribution is negligible during HAT reactions.[83] As a result, the interaction between the HAT reaction and a polar solvent environment is relatively weak. As mentioned above, the derivation of the rate constant expression in Eq. (7) requires sufficiently large solvent reorganization energy. Specifically, the reactive flux correlation function associated with the charge transfer reaction must decay on a faster timescale than the solvent relaxation.[8,79] The specific condition on the solvent reorganization energy depends on the derivation, but an example of such a condition is that $\lambda_s \gg \hbar^2/\left(k_B T \tau_L^2\right)$, where τ_L is the solvent longitudinal relaxation time.[79] When the solvent reorganization energy is not large enough, divergent integrals arise in the standard golden rule treatment used to derive this rate constant expression. If the solvent reorganization energy for HAT is large enough to avoid these difficulties, then Eq. (7) can be used. In many cases, however, the solvent reorganization energy is small enough that HAT reactions require special treatment. The limit of weak solvation, as well as the derivation of rate constant expressions in this limit, has been discussed by Borgis and Hynes[8] for HAT in solution. The resulting rate constant expressions are related to those derived by Trakhtenberg et al.[73] for HAT in solids. These studies also treat the low-temperature limit for the solvent, where the solvent must be treated quantum mechanically.[8] In addition, rate constant expressions that include coupling between the proton donor-acceptor vibrational mode and the solvent modes to avoid the divergent integrals in the weak solvation limit have been derived.[106] The reader is referred to these sources for the various analytical rate constant expressions for HAT. A variety of other general approaches have also been developed for systems exhibiting weak system-bath coupling.[107–110]

In addition, intramolecular solute modes are expected to play a more dominant role for HAT reactions because of the relatively weak coupling between the HAT reaction and the solvent. Thus, describing HAT reactions in terms of a collective solvent coordinate, as in Figures 2–4, is often not appropriate. Instead, HAT reactions should be described in terms of the specific solute and environmental motions that alter the shape of the proton potentials (i.e., the relative energies of the wells in Figure 2). In general, HAT reactions may require an explicit dynamical treatment of intramolecular solute motions, as well as key environmental molecular motions, with either classical or quantum mechanical methods. Thus, HAT rate constant expressions that include explicit solute and/or environmental motions treated either classically or quantum mechanically need to be explored for a complete description of such reactions.

2.2.5 Limits of applicability of various treatments—As discussed above, these theoretical treatments and analytical rate constant expressions are based on certain well-defined approximations and are only valid in the regimes for which these approximations are justified. For example, these treatments assume that the hydrogen coordinate and proton donor-acceptor mode can be separated from the other nuclear degrees of freedom. Many of these treatments also assume the validity of linear response theory for the solvent responding to the charge transfer reaction and a large enough solvent reorganization energy to ensure convergence of various integrals. The relative magnitudes of the solvent reorganization energies are expected to be as follows: $\lambda_{\mathrm{s}}^{\mathrm{EPT}} > \lambda_{\mathrm{s}}^{\mathrm{PT}} > \lambda_{\mathrm{s}}^{\mathrm{HAT}}$. Although the solvent reorganization energies for proton, hydride, and EPT reactions are expected to be large enough to warrant these types of treatments, the solvent reorganization energy for HAT may be too small, and other methods involving the dynamical treatment of solute modes may be required for HAT reactions, as discussed in Sec. 2.2.4.

In addition, the use of the various rate constant expressions requires the reaction to be in the appropriate regime in terms of electronic and vibrational nonadiabaticity. Proton and hydride transfer reactions are typically electronically adiabatic but could be vibrationally adiabatic or nonadiabatic, leading to the applicability of Eq. (2) or Eq. (7), respectively. Vibrational nonadiabaticity requires a small enough coupling between the reactant and product diabatic proton vibrational states and usually occurs for reactions with relatively high proton transfer barriers. HAT and EPT reactions are typically vibronically nonadiabatic in that the electron-proton subsystem does not respond instantaneously to the solvent environment. As discussed in Section 2.2.2, the degree of electron-proton nonadiabaticity can be determined using a semiclassical formalism to estimate the relative timescales for the electronic transition and proton tunneling or by calculating the nonadiabatic coupling between the lowest two adiabatic electronic states along the proton coordinate. HAT reactions are defined to be electronically adiabatic and hence resemble electronically adiabatic but vibrationally nonadiabatic proton transfer reactions, except that the solvent reorganization energy may be too small for the above treatments. EPT reactions are defined to be electronically nonadiabatic, leading to the applicability of Eq. (19), (20), or (22). We emphasize that the rate constants for vibrationally nonadiabatic proton transfer and for EPT are of similar form but are fundamentally different due to the coupling term given in Eq. (11) for the former and Eq. (16) for the latter. Although the dependence of both types of coupling on the proton donor-acceptor distance is assumed to be exponential with exponential factors of similar magnitude, the isotope dependence of these two types of coupling is different.

A comprehensive analysis of the limitations of nonadiabatic treatments is given in Ref. 22. These authors enumerate three concerns about such treatments. First, the Fermi golden rule approach is valid only when the coupling is small, and the Boltzmann averaging over the proton donor-acceptor distance may involve situations in which this coupling becomes too

large for a perturbation theory treatment. Second, the assumption that the hydrogen coordinate and proton donor-acceptor mode are separable from the other modes may not be justified for some systems. Note that all other modes in the system contribute to the collective solvent coordinate and thus impact the free energy barrier (i.e., the term in the rate constant associated with the probability of obtaining configurations conducive to electron and/or proton tunneling). Third, the treatment of these reactions in terms of diabatic states may not be appropriate, which is related to the first concern about small enough coupling. These authors, as well as others,[111–113] point out that many proton and hydride transfer reactions may be better characterized as partially vibrationally adiabatic and may only approach the nonadiabatic limit. Clearly when reactions are not in either the adiabatic or nonadiabatic limit, but rather are in an intermediate regime, the rate constant expressions given above are no longer valid. The nonadiabatic limit is expected to be much more suitable for EPT reactions, which involve electron transfer as well as proton transfer, than for proton and hydride transfer reactions. EPT reactions are more similar to electron transfer reactions, and the assumptions underlying Marcus theory for nonadiabatic electron transfer reactions[114–115] are likely to be valid for EPT reactions. Thus, the first and third issues mentioned above are not as problematic for EPT reactions. Simulation methods to study systems in the intermediate regime are discussed in Section 3.

We also point out that more general nonadiabatic rate constant expressions depending on the longitudinal solvent relaxation time as well as the electronic coupling have been derived for electron transfer reactions[116–118] and more recently extended to EPT reactions.[119] The nonadiabatic rate constant expressions given in Section 2 are valid in the Golden Rule limit, which is associated with weak electronic coupling and fast solvent relaxation. In this limit, the rate constant is determined by the nonadiabatic transitions in the crossing region, and it depends on the square of the electronic coupling but not on the solvent relaxation time. In the solvent-controlled nonadiabatic limit, which is associated with relatively strong electronic coupling and slow solvent relaxation, the rate constant is independent of the electronic coupling but is inverseley proportional to the longitudinal solvent relaxation time. Although the solvent-controlled limit is sometimes referred to as the adiabatic limit, the overall treatment is nonadiabatic in that transitions between electronic states are involved.[120] The more general nonadiabatic rate constant expressions[116–119] span the Golden Rule and solvent-controlled limits.

Finally, we address the issue of whether these types of models implicate the significance of *dynamical* effects in condensed phase hydrogen tunneling reactions. In the literature, the proton donor-acceptor mode R has been denoted a “promoting mode” that could be dynamically coupled to the chemical reaction.[39,121–123] All of the treatments discussed above assume that the system is at equilibrium. For example, the reactant states are occupied according to the equilibrium Boltzmann distribution with probabilities P_μ. Moreover, the proton donor-acceptor mode R is represented by an equilibrium Boltzmann distribution $P(R)$ and thus is assumed to always remain at thermal equilibrium. The solvent is also assumed to remain at equilibrium, and the tunneling-ready configurations are reached by thermal fluctuations. Thus, the so-called promoting mode is not dynamically coupled to the chemical reaction (i.e., there is no vibrational energy transfer or other type of nonequilibrium effect). Nevertheless, the equilibrium proton donor-acceptor motion plays a key role in the tunneling reaction. Note that the types of dynamical effects investigated for electron transfer reactions in donor-bridge-acceptor systems could potentially be relevant for proton transfer systems as well.[124–125]

3. Simulation methods for hydrogen tunneling

3.1 Hybrid quantum/classical molecular dynamics methods

Our group developed a hybrid quantum/classical molecular dynamics approach for the simulation of proton and hydride transfer reactions in solution and enzymes.[13–15] In this approach, the potential energy surface is described by an empirical valence bond (EVB) model, and the transferring hydrogen nucleus is represented as a quantum mechanical wavefunction on a three-dimensional grid. The overall rate constant is expressed as the product of the transmission coefficient and the transition state theory rate constant, as in Eq. (3). The transition state theory rate constant is calculated from the free energy barrier, which is determined from the free energy profile generated along a collective reaction coordinate. The transmission coefficient, which accounts for dynamical recrossings of the dividing surface, is calculated with a reactive flux method, in which an ensemble of trajectories is started at the dividing surface and propagated backward and forward in time. This approach assumes that the reaction is electronically adiabatic, but the vibrationally nonadiabatic effects are including using a surface hopping method to introduce nonadiabatic transitions among the proton vibrational states during the calculation of the transmission coefficient. Nuclear quantum effects such as zero point energy and hydrogen tunneling, as well as the motion of the entire solvated enzyme, are included during the generation of the free energy profiles and the real-time dynamical trajectories used to determine the transmission coefficient.

3.1.1 EVB potential—EVB potentials have been used successfully to simulate a wide range of proton and hydride transfer reactions in solution and enzymes.[12–14,126–128] In the simplest model, a proton or hydride transfer reaction is described in terms of two VB states, as given in Eq. (1). In state (*a*), the hydrogen is bonded to its donor, and in state (*b*), the hydrogen is bonded to its acceptor. The matrix elements of the Hamiltonian in the basis of these two VB states are described by molecular mechanical forcefield terms. The electronic ground state potential energy surface is obtained by diagonalizing the 2×2 EVB Hamiltonian matrix to determine the lowest-energy state at each nuclear configuration.

3.1.2 Nuclear quantum effects—A variety of methods have been developed to include the nuclear quantum effects in simulations of enzyme reactions. In this subsection, we describe a hybrid quantum/classical grid-based approach, in which the transferring hydrogen nucleus is treated quantum mechanically using grid-based methods, while all other nuclei are treated classically. In the next subsection, we will describe methods based on the Feynman path integral formalism. For the hybrid quantum/classical grid-based approach, the nuclear quantum effects of the transferring hydrogen are incorporated by representing this nucleus as a three-dimensional vibrational wavefunction. The adiabatic vibrational wavefunctions for the transferring hydrogen nucleus are calculated for fixed classical nuclear coordinates at each time step of the molecular dynamics trajectory by solving a three-dimensional time-independent Schrödinger equation for the hydrogen nucleus moving in the potential created by the classical nuclei. Typically this calculation is performed with a Fourier grid Hamiltonian method.[129–131] To ensure proper feedback between the classical and quantum subsystems, the classical nuclei are propagated according to forces averaged over the occupied proton vibrational wavefunction.

3.1.3 Transition state theory rate constant—In this hybrid approach,[13–15] the free energy profile is generated along a collective solvent coordinate defined to be the difference in energies of the two EVB states averaged over the occupied proton vibrational state. Typically the free energy barrier is significantly greater than the thermal energy, and biasing potentials must be used to generate the entire free energy profile. In this procedure,

independent equilibrium molecular dynamics trajectories are propagated with different mapping potentials to generate portions of the free energy curve along the entire collective reaction coordinate. Each mapping potential is chosen to be a linear combination of the two EVB state energies with a mapping parameter that is varied from zero to unity, thereby evolving the system from reactant to product. All of these portions of the free energy curve are unbiased and combined using a statistical method, such as the weighted histogram analysis method (WHAM),[132–133] to generate the entire free energy profile associated with the true potential energy surface. These free energy profiles are generated with the hybrid quantum/classical approach, in which the transferring hydrogen nucleus is treated quantum mechanically, remaining in its proton vibrational ground state. Thus, the resulting free energy profiles include the nuclear quantum effects associated with the transferring hydrogen in its vibrational ground state.

For a general reaction coordinate ξ with dividing surface defined as $\xi=\xi^{\ddagger}$, various expressions for the transition state theory rate constant have been derived.[134–138] For example, the transition state theory rate constant has been derived to be:[138]

$$k^{\mathrm{TST}}=\left\{\left(\frac{Z_{\xi}k_{\mathrm{B}}T}{2\pi}\right)^{\frac{1}{2}}\right\}_{\xi^{\ddagger}}^{\mathrm{cond}}\frac{e^{-W(\xi^{\ddagger})/k_{\mathrm{B}}T}}{\int_{-\infty}^{\xi^{\ddagger}}d\xi e^{-W(\xi)/k_{\mathrm{B}}T}}, \quad (24)$$

where $W(\xi)$ is the potential of mean force (PMF), $\{f(\mathbf{R})\}_{\xi^{\ddagger}}^{\mathrm{cond}}$ is the conditional configurational average defined in Ref. 138, and Z_{ξ} is the Jacobian factor defined as

$$Z_{\xi}\equiv\sum_{i=1}^{3N}\frac{1}{M_i}\left(\frac{\partial\xi}{\partial R_i}\right)^2 \quad (25)$$

for N atoms with components of spatial coordinates R_i and masses M_i. Often the simpler approximate form of this rate constant expression is used:

$$k^{\mathrm{TST}}=\frac{k_{\mathrm{B}}T}{h}\exp\left(-\frac{\Delta G^{\ddagger}}{k_{\mathrm{B}}T}\right), \quad (26)$$

where $\Delta G^{\ddagger}$ is chosen to be the free energy barrier associated with the PMF along the collective reaction coordinate.[139–141]

3.1.4 Transmission coefficient—In standard classical molecular dynamics simulations, the transmission coefficient κ may be calculated using reactive flux methods for infrequent events.[68,142–144] In this approach, an equilibrium ensemble of trajectories is started at the dividing surface and integrated backward and forward in time. The transmission coefficient is determined from the flux-weighted average of a quantity that accounts for multiple crossings of the dividing surface within this ensemble of trajectories. If all trajectories start in reactants and end in products, passing through the dividing surface only once, the transmission coefficient κ is unity. As the number of recrossings of the dividing surface increases within this ensemble of trajectories, the transmission coefficient will decrease to a value greater than zero and less than unity.

In the hybrid quantum/classical molecular dynamics approach, the dynamical trajectories for the reactive flux calculations are propagated with the molecular dynamics with quantum transitions (MDQT) surface hopping method.[145–146] In the implementation of MDQT for proton or hydride transfer, the classical nuclei evolve according to Newton's equations of

motion, and the adiabatic proton vibrational states are calculated at each time step. An ensemble of trajectories is propagated, and each trajectory moves classically on a single adiabatic proton vibrational surface except for instantaneous transitions among the adiabatic vibrational states. These transitions are incorporated according to a probabilistic algorithm based on the quantum amplitudes obtained by integrating the time-dependent Schrödinger equation to propagate the time-dependent proton vibrational wavefunction, which is expanded in a basis of the adiabatic proton vibrational states. This probabilistic algorithm, often denoted the "fewest switches" algorithm, is designed to ensure that at each time *t*, the fraction of trajectories in state *n* is the quantum probability for this state, as determined by the quantum amplitudes, except for complications arising from forbidden transitions. The MDQT method has been shown to agree well with exact quantum results for one-dimensional model PT and PCET systems,[147–148] as well as for PT in a dissipative bath.[149]

The MDQT method has been extended in the framework of the reactive flux approach for the simulation of infrequent events in reactions evolving on multiple potential energy surfaces.[150] In this approach, trajectories are started at the dividing surface and propagated backward in time with a fictitious surface hopping algorithm that does not depend on the quantum amplitudes. Subsequently, the trajectory is propagated forward in time, retracing the exact same trajectory, integrating the quantum amplitudes and calculating the probabilities for nonadiabatic transitions for each time step using the true surface hopping algorithm. The trajectories are weighted in a manner that leads to the identical results as would have been obtained with the true surface hopping algorithm in the forward direction from reactants to products. Thus, the MDQT method can be used to calculate the transmission coefficient for proton and hydride transfer reactions in solution and enzymes.[13–15,26] The transmission coefficient calculated in this manner incorporates vibrationally nonadiabatic effects, as well as dynamical recrossings of the dividing surface.

The total rate constant is the product of the transmission coefficient and the transition state theory rate constant, as given in Eq. (3). This approach provides a description of hydrogen tunneling that is valid in the vibrationally adiabatic and nonadiabatic limits, as well as the intermediate regime. In terms of the physical assumptions, the total rate constant should be consistent with Eq. (3), where the transition state theory rate constant is given by Eq. (2), in the vibrationally adiabatic limit and with Eq. (4) in the vibrationally nonadiabatic limit for proton transfer reactions. Moreover, this approach includes the motion of the entire solvated enzyme during the calculation of both the transition state theory rate constant and the transmission coefficient. The main approximations underlying this approach are the separation of the transferring hydrogen from all other nuclear degrees of freedom and the neglect of zero point energy contributions from other modes in the system. Additional nuclear degrees of freedom, such as the proton donor-acceptor mode, can also be treated quantum mechanically,[151] but the expense of the grid-based vibrational wavefunction calculation prevents the quantum mechanical treatment of a large number of modes.

3.2 Path integral methods

An alternative approach for including nuclear quantum effects is the use of Feynman path integrals, where the quantum nuclei are represented by rings of beads.[16,152–156] The path integral quantum transition state theory (QTST) formulates the quantum reaction rate constants in terms of a quantum activation free energy factor and a dynamical prefactor.[154–158] An advantage of path integral methods is that multiple nuclei can be treated quantum mechanically in a computationally efficient manner. Because these methods are formally complex and have been reviewed extensively in the literature,[21,159] the reader will be referred to the original papers and these reviews for the details of the methodology.

Equilibrium path integral approaches can be used to include nuclear quantum effects in the calculation of the activation free energy barrier. A particularly powerful approach is the quantized classical path (QCP) method,[160] which applies a quantum path integral correction to the classical PMF. In typical implementations of QCP to proton and hydride transfer in enzymes, the classical PMF is generated along a collective reaction coordinate using an EVB potential or an alternative quantum mechanical/molecular mechanical (QM/MM) potential in conjunction with the umbrella sampling techniques described in Section 3.1. The nuclear quantum contribution is determined for each configuration sampled during the classical molecular dynamics trajectories by performing free-particle path integral calculations while constraining the centroid of the beads to be the position of the corresponding classical particle. This method is efficient because the path integral sampling of the quantum nuclei is performed separately from the classical molecular dynamics simulation of the entire system. Moreover, this efficiency can be improved by combining the QCP approach with the bisection path integral sampling method.[161–162] A related method that does not utilize the centroid constraint has also been developed.[163]

The QCP approach provided the foundation for the development of an integrated path integral and free energy perturbation-umbrella sampling method for computing KIEs for proton and hydride transfer reactions in solution and enzymes.[164] The key aspect of this method is that only a single simulation of a given isotopic reaction (i.e., hydrogen transfer) is performed, and the KIEs are obtained by perturbing the mass from one isotope to another (i.e., from hydrogen to deuterium) using free energy perturbation techniques. This type of mass perturbation in conjunction with the free-particle bisection path integral sampling scheme leads to significant improvements in accuracy for KIE calculations and therefore allows the calculation of secondary as well as primary KIEs. Note that these QCP-type approaches provide corrections to the activation free energy barrier but do not enable the incorporation of nuclear quantum effects in the calculation of dynamical quantities, such as the dynamical prefactor in the QTST rate constant expression.

A variety of approximate methods have been developed for utilizing the Feynman path integral formalism to calculate real-time correlation functions in condensed phase systems. These types of methods are well-suited for the study of dynamical aspects of hydrogen tunneling reactions in solution and enzymes. For example, the centroid molecular dynamics method[19–20,165] has been used to study proton tunneling in solution and enzymes.[166] The ring polymer molecular dynamics (RPMD) method[21] has also been used for this purpose.[167–168] A known limitation of such methods is the lack of real-time coherence, which prevents the description of quantum coherences that persist beyond the thermal time. As a result of this limitation, the standard RPMD method is unable to even qualitatively reproduce the inverted region behavior of Marcus theory for electron transfer.[169] This limitation may prevent RPMD from being generally applicable to nonadiabatic EPT reactions, although it may still be very useful for adiabatic proton and hydride transfer reactions, and extensions may be developed to circumvent this problem.

3.3 Ensemble-averaged variational transition state theory with multidimensional tunneling

Another powerful approach for studying proton and hydride transfer reactions in solution and enzymes is the ensemble-averaged variational transition state theory with multidimensional tunneling (EA-VTST/MT) approach.[22,24,170–172] The details of this approach are described elsewhere,[22,173] and only the basic steps are summarized herein. In this approach, the rate constant is expressed as

$$k=\Gamma(T)\kappa(T)k^{(1)}(T), \quad (27)$$

where $k^{(1)}(T)$ is denoted the stage-1 quasiclassical rate constant, similar to the TST rate constant described in Section 3.1, $\Gamma(T)$ accounts for dynamical recrossings, and $\kappa(T)$ accounts for contributions from the nonclassical transmission through the barrier, typically dominated by tunneling. This notation differs from that in Section 3.1 but is consistent with the majority of papers on EA-VTST/MT. In the EA-VTST/MT approach, the system is divided into a primary and secondary zone, and the overall procedure involves three stages that are briefly described below.

Stage 1 consists of two steps. In the first step, the classical mechanical PMF is obtained from umbrella sampling molecular dynamics along a reaction coordinate, which could be a geometry-based reaction coordinate or a collective reaction coordinate such as the energy gap reaction coordinate described in Section 3.1. Note that the derivations of the analytical rate constant expressions for proton and hydride transfer given in Section 2.1 are based on the energy gap reaction coordinate, but applications of the EA-VTST/MT approach have illustrated that similar results can be obtained with a geometry-based reaction coordinate and an energy gap reaction coordinate.[174] The difference between the classical PMF at its maximum and at the reactants is denoted the PMF of activation. The classical free energy of activation is obtained by combining the PMF of activation with the classical free energy associated with the reaction coordinate. In the second step of stage 1, the quantization effects on the vibrational free energies for atoms in the primary zone are included in the free energy of activation using a quasiclassical method based on quantum mechanical harmonic vibrational partition functions. The stage-1 quasiclassical rate constant, $k^{(1)}(T)$, is given by Eq. (26) using the quasiclassical free energy of activation obtained in this stage.

In stage 2, the prefactors are calculated together through an ensemble averaging procedure, where the overall prefactor is expressed as

$$\gamma=\frac{1}{N}\sum_{i=1}^{N}\Gamma_i\kappa_i. \quad (28)$$

In this expression, N is the number of members in the ensemble sampled from the variational transition states obtained from stage 1, and Γ_i and κ_i are the recrossing and tunneling corrections for ensemble member i. Various approximate methods have been developed to calculate the prefactors accounting for recrossings and tunneling. For example, the values of κ_i can be calculated by optimizing the tunneling paths between small-curvature tunneling (SCT) paths or large-curvature tunneling (LCT) paths. In stage 2, typically the secondary zone is fixed during the calculation of each Γ_i and κ_i, and only the fluctuations of the primary zone are included directly in the reaction path dynamics. However, fluctuations of the secondary zone are incorporated via the ensemble average performed in Eq. (28). In stage 3, the free energy change due to motion of the secondary zone can be included, although often this stage is not necessary.

An advantage of the EA-VTST/MT approach is that quantized vibrations, including zero point energy, and thermally activated multidimensional tunneling are incorporated for the primary zone. The equilibrium fluctuations of the secondary zone are included through the ensemble averaging procedure. Although there is no direct correspondence between this approach and the definitions of vibrationally adiabatic and nonadiabatic given in Section 2, the range of methods available for calculating the multidimensional tunneling contributions in the EA-VTST/MT approach most likely spans the vibrationally adiabatic and nonadiabatic limits, as well as the intermediate regime.[22] For proton transfer reactions, the total rate constant is related to Eq. (3), where the transition state theory rate constant is given by Eq. (2), in the vibrationally adiabatic limit and to Eq. (4) in the vibrationally nonadiabatic

limit, although additional degrees of freedom are quantized, typically a geometry-based reaction coordinate is used, and the tunneling contributions are calculated using different approximations. Furthermore, this approach assumes that the reaction is electronically adiabatic and therefore is not directly applicable to reactions in the electronically nonadiabatic regime, such as typical EPT reactions.

3.4 Calculating rate constants and simulating dynamics of nonadiabatic EPT reactions

The rate constants for EPT reactions can be calculated with the expressions in Eqs. (17), (19), (20), and (22).[11] These rate constant expressions depend on the reaction free energies $\Delta G^0_{\mu\nu}$, the solvent reorganization energy λ_s, the electronic coupling V^{el}, the overlaps $S_{\mu\nu}$ between the reactant and product proton vibrational wavefunctions, and the Boltzmann probabilities P_μ for the reactant states. In practice, the proton potential energy curves for the reactant and product states can be used to calculate the proton vibrational wavefunctions and energy levels, thereby providing the proton vibrational wavefunction overlaps $S_{\mu\nu}$, the vibrational energy level contributions to $\Delta G^0_{\mu\nu}$, and the Boltzmann probabilities P_μ for the reactant states. When the proton donor-acceptor motion is included, the exponential factor α representing the distance dependence of the vibronic coupling, the equilibrium proton donor-acceptor distance R, and the effective mass and frequency, M and Ω, of the proton donor acceptor mode (or, alternatively, the force constant $M\Omega^2$) are also required. Note that the rate constant expression given in Eq. (19) includes the quantity $\lambda^{(\alpha)}_{\mu\nu}$, which is defined in Eq. (8) and depends on the effective mass M but not on the effective frequency Ω. Thus, this rate constant depends on both the effective mass and the effective frequency. In contrast, the rate constants given in Eqs. (20) and (22), as well as the KIE given in Eq. (21), depend on the force constant $M\Omega^2$ rather than the individual effective mass and frequency. In this case, the rate constant and KIE are independent of the choice of effective mass.

All of these parameters can be determined using a variety of experimental and theoretical methods. The reaction free energy or driving force for the ground states, ΔG^0_{00}, can be estimated from experimentally measured reduction potentials and pK_a values[175] or, in the absence of such data, from electronic structure calculations.[43,176] The solvent reorganization energy, λ_s, can be estimated from experimental measurements of the EPT reaction or associated ET reaction, as the reorganization energies are often similar for these related processes.[177] Alternatively, the solvent reorganization energy can be calculated using theoretical methods, specifically dielectric continuum models[77,178–179] or molecular dynamics simulations,[44] analogous to the methods used for ET. The electronic coupling can be calculated with the same electronic structure methods used to calculate this parameter in ET theory.[180–182] The reactant and product proton potential energy curves can be obtained from electronic structure methods for the diabatic electronic states, and the associated proton vibrational wavefunctions can be calculated numerically with Fourier grid methods.[129–130] The exponential factor α in the vibronic coupling can be determined from the dependence of the overlap $S_{\mu\nu}$ on the proton donor-acceptor distance. The equilibrium proton donor-acceptor distance and associated frequency can also be obtained from electronic structure calculations or, alternatively, from molecular dynamics simulations.[44]

The dynamical effects of EPT reactions can also be investigated computationally. The EPT rate constant expressions given in Eqs. (19) and (20) were derived from a dynamical rate constant expression involving the time integral of the probability flux correlation function, which depends on the time correlation functions of the energy gap and the proton donor-acceptor mode, as well as the parameters in the vibronic coupling.[11,90] The time correlation functions can be calculated from classical molecular dynamics simulations on the reactant vibronic surface.[44,93,183] This procedure includes equilibrium dynamical effects of the

proton donor-acceptor mode and the solvent. In many cases, however, the approximations used to derive the rate constant expressions given in Eqs. (17), (19), (20), and (22) are valid, and the calculation of time correlation functions is not necessary. In other words, the dynamical effects are often negligible for EPT reactions.[44,93,183]

In some cases, nonequilibrium dynamical effects are significant and even dictate the mechanisms and rates of EPT reactions. For example, photoinduced EPT reactions are initially in a nonequilibrium configuration due to the virtually instantaneous optical excitation, and the nonequilibrium dynamics of the solvent and solute during the relaxation process play a central role.[184] These types of processes can be simulated using the MDQT surface hopping algorithm[145–146] and other methods described in Section 3.1. For EPT processes, however, the classical nuclei evolve on electron-proton vibronic surfaces rather than purely electronic or vibrational surfaces. The electron-proton vibronic surfaces can be generated from a four-state EVB model, as given in Eq. (12), combined with proton vibrational states calculated for each diabatic electronic state using a grid-based method. The solvent can be treated either as explicit solvent molecules or as a dielectric continuum, in which case the solvent is represented by two collective solvent coordinates.[185–188] The RPMD method has also been used to investigate the dynamics of model thermal EPT reactions in solution.[189]

4. Applications to enzymes

The contribution of hydrogen tunneling to enzyme-catalyzed reactions has been examined by many groups across a wide array of enzymes. From the experimental perspective, studies of hydrogen tunneling have focused on the magnitude and temperature dependence of the KIEs.[99,190–196] On the theoretical side, the computational techniques discussed in Section 3 have been used to study a wide range of enzymatic reactions.[22] Enzymatic systems for which hydrogen tunneling has been implicated include, among others, morphinone reductase,[197–198] aromatic amine hydrogenase,[199] dihydrofolate reductase,[26,167,192–195,200–201] copper amine oxidase,[202–203] and xylose isomerase.[170,204] The reader is referred to these papers for in-depth discussions of each specific enzymatic system.

In this section, we consider the role of hydrogen tunneling for two different enzymes, liver alcohol dehydrogenase (LADH) and soybean lipoxygenase (SLO). LADH catalyzes proton and hydride transfer reactions that are predominantly adiabatic, while SLO catalyzes an EPT reaction that has been shown to be vibronically nonadiabatic. Thus, these two enzymes provide case studies in two fundamentally different regimes. Both systems have been studied extensively with experimental and theoretical methods by multiple research groups. Moreover, a comparison between these two systems highlights the multiple types of hydrogen tunneling that can occur in enzymatic reactions.

4.1 Liver alcohol dehydrogenase (LADH)

Liver alcohol dehydrogenase (LADH) catalyzes the reversible oxidation of alcohols to the corresponding aldehydes or ketones. As depicted in Figure 8, the mechanism is thought to proceed through an initial deprotonation of the alcohol substrate via a proton relay, followed by hydride transfer from the C1 of the zinc-bound alkoxide to C4 of the nicotinamide adenine dinucleotide (NAD^+) cofactor. Although product release is often rate limiting, the chemical step of hydride transfer can be “unmasked” from the chemical complexity of the overall catalytic cycle by mutagenesis of hydrophobic residues near the substrate binding site, such as residues 57 and 93, to increase the rate of product release. The primary KIEs were measured experimentally to be $k_H/k_D = 3.78 \pm 0.07$ and $k_D/k_T = 1.89 \pm 0.01$ for the benzyl alcohol substrate in wild-type (WT) LADH. The secondary KIEs at the C1 position

were also measured for WT LADH and several mutants, and the corresponding Swain-Schaad exponent, defined as $\ln(k_H/k_T)/\ln(k_D/k_T)$, was measured to be 8.5 and 6.1 for the unmasked enzymes Leu57Phe and Phe93Trp, respectively.[205] As discussed in the Introduction, typically a Swain-Schaad exponent greater than 3.3 is considered to be a manifestation of tunneling, and these relatively large values were interpreted to be indicative of significant hydrogen tunneling in the hydride transfer reaction catalyzed by LADH. In addition, decreasing the size of residue 203 from Val to a smaller residue, such as Ala, was found to decrease both the catalytic efficiency and the degree of tunneling as measured by the Swain-Schaad exponent.[5] However, as pointed out by Warshel,[32] it is difficult to distinguish the impact on hydride transfer from other steps in the catalytic cycle.

This wealth of experimental data inspired many theoretical studies on the LADH-catalyzed reaction.[23–25,27–36] All of these studies have assumed that the reaction is electronically adiabatic, as is reasonable for this type of hydride transfer reaction. In this system, the catalytic zinc ion coordinates to the enzyme-bound substrate and is thought to facilitate the initial proton transfer reaction by stabilizing the resulting alkoxide ion. In terms of the hydride transfer step, however, the catalytic zinc ion does not appear to play an active role. Instead, the hydride transfer reaction involves mainly electronic redistribution within the substrate to form an aldehyde or ketone and within the NAD^+ cofactor to form NADH. These types of relatively localized bond rearrangements are expected to be electronically adiabatic, similar to the benzyl/toluene self-exchange reaction discussed in Section 2.2.2.

Investigations using the hybrid quantum/classical molecular dynamics method, the EA-VTST/MT approach, and the EVB/QCP method described in Section 3 confirmed the significance of hydrogen tunneling in the LADH-catalyzed hydride transfer reaction.[13–14,23–24,28,206] These calculations utilized unsubstituted benzyl alcohol as the substrate and focused on the hydride transfer step. The calculations with the hybrid quantum/classical molecular dynamics method used an EVB potential energy surface and represented the transferring hydrogen nucleus as a three-dimensional vibrational wavefunction obtained with grid-based methods.[13–14] These calculations illustrated that nuclear quantum effects decrease the free energy barrier by ~1.8 kcal mol^{-1} and that the transmission coefficient, which accounts for dynamical barrier recrossings, is nearly unity.[13–14] Moreover, the calculated primary deuterium and tritium KIEs were in qualitative agreement with experimental data. A similar reduction in the free energy barrier was observed in the EA-VTST/MT and EVB/QCP calculations.[23–24] The EA-VTST/MT calculations used a semiempirical method for the QM part of the QM/MM potential, as well as some additional VB terms, to generate the potential energy surface.[23–24] These calculations indicated that quantum mechanical tunneling accounts for ~60% of the reactive flux and provided primary and secondary KIEs, as well as the corresponding Swain-Schaad exponents, that were in qualitative agreement with the experimental data.[23–24] Subsequent calculations using a potential energy surface obtained by the self-consistent-charge–density-functional-tight-binding method (SCC-DFTB) together with canonical variational TST with small-curvature semiclassical tunneling (CVT-SCT) provided similar results and also concluded that hydride tunneling was important for determining the calculated KIEs and Swain-Schaad exponents.[28] The EVB/QCP calculations illustrated that the reduction in the free energy barrier due to nuclear quantum effects is similar in the protein and in aqueous solution and therefore does not represent a catalytic effect of the enzyme.[25]

Various theoretical studies have addressed the issues of protein motion and the role of residue Val203 in LADH. Our group analyzed key geometrical parameters during the equilibrium and nonequilibrium hybrid quantum/classical molecular dynamics simulations.[13–15] As indicated by the transmission coefficient value of nearly unity, dynamical recrossings are relatively insignificant for this system. Thus, the thermally

averaged changes in distances and angles along the collective reaction coordinate, as determined from the equilibrium simulations, are more important than the nonequilibrium motions influencing the barrier recrossings. The calculations indicated that the thermally averaged hydride donor-acceptor distance decreases to ~2.7 Å as the reaction evolves from the reactant to the transition state, which was defined to correspond to zero collective solvent coordinate (i.e., energy gap reaction coordinate). In addition, the thermally averaged distance between Val203 and the acceptor carbon was found to increase as the reaction evolves from the reactant to the transition state, suggesting that the relative motion of Val203 and the acceptor carbon contributes to the collective reaction coordinate and thus impacts the free energy barrier. These results suggest that the mutation of Val203 to a smaller residue may alter the equilibrium conformational sampling in a manner that changes the free energy barrier and therefore the hydride transfer rate. As discussed previously,[207–210] the free energy barrier is a measure of the relative probabilities of sampling transition state and reactant state configurations, and altering the equilibrium conformational sampling through mutation can influence the free energy barrier. Note that these simulations provide no evidence of a *dynamical* effect of Val203 or any other protein motions in the sense that the transmission coefficient is nearly unity, and there is no evidence of the direct dynamical coupling of any protein modes to the chemical reaction.

In addition, classical molecular dynamics simulations of the reactive complex, in conjunction with a cross-correlation analysis, were used to identify correlated and anticorrelated motions that involve the entire protein.[35–36] This analysis identified a pushing motion of Val203 that moves the C4 of NAD^+ toward the substrate to form near-attack conformers (NACs), which are reactive conformations shown to be associated with the transition states of lowest energy.[36] These pushing motions occur on a much faster timescale than the turnover rate of the enzyme, but they could potentially influence the equilibrium sampling of conformations favorable for hydride transfer.

Another theoretical study focused on the role of so-called protein-promoting vibrations in LADH.[27] A spectral analysis of classical molecular dynamics simulations was interpreted to suggest that the substrate-NAD^+ motion is a rate-promoting vibration that is symmetrically coupled to the reaction coordinate. Moreover, the substrate-NAD^+ and NAD^+-Val203 motions were found to be in resonance, leading the authors to conclude that the promoting vibration is induced by the motion of Val203. The authors conclude the following: “The action of the enzyme in speeding the chemical reaction, however, is postulated to be intimately connected to the directed vibrational motion identified in this paper. Thus, it appears that evolution has designed the protein matrix of an enzyme not just to hold substrates or stabilize transition state formation, but rather to channel energy in a specific chemically relevant direction.” The relevance of protein-promoting vibrations is not well-accepted in the community. As mentioned above, the other simulations of the LADH reaction did not identify such protein-promoting modes that are dynamically coupled to the chemical reaction. Instead, these other simulations illustrated the impact of equilibrium conformational sampling on the free energy barrier.[207,209–210] Moreover, other studies illustrated that the same type of coupling of different modes to the reaction coordinate are noncoherent and thus statistical and also exist in the solution reaction as well as the protein reaction.[32] Perhaps the most convincing argument is that these promoting vibrations occur on the femtosecond timescale, whereas most enzyme reactions, including LADH, occur on the millisecond or slower timescale. Thus, these promoting vibrations could be slowed down by many orders of magnitude and still would not impact the rate constant, which is typically determined by the free energy barrier rather than any type of fast dynamics at the top of the barrier. Given these relative timescales, it is difficult to understand how there could be evolutionary pressure to create these types of femtosecond protein-promoting vibrations.

Overall, the current evidence that dynamical effects and, in particular, protein-promoting vibrations contribute significantly to enzyme catalysis is not convincing.

4.2 Soybean lipoxygenase (SLO)

Soybean lipoxygenase (SLO) catalyzes the oxidation of unsaturated fatty acids. As depicted in Figure 9, SLO catalyzes the net hydrogen atom transfer from the linoleic acid substrate to the iron cofactor. Kinetic studies have shown that this hydrogen abstraction step is rate-limiting above 32 °C.[211] This reaction is thought to occur through an EPT mechanism involving the concerted transfer of an electron from the π-system of the substrate to the iron of the cofactor and a proton from the C11 carbon of the substrate to the hydroxyl ligand of the cofactor.[37] This EPT mechanism was deduced on the basis of an orbital analysis of density functional theory calculations[212] and a thermodynamic analysis indicating that the single PT and ET reactions are highly endothermic, whereas the concerted reaction is slightly exothermic.[43] According to experimental studies, the deuterium KIE of this reaction is unusually high, with a value of ~80 at room temperature, and the temperature dependence of the rate constant and KIE is relatively weak.[37,213]

In addition, relatively distal mutations were found to significantly impact the magnitude and temperature dependence of the KIE. A particularly interesting mutation site is isoleucine 553 (Ile553), which borders the bound linoleic acid substrate but is ~15 Å from the active site iron. The experimental data show negligible structural changes due to these mutations but indicate that the magnitude and temperature dependence of the KIE increase as residue 553 becomes less bulky (i.e., along the series comprised of leucine, valine, alanine, and glycine).[213–214] These intriguing mutation data, as well as the unusually large KIE and weak temperature dependence of WT SLO, have attracted a wide range of theoretical studies.[38–41,212,215–218]

In an effort to dispel the belief that the TST framework is insufficient for describing this type of behavior, Truhlar showed that a very simple conventional model is capable of describing a large KIE with weak temperature dependence.[219] Within a TST framework, he calculated a quasiclassical KIE due to a small change in zero point energy and a contribution to the KIE from a one-dimensional parabolic tunneling transmission coefficient. Using physically reasonable parameters, he was able to design a simple conventional model that is qualitatively consistent with the experimental data for WT SLO. This exercise illustrates that a simple electronically adiabatic model is capable of describing the experimental data at a qualitative level, although it provides limited mechanistic insight and, as will be discussed below, there is evidence that the reaction is likely electronically nonadiabatic according to the definition of electron-proton nonadiabaticity given in Section 2.2.2.

Warshel and coworkers also assumed that this reaction is electronically adiabatic and used an EVB potential to describe the ground state potential energy surface of the entire solvated enzyme. In their initial studies,[40,42] the QCP approach based on path integrals was used to incorporate the nuclear quantum effects of the transferring hydrogen or deuterium. These calculations reproduced the magnitude but not the temperature dependence of the experimentally measured KIE. Subsequently, they used a grid-based method for propagation of one-dimensional hydrogen vibrational wavefunctions,[218] but the authors state that the QCP approach is more suitable for these types of simulations. An important conclusion of the EVB/QCP calculations is that nuclear quantum effects are similar in the enzyme and in reference solution reactions, and therefore these effects do not contribute to the catalytic property of the enzyme relative to aqueous solution.[40,42]

The EA-VTST/MT approach has also been applied to the SLO reaction using a QM/MM potential with a semiempirical QM region.[41] This approach also assumes an electronically

adiabatic reaction and severely underestimates the experimentally observed KIE. As a result, the authors introduced an empirical shift of ~10 kcal mol^{-1} to the potential energy barrier. After introducing this correction, they were able to reproduce the experimentally observed KIE, but they did not attempt to investigate the temperature dependence of the KIE. A conclusion of this work is that the KIE depends strongly on the width of the proton transfer barrier, which is certainly valid for any hydrogen tunneling reaction. Analogous simulations of the Ile553Ala mutant suggested that the proton donor-acceptor distance becomes larger and more flexible in the mutant.[41] This observation was interpreted to arise from a decompressed active site for the Ile553Ala mutant, in comparison to a compressed active site for WT SLO. These results were qualitatively consistent with prior modeling studies,[213] as will be discussed below.

In contrast to the studies discussed so far in this subsection, several analyses of the SLO reaction have assumed that the reaction is electronically nonadiabatic. Given that the electron transfers from the π-backbone of the linoleic acid substrate to the iron of the cofactor and is spatially separated from the proton transfer, this reaction is likely to be electronically nonadiabatic according to the definition given in Section 2.2.2. An analysis of the orbitals and spin density for a model system of the SLO active site indicates that the electron transfers directly from an orbital localized on the substrate to an orbital localized on the iron without ever becoming localized on the proton, which transfers from the carbon to the oxygen.[212] According to this analysis, the SLO reaction is qualitatively similar to the self-exchange reaction of the phenoxyl/phenol system, where the electron transfers between orbitals that are approximately perpendicular to and well-separated from the orbitals involved in the proton transfer reaction.[80,82] As discussed above, the phenoxyl/phenol self-exchange reaction has been shown to be electronically nonadiabatic through a semiclassical analysis that provides estimates of the electronic transition and proton tunneling timescales and the calculation of the nonadiabatic coupling along the proton coordinate.[82–83] Moreover, as will be discussed in the remainder of the subsection, these electronically nonadiabatic models can successfully reproduce the experimental KIE and temperature dependence utilizing physically reasonable parameters. Thus, the assumption of electronic nonadiabaticity is consistent with the experimental data, although apparently some electronically adiabatic models can also lead to qualitatively consistent results.

Klinman and coworkers used the thermally averaged nonadiabatic rate constant expression in Eq. (22) to analyze the kinetic data for WT SLO, as well as several mutants of SLO.[98,213–214] They were able to reproduce the experimentally observed large KIE and its weak temperature dependence. According to their modeling analysis,[213] the nearly temperature-independent KIE for WT SLO arises from a compressed hydrogen transfer distance with little modulation (i.e., a stiff gating frequency), whereas the greater temperature dependence for the Ile553Ala mutant arises from a more relaxed active site with extensive gating to facilitate hydrogen transfer. A further analysis of the entire series of Ile553 mutants[214] confirmed the importance of distance sampling in the context of the proton donor-acceptor motion. In these analyses, the parameters were fit to the experimental data without any atomic level calculations.

Our group has also studied the reaction catalyzed by SLO and the series of Ile553 mutants using several different nonadiabatic approaches.[43–44,220] Our initial study was based on a thermally averaged rate constant related to Eq. (22) except that all parameters, rather than only the overlap factor, depended on the proton donor-acceptor distance.[43] The solvent reorganization energy was calculated with a dielectric continuum model, and the inner-sphere reorganization energy was determined from the Fe-ligand bond length changes and associated force constants. The EPT reaction was described by a four-state EVB model, which provided the proton potentials for the reactant and product diabatic states, including

anharmonic effects. Both classical and quantum mechanical treatments of the proton donor-acceptor motion were explored and gave similar results. As depicted in Figure 10 (dashed blue lines), these calculations reproduced the temperature dependence of the rate constants and KIE for WT SLO.

This analysis provided an explanation for the weak temperature dependence of the rate constant and the unusually high KIE.[43] The weak temperature dependence of the rate constant is due to a relatively small free energy barrier, which results from a balance between the total reorganization energy and the reaction free energy. The unusually high KIE of ~80 is due to the small overlap of the reactant and product proton vibrational wavefunctions, which results from the weak hydrogen-bonding interaction at the C-H---O interface and the dominance of the lowest energy reactant and product vibronic states. According to the concerted PCET theory discussed in Subection 2.2.3,[11] the KIE for a given pair of reactant/product states is approximately proportional to the square of the ratio of the hydrogen and deuterium vibrational wavefunction overlaps, and this ratio increases as the overlap decreases. Thus, when all other parameters remain fixed, the KIE is predicted to increase as this overlap decreases and hence to be larger for relatively weak hydrogen-bonding interfaces. Moreover, this overlap decreases as the proton donor-acceptor distance, which is the C–O distance for this system, increases. As depicted schematically in Figure 7, this initial study illustrated that the dominant proton donor-acceptor distance is significantly smaller than the equilibrium distance and is determined by a balance between the larger coupling and the smaller Boltzmann probability as the distance decreases. In other words, the smaller proton donor-acceptor distances are energetically unfavorable, but these distances are sampled through thermal fluctuations and contribute significantly to the overall rate constant due to the much larger vibronic coupling. Nevertheless, the relatively weak hydrogen-bonding interaction at the C-H---O interface prevents optimal overlap and therefore leads to an unusually high KIE.

Our second study of SLO examined the dynamical behavior of the entire solvated enzyme by utilizing the probability flux correlation function formalism.[44] In this approach, the rate constant is represented by the time integral of a probability flux correlation function that depends on the vibronic couplings and on time correlation functions of the energy gap and the proton donor-acceptor mode. The vibronic couplings were obtained from hydrogen vibrational wavefunctions for model systems, and the time correlation functions were calculated from all-atom classical molecular dynamics simulations of the entire solvated enzyme. As depicted in Figure 10 (solid blue line), these calculations reproduced the experimentally observed magnitude and temperature dependence of the KIE for SLO without fitting any parameters directly to the experimental kinetic data. Our analysis indicated that only the equilibrium motions of the energy gap and the proton donor-acceptor mode influenced the rate constant, and we verified that the approximations leading to the analytical rate constant given in Eq. (20) are valid for this system.

Furthermore, we found that the temperature dependence of the KIE is determined predominantly by the proton donor-acceptor frequency Ω and the distance dependence of the vibronic couplings (i.e., α in Eq. (20)) for hydrogen and deuterium. Considering only the nonadiabatic transition between the two ground vibronic states, the KIE can be approximated by the expression in Eq. (21). As discussed above, the ratio of hydrogen and deuterium overlaps increases as the overlap decreases (i.e., as the equilibrium proton donor-acceptor distance increases). According to this analysis, the weak temperature dependence of the KIE for this system is due in part to the dominance of the local component of the proton donor-acceptor motion (i.e., the C–O mode). In other words, the frequency Ω is low enough to allow the high-temperature treatment of this mode, as used in the derivation of Eq. (20), but high enough to result in weak temperature dependence.

Our third study of SLO focused on the Ile553 mutant series.[220] All-atom classical molecular dynamics simulations illustrated that mutation of Ile553 to less bulky residues influenced the mobility, geometrical conformation, and orientation of the linoleic acid within the active site. These effects altered the proton donor-acceptor equilibrium distance and frequency, thereby changing the magnitude and temperature dependence of the KIE. According to this analysis, as the Ile553 residue becomes less bulky, the equilibrium proton donor-acceptor distance increases and the associated frequency decreases, leading to an increase in the magnitude and temperature dependence of the KIE. These trends can be understood in the context of the approximate KIE given in Eq. (21), where a longer proton donor-acceptor distance leads to a larger ratio of overlaps, and a smaller frequency Ω leads to a greater temperature dependence from the exponential factor. These trends are qualitatively similar to those observed in Refs. [98,214], although the values for the equilibrium distances and frequencies differ.

As illustrated by these various studies, the SLO reaction can be described by several different theories that are based on fundamentally different assumptions and approximations. In these situations, an effective way to determine which theoretical description is correct is to make experimentally testable predictions. This type of feedback between theory and experiment will be essential for further refining theories of hydrogen tunneling in enzymes and for determining which theory is suitable for each individual system. Given the complexity of enzymatic reactions, however, as well as the complications that arise in the analysis of the temperature dependence of KIEs, definitive answers may not be available in the near future.

5. Applications to biomimetic systems

The tremendous kinetic efficiency achieved by enzymatic systems has led researchers to use the active sites of proteins as inspiration for the design of molecular catalysts. Biomimetic systems have been used to directly catalyze chemical reactions by designing molecules to mimic the active sites of enzymes such as hydrogenases, or by using macrocyclic and polymeric systems to sequester reacting species in hydrophobic cavities that are reminiscent of the active sites found in enzymatic systems.[221] The wealth of organic synthetic reactions that have been effectively catalyzed by biomimetic systems includes Diels-Alder cycloadditions,[222–224] transamination reactions to form amino acids,[225–226] and the acylation and phosphorylation of molecular alcohols.[227–229] While detailed mechanistic details have been elucidated for a number of these systems, the role of hydrogen tunneling has not been extensively studied in these particular systems.

In this section, we discuss two types of biomimetic systems for which hydrogen tunneling has been shown to play an important role. The first type is comprised of complexes with redox-active tyrosines designed to mimic biological systems such as photosystem II (PSII) and class 1 ribonucleotide reductases (RNR). The second type is comprised of hydrogen oxidation and production catalysts designed to mimic hydrogenase enzymes. In both types of systems, the catalyzed reaction proceeds via an EPT mechanism that is expected to be vibronically nonadiabatic for the reasons discussed in Section 2. In these types of biomimetic systems, the EPT reaction is induced either electrochemically or photochemically, thereby enabling an exquisite level of control over the reactive process and the experimental conditions. As a result, the combination of experimental and theoretical studies of biomimetic systems provides a level of detailed mechanistic information that is currently not attainable for enzymatic systems.

5.1 Redox-active tyrosines

PCET reactions involving redox-active tyrosines play an important role in a variety of biological processes. Typically these PCET reactions are concerted in that they occur in a single kinetic step, thereby avoiding the high-energy intermediates associated with initial ET or PT (i.e., the pK_a is 10 for neutral tyrosine and –2 for oxidized tyrosine).[230] Moreover, these PCET reactions are bidirectional, also denoted multi-site, in that the electron and proton are transferred in different directions to different sites. An important example is the oxidation of water to O_2 by PSII,[231–232] a process that requires the oxidation of a tyrosine to a neutral tyrosyl radical.[233–234] Specifically, the electron is transferred from tyrosine-Z to an oxidized chlorophyll P680, and the proton is transferred from tyrosine-Z to a hydrogen-bonded histidine residue.[235–237] Another example is RNR, an enzyme that catalyzes the conversion of nucleotides to 2′-deoxynucleotides and plays an important role in DNA replication and repair. The mechanism of class 1 RNRs is thought to involve a series of PCET reactions along a 35 Å pathway of redox-active aromatic residues, including several tyrosine residues.[238–239] The design of biomimetic systems that mimic these types of tyrosine oxidation reactions is important for elucidating the fundamental physical principles underlying bidirectional PCET reactions as well as developing catalysts for solar fuel generation by artificial photosynthesis.

To investigate these types of PCET reactions, a tyrosine-bound rhenium-polypyridyl complex, depicted in Figure 11, was synthesized and characterized both experimentally and theoretically.[240–242] In this system, photoexcitation leads to a metal-to-ligand charge-transfer (MLCT) excited state, followed by electron transfer from the tyrosine to the formally oxidized Re of the MLCT state and proton transfer from the tyrosine to the bulk solvent. At pH < 9, the rate constant was found to increase with pH, and a hydrogen/deuterium KIE of ~3.0 was observed for the relatively high pH values within this range, indicative of a concerted PCET mechanism (i.e., an EPT mechanism) for tyrosyl radical generation. In principle, the proton acceptor for this reaction could be either water or the phosphate buffer. The rate constant is independent of pH for 4 < pH < 8 in the absence of the phosphate buffer, however, and the dependence of the rate constant on phosphate buffer concentration is absent at low pH, where the dominant buffer species is $H_2PO_4^-$. These experimental data suggest that the proton transfers to HPO_4^{2-} but not to $H_2PO_4^-$ and that the pH dependence arises from the titration between these two forms of the phosphate buffer.[241] As pointed out in Ref. 241, however, at sufficiently low total buffer concentration and/or pH, water is expected to be the dominant proton acceptor because of its high concentration relative to HPO_4^{2-}.

Our group investigated the rhenium-tyrosine complex shown in Figure 11 with the concerted PCET theory discussed in Section 2.2.3 using the rate constant expression given in Eq. (17) for fixed proton donor-acceptor distances.[242] When phosphate buffer is the proton acceptor, the hydrogen-bonding interaction will be strong with a nearly linear geometry (∠O-H-O=178°), a short proton donor-acceptor distance ($R_{OO} \approx 2.5$ Å), and a relatively high proton donor-acceptor frequency (i.e., the O—O frequency at the hydrogen-bonding interface). For these types of stiff hydrogen-bonding interfaces, the expressions in Eqs. (19)–(22), which were derived for the low-frequency proton donor-acceptor regime, are inapplicable, and Eq. (17) is expected to provide more reliable results. Alternatively, expressions have been derived for the high-frequency proton donor-acceptor regime,[90] although the results are expected to be similar to those obtained with Eq. (17) in this case. The calculations were performed with either a phosphate buffer species, HPO_4^{2-}, as the proton acceptor or a water molecule as the proton acceptor. The calculations with the phosphate buffer acceptor reproduced the experimentally measured pH dependence of the overall rate constant and the KIE. The calculations with the water acceptor were not in agreement with the experimental

data for parameters varied within physically reasonable ranges. Note that the proton donor-acceptor motion may be relevant for the model in which water is the proton acceptor but was not considered in this early study.[242]

These theoretical results are consistent with the conclusion that the phosphate buffer species is most likely the proton acceptor for this system when the concentration of HPO_4^{2-} is sufficiently high. In this case, the pH dependence of the overall rate constant arises from the titration between the HPO_4^{2-} and $H_2PO_4^-$ forms of the phosphate buffer. Moreover, the calculations suggest that the phosphate buffer species is favored over water as the proton acceptor in part because the proton donor-acceptor distance is ~0.2 Å smaller for the phosphate acceptor due to its negative charge. Detailed analysis of the theoretical calculations provided further insight into the physical quantities impacting the overall rate constant, including the reorganization energies, reaction free energies, and vibronic couplings for the various pairs of reactant/product vibronic states.[242]

Hammarström and coworkers investigated PCET reactions in a series of tyrosine-bound ruthenium-tris-bipyridine complexes, as depicted in Figure 12.[48–52] Following photoexcitation of the complex, the excited state of Ru is quenched by an external quencher, methyl viologen, followed by electron transfer from the tyrosine to the oxidized Ru and proton transfer from the tyrosine to either an internal proton acceptor or to the bulk solvent. These authors examined substituted phenols both with and without an intramolecular hydrogen bond to a carboxylate group.[52] The proton acceptor was primarily the carboxylate for phenols with the internal hydrogen bond (Figure 12), and the proton acceptor was thought to be water for phenols without this internal hydrogen bond. In a particularly interesting study,[53] the kinetics of the PCET reactions for the two different systems with internal hydrogen bonds depicted in Figure 12 were compared directly. As illustrated in this figure, the phenolic group was either salicylic acid, which is associated with a resonance-assisted hydrogen-bonded construct, or *o*-hydroxyphenyl-acetic acid. They found that both the rate constant and the KIE were smaller for the salicylic acid system than for the *o*-hydroxyphenyl-acetic acid system.

The experimental data for the complexes in Figure 12 were modeled[53] with the EPT rate constant expressions given in Eq. (17), which assumes a fixed proton donor-acceptor distance, and Eq. (22), which describes the proton donor-acceptor motion as a classical harmonic oscillator using the thermal averaging procedure discussed in Section 2.2.3. The authors were able to reproduce the experimentally determined magnitude and temperature dependence of the rate constants and KIEs for both systems using Eq. (22) with physically reasonable parameters. The results obtained with Eq. (17), which assumes a fixed proton donor-acceptor distance, were less satisfactory. In this system, the proton donor-acceptor mode is expected to be associated with a relatively low frequency because of the non-linearity of the intramolecular hydrogen bond between the phenol hydroxyl group and the carboxylate group (Fig. 12). As a result, inclusion of this mode leads to significant contributions to the overall rate constant from proton donor-acceptor distances shorter than the equilibrium distance, thereby increasing the rate constant and decreasing the KIE relative to the values that would be calculated at the fixed equilibrium proton donor-acceptor distance. Comparison of the theoretical results for the two different systems indicates that the rate constants and KIEs are determined by a balance among several factors, including the inner- and outer-sphere reorganization energies, the equilibrium proton donor-acceptor distance and associated frequency, and the vibronic couplings for the various pairs of reactant/product states.

In addition to these types of photoinduced PCET processes in tyrosine-bound rhenium and ruthenium polypyridyl systems, a variety of simpler phenolic systems without metal centers

have been studied electrochemically[45–46,243–248] and, in some cases, with thermal oxidants[47] and photo-oxidants.[249] Mayer and coworkers investigated PCET reactions in a series of phenols with pendant, hydrogen-bonded bases, such as the phenol-amine systems depicted in Figure 13.[47,243–244,250–251] On the basis of the experimentally measured KIE and driving force dependence of the rates, as well as thermochemical arguments, the authors deduced that electrochemical oxidation of these systems occurs by a concerted PCET mechanism (i.e., an EPT mechanism), where the electron transfers from the phenol to the electrode and the proton transfers from the phenol to the amine in a single kinetic step.[243–244] The sequential mechanism is disfavored because of the high-energy intermediates arising from initial ET or PT.

Mayer and coworkers examined the effects of varying the proton donor-acceptor distance and the driving force by synthesizing and characterizing several different series of substituted phenol-amine compounds.[46–47] For related series of compounds with different substituents, they found that the rate constants were correlated primarily with changes in ΔG^0, the reaction free energy,[46,248] as also observed by Thorp and Meyer.[245] Furthermore, they analyzed the plots of the $\log(k^{EPT})$ versus ΔG^0 with the semiclassical Marcus theory rate constant expression, which is equivalent to Eq. (17) when only the ground reactant and product vibronic states are included.[249] Fitting the experimental data to this expression provided values for the reorganization energy and vibronic coupling for each series of related compounds. On the basis of the maximum rate constant measured and the associated value of the vibronic coupling, which was 20–30 cm^{-1}, the authors deduced that these reactions are nonadiabatic.

Mayer and coworkers also performed a direct comparison of two compounds with different proton donor-acceptor distances, namely a phenol compound with an *ortho* CPh_2NH_2 substituent and a bicyclic amino-indanol compound, as depicted in Figure 13.[47] The bicyclic compound, which has a longer proton donor-acceptor distance, has a similar rate constant and a smaller KIE compared to the substituted phenol compound. The authors analyzed these reactions in the framework of the concerted PCET theory described in Section 2.2.3.[79,90] As discussed above in the context of applying this theory to SLO in Section 4.2,[44] typically the KIE increases with increasing equilibrium proton donor-acceptor distance when all other parameters remain fixed because the ratio of hydrogen and deuterium vibrational wavefunction overlaps increases. However, an inverse relationship can occur in certain situations, such as when excited proton vibrational states are involved or when the species with the longer distance has a lower effective proton donor-acceptor frequency.[94] In other words, the approximate expression in Eq. (21) for the KIE depends on this frequency Ω as well as the ratio of overlaps, and the expression for the KIE is more complicated than that in Eq. (21) when contributions from excited states are included. For the particular compounds studied by Mayer and coworkers,[47] the authors determined that the results could be explained in terms of the involvement of excited proton vibrational states and differences in the effective proton donor-acceptor frequencies (i.e., the O—N frequency at the intramolecular hydrogen-bonding interface).[47] This analysis illustrates that changing the proton donor-acceptor distance may also alter other parameters that significantly impact EPT rate constants and KIEs.

Recently Mayer and coworkers[252] performed a more comprehensive theoretical analysis of three phenol-base compounds using the EPT rate constant expressions obtained from the multistate continuum theory.[76,79,90] Specifically, these authors utilized the EPT rate constant in Eq. (17) in conjunction with a procedure related to the thermally averaged rate constant in Eq. (22) to include the proton donor-acceptor motion (i.e., the changes in the O—N distance at the hydrogen-bonding interface). This concerted PCET theory was able to reproduce the experimentally observed KIEs for all three compounds and the relative rate constants of two

of the compounds but not the relative rate constant of the third compound. These discrepancies may have been due to simplifications in the computational procedure used to determine the input quantities to the rate constant expressions. The analysis indicated that all three compounds have similar dominant proton donor-acceptor distances (i.e., the distance *R* that contributes the most to the thermally averaged rate constant in Eq. (22)), despite the significant differences in the equilibrium proton donor-acceptor distances, which range from 2.56 – 2.76 Å.[252] The ground vibronic states dominated for hydrogen transfer, but excited vibronic states contributed significantly for deuterium transfer. This analysis further illustrates that the EPT rate constants and KIEs are determined by a complex interplay among various factors.

Overall, these studies of biomimetic redox-active tyrosine systems have provided significant insight into the underlying physical principles of bidirectional PCET reactions. The nonadiabatic concerted PCET theory described in Section 2.2.3 is clearly capable of reproducing a wide range of experimental data for these types of systems. Moreover, this theory can be used to make experimentally testable predictions in terms of the behavior of the rate constants and KIEs as functions of physical properties such as proton donor-acceptor distance and driving force. Unfortunately, it is difficult to design experimental systems in which only one property is changed, and EPT rate constants are determined by a subtle balance among many factors. Nevertheless, this PCET theory can be used to help interpret experimental data and guide the design of systems with specified properties.

5.2 Hydrogenase mimics for hydrogen production and oxidation

Hydrogenase enzymes efficiently catalyze the production and oxidation of molecular hydrogen. The [FeFe] and [NiFe] hydrogenases have been studied extensively with a wide range of experimental methods. The presence of an amine ligand in the second coordination sphere of the [FeFe] hydrogenase is thought to play an important mechanistic role.[253–256] In particular, this pendant amine may participate in a proton relay to shuttle protons to and from the metal center during the H_2 production and oxidation processes. The design of molecular electrocatalysts that mimic the catalytic centers of hydrogenase enzymes is relevant to the development of hydrogen-based fuel cells and storage devices for energy harvested from solar, wind, and other environmentally benign processes.[59] Several groups have synthesized and characterized structural models of [FeFe] hydrogenases that also exhibit some degree of catalytic activity.[257–264] These models have been examined with electronic structure methods to analyze the structures and energetics along proposed reaction pathways.[265–269]

In contrast to these structural models, DuBois and coworkers have designed biologically inspired functional models of hydrogenases.[54–58] As depicted in Figure 14, these models contain only a single metal, typically nickel, as well as pendant amines to serve as proton relays for the Ni center. In the $Ni(P_2N_2)_2$ systems, the phosphorus atoms are directly bonded to the nickel center, and the nitrogen atoms of the ligands are in the second coordination sphere to enable them to act as proton relays. A proposed mechanism for H_2 production and oxidation is depicted in Figure 15. These complexes have been shown to produce H_2 at turnover frequencies as large as 10^3–10^5 s^{-1} with moderate overpotentials.[56–57,60,270] These systems have been studied computationally to analyze the dependence of the reduction potentials and pK_a's on the substituents, to generate Pourbaix diagrams and thermodynamic cycles, and to examine the ring isomerization processes and intramolecular proton transfer reactions.[271–280] Although these theoretical studies do not account for hydrogen tunneling, they have provided useful mechanistic insights.

To investigate the role of hydrogen tunneling in these catalysts, our group applied the PCET theory described in Section 2.2.3 to the $Ni(P_2N_2)_2$ complexes.[61] This study utilized an

extension of the thermally averaged rate constant given in Eq. (22) for electrochemical concerted PCET reactions.[176,281–282] The expressions for the anodic and cathodic rate constants are similar to the homogeneous expression in Eq. (22) except that the effective free energy barrier depends on the energies of the electronic states in the electrode and the applied overpotential, and the rate constant is averaged over the Fermi distribution function and the density of states for the electrode. Our calculations focused on the catalytic step that involves electron transfer between the nickel complex and the electrode as well as intramolecular proton transfer between the nickel and the nitrogen atoms, as indicated by the square brackets in Figure 15. We examined the sequential mechanisms, in which either the electron or proton transferred first, as well as the concerted PCET mechanism (i.e., the EPT mechanism). We calculated the electrochemical rate constants as functions of overpotential for the EPT mechanism and the two ET reactions in the sequential mechanisms. These calculations indicated that the favored mechanism will depend on the experimental conditions, such as the applied overpotential, as well as the substituents on the molecular electrocatalyst. Moreover, the calculations predict that the EPT rate constant will increase as the equilibrium distance between the nickel and nitrogen atoms decreases and as the pendant amines become more flexible to facilitate the contraction of this distance with a lower energy penalty.

On the basis of this prediction, we examined related catalysts with more flexible pendant amines, as depicted in Figure 14.[62] The overall objective of catalyst design is to maximize the turnover frequency and minimize the overpotential. Because the concerted PCET mechanism is typically associated with a lower overpotential, we made an effort to theoretically design catalysts that will favor the concerted mechanism for the step shown in square brackets in Figure 15. Our analysis focused on the probability function $P(R)$, which represents the Boltzmann probability for the catalyst to sample each Ni–N distance R, as given by Eq. (23). The overall rate constant given in Eq. (22) is the integral of the product of this probability function, $P(R)$, and the EPT rate constant, $k^{EPT}(R)$, as illustrated schematically in Figure 7. Assuming that $k^{EPT}(R)$ is similar for these complexes, the objective is to decrease the equilibrium proton donor-acceptor distance R and the associated frequency Ω (i.e., to shift the maximum of $P(R)$ to smaller R and to increase the width of $P(R)$). We found that the probability functions for the $Ni(P_2N_2)_2$, $Ni(PNP)_2$, and $Ni(7P_2N)_2$ catalysts are very similar, but the probability function for the Ni(PN) catalyst with phenyl substituents is centered at a significantly larger Ni–N distance and is broader. Despite the greater flexibility of the Ni(PN) catalyst, which leads to the broader probability distribution function, the Ni–N equilibrium distance is so much larger that the concerted mechanism is expected to be less favorable for this catalyst. When the phenyl groups are replaced with methyl groups, however, the equilibrium Ni–N distance decreases significantly, although it is still larger than the distance for the other catalysts shown in Figure 14. Furthermore, the inner-sphere reorganization energy is smaller for the Ni(PN) catalyst than for the $Ni(P_2N_2)_2$ catalysts with equivalent substituents, so the rate constant $k^{EPT}(R)$ is expected to be greater for the Ni(PN) catalyst.[62] As a result, it is possible that the overall rate constant given in Eq. (22) will be large enough for the Ni(PN) catalyst with methyl substituents to favor the concerted PCET mechanism.

Overall, these calculations illustrate that the equilibrium proton donor-acceptor distance and its effective frequency play an important role in determining the rate constant of the concerted PCET mechanism.[61–62] Unfortunately, these two characteristics often compete against each other because greater flexibility of the pendant amine is typically associated with a larger equilibrium Ni–N distance. Reducing the bulkiness of the substituents on the other ligands, however, may result in a smaller equilibrium Ni–N distance for such flexible amines. Note that a complete understanding of these types of catalysts requires analysis of the entire catalytic cycle, such as the one shown in Figure 15, because another step may

require a larger overpotential or slow down the overall turnover frequency. Nevertheless, these types of design principles will be useful for developing the next generation of hydrogen production catalysts.

6. Concluding remarks

In this review, we discuss a wide range of theoretical and computational treatments of hydrogen tunneling in enzymatic and biomimetic systems. An important take-home message is that each method involves approximations and is valid only within the specified regime (e.g., electronically/vibrationally adiabatic or nonadiabatic, low-frequency or high-frequency proton donor-acceptor mode, small or large solvent reorganization energy, and so forth). Thus, each method should be applied only to systems that fall within this specified regime. In some cases, the appropriate regime may not be clear, and a comparison of various theoretical methods may help identify the appropriate regime. Another important take-home message is that a strong connection to experimental studies is critical for testing and improving theoretical and computational methods. To assist these efforts, theoretical approaches can be used to interpret existing experimental data but should also be used to make experimentally testable predictions. Overall, the applications discussed in this review illustrate the power of combined theoretical and experimental studies in elucidating the detailed mechanisms of hydrogen tunneling processes in condensed phases.

Acknowledgments

We are grateful to Soumya Ghosh, Phil Hanoian, Samantha Horvath, and Alexander Soudackov for helpful comments and useful discussions. The theoretical development portion of this review was supported by the National Science Foundation under CHE-10-57875. The biological portion of this review was funded by NIH Grant No. GM056207. The biomimetic portion was supported as part of the Center for Molecular Electrocatalysis, an Energy Frontier Research Center funded by the U. S. Department of Energy, Office of Science, Office of Basic Energy Sciences.

References

1. Klinman JP. Biochim Biophys Acta, Bioenerg. 2006; 1757:981.
2. Swain CG, Stivers EC, Reuwer JF, Schaad LJ. J Am Chem Soc. 1958; 80:5885.
3. Saunders WH. J Am Chem Soc. 1985; 107:164.
4. Cha Y, Murray CJ, Klinman JP. Science. 1989; 243:1325. [PubMed: 2646716]
5. Bahnson BJ, Colby TD, Chin JK, Goldstein BM, Klinman JP. Proc Natl Acad Sci U S A. 1997; 94:12797. [PubMed: 9371755]
6. Bell, RP. The Tunnel Effect in Chemistry. Chapman and Hall; London ; New York: 1980.
7. Hammes-Schiffer S. Energy Environ Sci. 2012; 5:7696.
8. Borgis D, Hynes JT. Chem Phys. 1993; 170:315.
9. Borgis DC, Lee SY, Hynes JT. Chem Phys Lett. 1989; 162:19.
10. Kiefer PM, Hynes JT. Solid State Ionics. 2004; 168:219.
11. Hammes-Schiffer S, Soudackov AV. J Phys Chem B. 2008; 112:14108. [PubMed: 18842015]
12. Warshel, A. Computer Modeling of Chemical Reactions in Enzymes and Solutions. Wiley; New York: 1991.
13. Billeter SR, Webb SP, Agarwal PK, Iordanov T, Hammes-Schiffer S. J Am Chem Soc. 2001; 123:11262. [PubMed: 11697969]
14. Billeter SR, Webb SP, Iordanov T, Agarwal PK, Hammes-Schiffer S. J Chem Phys. 2001; 114:6925.
15. Hammes-Schiffer S, Billeter SR. Int Rev Phys Chem. 2001; 20:591.
16. Feynman, RP.; Hibbs, AR. Quantum mechanics and path integrals. McGraw-Hill; New York: 1965.

17. Hwang JK, Warshel A. J Phys Chem. 1993; 97:10053.
18. Lobaugh J, Voth GA. J Chem Phys. 1994; 100:3039.
19. Cao JS, Voth GA. J Chem Phys. 1993; 99:10070.
20. Cao JS, Voth GA. J Chem Phys. 1996; 104:273.
21. Habershon S, Manolopoulos DE, Markland TE, Miller TF III. Annu Rev Phys Chem. 2013; 64:387. [PubMed: 23298242]
22. Pu JZ, Gao JL, Truhlar DG. Chem Rev. 2006; 106:3140. [PubMed: 16895322]
23. Alhambra C, Corchado JC, Sanchez ML, Gao JL, Truhlar DG. J Am Chem Soc. 2000; 122:8197.
24. Alhambra C, Corchado J, Sanchez ML, Garcia-Viloca M, Gao J, Truhlar DG. J Phys Chem B. 2001; 105:11326.
25. Villa J, Warshel A. J Phys Chem B. 2001; 105:7887.
26. Agarwal PK, Billeter SR, Hammes-Schiffer S. J Phys Chem B. 2002; 106:3283.
27. Caratzoulas S, Mincer JS, Schwartz SD. J Am Chem Soc. 2002; 124:3270. [PubMed: 11916410]
28. Cui Q, Elstner M, Karplus M. J Phys Chem B. 2002; 106:2721.
29. Tresadern G, McNamara JP, Mohr M, Wang H, Burton NA, Hillier IH. Chem Phys Lett. 2002; 358:489.
30. Kohen A, Jensen JH. J Am Chem Soc. 2002; 124:3858. [PubMed: 11942822]
31. Tresadern G, Faulder PF, Gleeson MP, Tai Z, MacKenzie G, Burton NA, Hillier IH. Theor Chem Acc. 2003; 109:108.
32. Warshel A, Villa-Freixa J. J Phys Chem B. 2003; 107:12370.
33. Schwartz SD. J Phys Chem B. 2003; 107:12372.
34. Luo J, Bruice TC. Biophys Chem. 2007; 126:80. [PubMed: 16737770]
35. Luo J, Bruice TC. Proc Natl Acad Sci U S A. 2002; 99:16597. [PubMed: 12481026]
36. Luo J, Bruice TC. Proc Natl Acad Sci U S A. 2004; 101:13152. [PubMed: 15331786]
37. Rickert KW, Klinman JP. Biochemistry. 1999; 38:12218. [PubMed: 10493789]
38. Knapp MJ, Klinman JP. Biochemistry. 2003; 42:11466. [PubMed: 14516198]
39. Mincer JS, Schwartz SD. J Chem Phys. 2004; 120:7755. [PubMed: 15267689]
40. Olsson MHM, Siegbahn PEM, Warshel A. J Am Chem Soc. 2004; 126:2820. [PubMed: 14995199]
41. Tejero I, Garcia-Viloca M, Gonzalez-Lafont A, Lluch JM, York DM. J Phys Chem B. 2006; 110:24708. [PubMed: 17134234]
42. Olsson MHM, Siegbahn PEM, Warshel A. J Biol Inorg Chem. 2004; 9:96. [PubMed: 14663649]
43. Hatcher E, Soudackov AV, Hammes-Schiffer S. J Am Chem Soc. 2004; 126:5763. [PubMed: 15125669]
44. Hatcher E, Soudackov AV, Hammes-Schiffer S. J Am Chem Soc. 2007; 129:187. [PubMed: 17199298]
45. Manner VW, DiPasquale AG, Mayer JM. J Am Chem Soc. 2008; 130:7210. [PubMed: 18479096]
46. Markle TF, Rhile IJ, DiPasquale AG, Mayer JM. Proc Natl Acad Sci U S A. 2008; 105:8185. [PubMed: 18212121]
47. Markle TF, Rhile IJ, Mayer JM. J Am Chem Soc. 2011; 133:17341. [PubMed: 21919508]
48. Sjödin M, Styring S, Akermark B, Sun LC, Hammarström L. J Am Chem Soc. 2000; 122:3932.
49. Sjödin M, Styring S, Åkermark B, Sun L, Hammarström L. Philos Trans R Soc, B. 2002; 357:1471.
50. Sjödin M, Ghanem R, Polivka T, Pan J, Styring S, Sun LC, Sundstrom V, Hammarström L. Phys Chem Chem Phys. 2004; 6:4851.
51. Sjödin M, Styring S, Wolpher H, Xu YH, Sun LC, Hammarström L. J Am Chem Soc. 2005; 127:3855. [PubMed: 15771521]
52. Sjödin M, Irebo T, Utas JE, Lind J, Merenyi G, Akermark B, Hammarström L. J Am Chem Soc. 2006; 128:13076. [PubMed: 17017787]
53. Johannissen LO, Irebo T, Sjödin M, Johansson O, Hammarström L. J Phys Chem B. 2009; 113:16214. [PubMed: 20000384]
54. DuBois MR, DuBois DL. Chem Soc Rev. 2009; 38:62. [PubMed: 19088965]

55. DuBois MR, DuBois DL. C R Chim. 2008; 11:805.
56. DuBois DL, Bullock RM. Eur J Inorg Chem. 2011:1017.
57. Kilgore UJ, Stewart MP, Helm ML, Dougherty WG, Kassel WS, DuBois MR, DuBois DL, Bullock RM. Inorg Chem. 2011; 50:10908. [PubMed: 21999814]
58. Yang JY, Bullock M, DuBois MR, DuBois DL. MRS Bull. 2011; 36:39.
59. Wiedner ES, Yang JY, Dougherty WG, Kassel WS, Bullock RM, DuBois MR, DuBois DL. Organometallics. 2010; 29:5390.
60. Helm ML, Stewart MP, Bullock RM, DuBois MR, DuBois DL. Science. 2011; 333:863. [PubMed: 21836012]
61. Horvath S, Fernandez LE, Soudackov AV, Hammes-Schiffer S. Proc Natl Acad Sci U S A. 2012; 109:15663. [PubMed: 22529352]
62. Fernandez LE, Horvath S, Hammes-Schiffer S. J Phys Chem Lett. 2013; 4:542.
63. Kiefer PM, Hynes JT. J Phys Chem A. 2004; 108:11809.
64. Staib A, Borgis D, Hynes JT. J Chem Phys. 1995; 102:2487.
65. Borgis D, Hynes JT. J Phys Chem. 1996; 100:1118.
66. Ando K, Hynes JT. Adv Chem Phys. 1999; 110:381.
67. Keck JC. J Chem Phys. 1967; 46:4211.
68. Anderson JB. J Chem Phys. 1973; 58:4684.
69. Chandler D. J Chem Phys. 1978; 68:2959.
70. Kiefer PM, Hynes JT. J Phys Org Chem. 2010; 23:632.
71. Hynes JT. J Phys Chem. 1986; 90:3701.
72. Trakhtenberg LI, Klochikhin VL, Pshezhetsky SY. Chem Phys. 1981; 59:191.
73. Trakhtenberg LI, Klochikhin VL, Pshezhetsky SY. Chem Phys. 1982; 69:121.
74. Kiefer PM, Hynes JT. J Phys Chem A. 2004; 108:11793.
75. Tachiya M. J Phys Chem. 1993; 97:5911.
76. Soudackov A, Hammes-Schiffer S. J Chem Phys. 1999; 111:4672.
77. Rostov I, Hammes-Schiffer S. J Chem Phys. 2001; 115:285.
78. Hammes-Schiffer S, Stuchebrukhov AA. Chem Rev. 2010; 110:6939. [PubMed: 21049940]
79. Soudackov A, Hammes-Schiffer S. J Chem Phys. 2000; 113:2385.
80. Mayer JM, Hrovat DA, Thomas JL, Borden WT. J Am Chem Soc. 2002; 124:11142. [PubMed: 12224962]
81. Huynh MHV, Meyer TJ. Chem Rev. 2007; 107:5004. [PubMed: 17999556]
82. Skone JH, Soudackov AV, Hammes-Schiffer S. J Am Chem Soc. 2006; 128:16655. [PubMed: 17177415]
83. Sirjoosingh A, Hammes-Schiffer S. J Phys Chem A. 2011; 115:2367. [PubMed: 21351757]
84. Georgievskii Y, Stuchebrukhov AA. J Chem Phys. 2000; 113:10438.
85. Landau LD. Physics Z Sowjetunion. 1932; 46:2.
86. Zener C. Proc R Soc London, Ser A. 1932; 137:696.
87. Frauenfelder H, Wolynes PG. Science. 1985; 229:337. [PubMed: 4012322]
88. Here the semiclassical framework refers to the use of the Wentzel-Kramers-Brillouin approximation.[89]
89. Kemble, EC. The fundamental principles of quantum mechanics, with elementary applications. 1. McGraw-Hill Book Company, inc; New York, London: 1937.
90. Soudackov A, Hatcher E, Hammes-Schiffer S. J Chem Phys. 2005; 122:014505.
91. Cukier RI, Nocera DG. Annu Rev Phys Chem. 1998; 49:337. [PubMed: 9933908]
92. Kuznetsov AM, Ulstrup J. Can J Chem. 1999; 77:1085.
93. Hatcher E, Soudackov A, Hammes-Schiffer S. Chem Phys. 2005; 319:93.
94. Edwards SJ, Soudackov AV, Hammes-Schiffer S. J Phys Chem A. 2009; 113:2117. [PubMed: 19182970]

95. Hammes-Schiffer S, Hatcher E, Ishikita H, Skone JH, Soudackov AV. Coord Chem Rev. 2008; 252:384. [PubMed: 21057592]
96. Knapp MJ, Klinman JP. Eur J Biochem. 2002; 269:3113. [PubMed: 12084051]
97. Meyer MP, Klinman JP. Chem Phys. 2005; 319:283. [PubMed: 21132078]
98. Meyer MP, Tomchick DR, Klinman JP. Proc Natl Acad Sci U S A. 2008; 105:1146. [PubMed: 18216254]
99. Klinman JP. Chem Phys Lett. 2009; 471:179. [PubMed: 20354595]
100. Bandaria JN, Cheatum CM, Kohen A. J Am Chem Soc. 2009; 131:10151. [PubMed: 19621965]
101. Roston D, Cheatum CM, Kohen A. Biochemistry. 2012; 51:6860. [PubMed: 22857146]
102. Klinman JP. Biochemistry. 2013; 52:2068. [PubMed: 23373460]
103. Kestner NR, Logan J, Jortner J. J Phys Chem. 1974; 78:2148.
104. Ulstrup J, Jortner J. J Chem Phys. 1975; 63:4358.
105. Bixon M, Giese B, Wessely S, Langenbacher T, Michel-Beyerle ME, Jortner J. Proc Natl Acad Sci U S A. 1999; 96:11713. [PubMed: 10518515]
106. Ohta Y, Soudackov AV, Hammes-Schiffer S. J Chem Phys. 2006; 125:144522. [PubMed: 17042624]
107. Suarez A, Silbey R. J Chem Phys. 1991; 94:4809.
108. Yan YJ, Shuang F, Xu RX, Cheng JX, Li XQ, Yang C, Zhang HY. J Chem Phys. 2000; 113:2068.
109. Shi Q, Geva E. J Chem Phys. 2004; 120:10647. [PubMed: 15268091]
110. Xu RX, Yan YJ. Phys Rev E: Stat, Nonlinear, Soft Matter Phys. 2007; 75
111. Warshel A, Chu ZT. J Chem Phys. 1990; 93:4003.
112. Schenter GK, Garrett BC, Truhlar DG. J Phys Chem B. 2001; 105:9672.
113. Kuznetsov, AM.; Ulstrup, J. Isotope Effects in Chemistry and Biology. Kohen, A.; Limbach, HH., editors. Taylor and Francis; Boca Raton, FL: 2006.
114. Marcus RA. Annu Rev Phys Chem. 1964; 15:155.
115. Marcus RA, Sutin N. Biochim Biophys Acta. 1985; 811:265.
116. Zusman LD. Chem Phys. 1980; 49:295.
117. Rips I, Jortner J. J Chem Phys. 1987; 87:2090.
118. Jortner J, Bixon M. J Chem Phys. 1988; 88:167.
119. Navrotskaya I, Hammes-Schiffer S. J Chem Phys. 2009:131.
120. Barzykin AV, Frantsuzov PA, Seki K, Tachiya M. Adv Chem Phys. 2002; 123:511.
121. Schwartz SD, Schramm VL. Nat Chem Biol. 2009; 5:551. [PubMed: 19620996]
122. Mincer JS, Nunez S, Schwartz SD. J Theor Comput Chem. 2004; 3:501.
123. Antoniou D, Schwartz SD. J Phys Chem B. 2001; 105:5553.
124. Berlin YA, Grozema FC, Siebbeles LDA, Ratner MA. J Phys Chem C. 2008; 112:10988.
125. Saito K, Sumi H. J Chem Phys. 2009; 131
126. Vuilleumier R, Borgis D. Chem Phys Lett. 1998; 284:71.
127. Vuilleumier R, Borgis D. J Chem Phys. 1999; 111:4251.
128. Kamerlin SCL, Warshel A. Faraday Discuss. 2010; 145:71.
129. Marston CC, Balint-Kurti GG. J Chem Phys. 1989; 91:3571.
130. Webb SP, Hammes-Schiffer S. J Chem Phys. 2000; 113:5214.
131. Webb SP, Agarwal PK, Hammes-Schiffer S. J Phys Chem B. 2000; 104:8884.
132. Kumar S, Bouzida D, Swendsen RH, Kollman PA, Rosenberg JM. J Comput Chem. 1992; 13:1011.
133. Roux B. Comput Phys Commun. 1995; 91:275.
134. Carter EA, Ciccotti G, Hynes JT, Kapral R. Chem Phys Lett. 1989; 156:472.
135. Paci E, Ciccotti G, Ferrario M, Kapral R. Chem Phys Lett. 1991; 176:581.
136. Sprik M, Ciccotti G. J Chem Phys. 1998; 109:7737.
137. Schenter GK, Garrett BC, Truhlar DG. J Chem Phys. 2003; 119:5828.

138. Watney JB, Soudackov AV, Wong KF, Hammes-Schiffer S. Chem Phys Lett. 2006; 418:268.
139. In Eq. (2), the prefactor corresponds to the harmonic frequency of oscillation of the solvent coordinate in the reactant well. In Eq. (26), the transition state theory rate constant appears to depend on Planck's constant, but this dependence is removed when the rate constant is expressed in terms of the ratio of the partition functions at the transition state and the reactant state because the transition state has one fewer degree of freedom than the reactant state.[140] This ratio is implicitly included in the exponential factor of Eq. (26) because the free energy barrier is the difference in free energy at the transition state and the reactant state, which differ by one degree of freedom.[141]
140. Johnston, HS. Gas Phase Reaction Rate Theory. Ronald Press Co; New York: 1966.
141. Hanggi P, Talkner P, Borkovec M. Rev Mod Phys. 1990; 62:251.
142. Wigner E. Phys Rev. 1932; 40:0749.
143. Bennett Charles, H. Algorithms for Chemical Computations. Vol. 46. American Chemical Soceity; 1977.
144. Keck JC. J Chem Phys. 1960; 32:1035.
145. Tully JC. J Chem Phys. 1990; 93:1061.
146. Hammes-Schiffer S, Tully JC. J Chem Phys. 1994; 101:4657.
147. Morelli J, Hammes-Schiffer S. Chem Phys Lett. 1997; 269:161.
148. Fang JY, Hammes-Schiffer S. J Chem Phys. 1997; 107:8933.
149. Kim SY, Hammes-Schiffer S. J Chem Phys. 2006; 124:244102. [PubMed: 16821968]
150. Hammes-Schiffer S, Tully JC. J Chem Phys. 1995; 103:8528.
151. Kim SY, Hammes-Schiffer S. J Chem Phys. 2003; 119:4389.
152. Berne BJ, Thirumalai D. Annu Rev Phys Chem. 1986; 37:401.
153. Chandler D, Wolynes PG. J Chem Phys. 1981; 74:4078.
154. Voth GA, Chandler D, Miller WH. J Chem Phys. 1989; 91:7749.
155. Voth GA. J Phys Chem. 1993; 97:8365.
156. Hall RW, Berne BJ. J Chem Phys. 1984; 81:3641.
157. Gillan MJ. Journal of Physics C-Solid State Physics. 1987; 20:3621.
158. Gillan MJ. Phys Rev Lett. 1987; 58:563. [PubMed: 10034973]
159. Wong KF, Sonnenberg JL, Paesani F, Yamamoto T, Vaníček Ji, Zhang W, Schlegel HB, Case DA, Cheatham TE, Miller WH, Voth GA. J Chem Theory Comput. 2010; 6:2566. [PubMed: 21116485]
160. Liu, H.; Warshel, A. Quantum Tunnelling in Enzyme-Catalysed Reactions. Allemann, RK.; Scrutton, NS., editors. Royal Society of Chemistry; Cambridge, UK: 2009.
161. Ceperley DM. Rev Mod Phys. 1995; 67:279.
162. Major DT, Gao JL. J Mol Graphics Modell. 2005; 24:121.
163. Wang Q, Hammes-Schiffer S. J Chem Phys. 2006; 125:184102. [PubMed: 17115733]
164. Major DT, Gao JL. J Chem Theory Comput. 2007; 3:949.
165. Voth GA. Adv Chem Phys. 1996; 93:135.
166. Wang ML, Lu ZY, Yang WT. J Chem Phys. 2006; 124:124516. [PubMed: 16599706]
167. Boekelheide N, Salomon-Ferrer R, Miller TF III. Proc Natl Acad Sci U S A. 2011; 108:16159. [PubMed: 21930950]
168. Warren JJ, Menzeleev AR, Kretchmer JS, Miller TF III, Gray HB, Mayer JM. J Phys Chem Lett. 2013; 4:519. [PubMed: 23493584]
169. Menzeleev AR, Ananth N, Miller TF III. J Chem Phys. 2011; 135:074106. [PubMed: 21861555]
170. Garcia-Viloca M, Alhambra C, Truhlar DG, Gao J. J Comput Chem. 2003; 24:177. [PubMed: 12497598]
171. Poulsen TD, Garcia-Viloca M, Gao JL, Truhlar DG. J Phys Chem B. 2003; 107:9567.
172. Truhlar DG, Gao JL, Garcia-Viloca M, Alhambra C, Corchado J, Sanchez ML, Poulsen TD. Int J Quantum Chem. 2004; 100:1136.

173. Truhlar DG, Gao JL, Alhambra C, Garcia-Viloca M, Corchado J, Sanchez ML, Villa J. Acc Chem Res. 2002; 35:341. [PubMed: 12069618]
174. Garcia-Viloca M, Truhlar DG, Gao J. Biochemistry. 2003; 42:13558. [PubMed: 14622003]
175. Mayer JM. Annu Rev Phys Chem. 2004; 55:363. [PubMed: 15117257]
176. Ludlow MK, Soudackov AV, Hammes-Schiffer S. J Am Chem Soc. 2010; 132:1234. [PubMed: 20067257]
177. Hammes-Schiffer S. Chem Rev. 2010; 110:6937. [PubMed: 21141827]
178. Basilevsky MV, Rostov IV, Newton MD. Chem Phys. 1998; 232:189.
179. Newton MD, Basilevsky MV, Rostov IV. Chem Phys. 1998; 232:201.
180. Cave RJ, Newton MD. Chem Phys Lett. 1996; 249:15.
181. Cave RJ, Newton MD. J Chem Phys. 1997; 106:9213.
182. Van Voorhis T, Kowalczyk T, Kaduk B, Wang LP, Cheng CL, Wu Q. Annu Rev Phys Chem. 2010; 61:149. [PubMed: 20055670]
183. Hatcher E, Soudackov A, Hammes-Schiffer S. J Phys Chem B. 2005; 109:18565. [PubMed: 16853391]
184. Chen ZF, Vannucci AK, Concepcion JJ, Jurss JW, Meyer TJ. Proc Natl Acad Sci U S A. 2011; 108:E1461. [PubMed: 22160681]
185. Hazra A, Soudackov AV, Hammes-Schiffer S. J Phys Chem B. 2010; 114:12319. [PubMed: 20809583]
186. Hazra A, Soudackov AV, Hammes-Schiffer S. J Phys Chem Lett. 2011; 2:36.
187. Soudackov AV, Hazra A, Hammes-Schiffer S. J Chem Phys. 2011; 135:144115. [PubMed: 22010706]
188. Auer B, Soudackov AV, Hammes-Schiffer S. J Phys Chem B. 2012; 116:7695. [PubMed: 22651684]
189. Kretchmer JS, Miller TF. J Chem Phys. 2013; 138:134109. [PubMed: 23574210]
190. Klinman JP, Kohen A. Annu Rev Biochem. 2013; 82:471. [PubMed: 23746260]
191. Knapp MJ, Seebeck FP, Klinman JP. J Am Chem Soc. 2001; 123:2931. [PubMed: 11457000]
192. Oyeyemi OA, Sours KM, Lee T, Kohen A, Resing KA, Ahn NG, Klinman JP. Biochemistry. 2011; 50:8251. [PubMed: 21859100]
193. Pu J, Ma S, Garcia-Viloca M, Gao J, Truhlar DG, Kohen A. J Am Chem Soc. 2005; 127:14879. [PubMed: 16231943]
194. Pu JZ, Ma SH, Garcia-Viloca M, Gao JL, Truhlar DG, Kohen A. J Am Chem Soc. 2005; 127:14879. [PubMed: 16231943]
195. Stojkovic V, Perissinotti LL, Willmer D, Benkovic SJ, Kohen A. J Am Chem Soc. 2012; 134:1738. [PubMed: 22171795]
196. Wang L, Goodey NM, Benkovic SJ, Kohen A. Philos Trans R Soc, B. 2006; 361:1307.
197. Masgrau L, Roujeinikova A, Johannissen LO, Hothi P, Basran J, Ranaghan KE, Mulholland AJ, Sutcliffe MJ, Scrutton NS, Leys D. Science. 2006; 312:237. [PubMed: 16614214]
198. Johannissen LO, Scrutton NS, Sutcliffe MJ. Angew Chem, Int Ed. 2011; 50:2129.
199. Johannissen LO, Hay S, Scrutton NS, Sutcliffe MJ. J Phys Chem B. 2007; 111:2631. [PubMed: 17305385]
200. Hammes-Schiffer S. Acc Chem Res. 2006; 39:93. [PubMed: 16489728]
201. Liu HB, Warshel A. J Phys Chem B. 2007; 111:7852. [PubMed: 17571875]
202. Murakawa T, Okajima T, Kuroda S, Nakamoto T, Taki M, Yamamoto Y, Hayashi H, Tanizawa K. Biochem Biophys Res Commun. 2006; 342:414. [PubMed: 16487484]
203. Taki M, Murakawa T, Nakamoto T, Uchida M, Hayashi H, Tanizawa K, Yamamoto Y, Okajima T. Biochemistry. 2008; 47:7726. [PubMed: 18627131]
204. Garcia-Viloca M, Alhambra C, Truhlar DG, Gao J. J Am Chem Soc. 2002; 124:7268. [PubMed: 12071725]
205. Bahnson BJ, Park DH, Kim K, Plapp BV, Klinman JP. Biochemistry. 1993; 32:5503. [PubMed: 8504071]

206. Villà J, Warshel A. The Journal of Physical Chemistry B. 2001; 105:7887.
207. Hammes-Schiffer S, Benkovic SJ. Annu Rev Biochem. 2006; 75:519. [PubMed: 16756501]
208. Hammes-Schiffer S. Biochemistry. 2013; 52:2012. [PubMed: 23240765]
209. Hammes GG, Benkovic SJ, Hammes-Schiffer S. Biochemistry. 2011; 50:10422. [PubMed: 22029278]
210. Benkovic SJ, Hammes GG, Hammes-Schiffer S. Biochemistry. 2008; 47:3317. [PubMed: 18298083]
211. Glickman MH, Klinman JP. Biochemistry. 1995; 34:14077. [PubMed: 7578005]
212. Lehnert N, Solomon EI. J Biol Inorg Chem. 2003; 8:294. [PubMed: 12589565]
213. Knapp MJ, Rickert K, Klinman JP. J Am Chem Soc. 2002; 124:3865. [PubMed: 11942823]
214. Meyer MP, Tomchick DR, Klinman JP. Proc Natl Acad Sci U S A. 2008; 105:19562.
215. Borowski T, Krol M, Chruszcz M, Broclawik E. J Phys Chem B. 2001; 105:12212.
216. Borowski T, Broclawik E. J Phys Chem B. 2003; 107:4639.
217. Siebrand W, Smedarchina Z. J Phys Chem B. 2004; 108:4185.
218. Mavri J, Liu HB, Olsson MHM, Warshel A. J Phys Chem B. 2008; 112:5950. [PubMed: 18069813]
219. Truhlar DG. J Phys Org Chem. 2010; 23:660.
220. Edwards SJ, Soudackov AV, Hammes-Schiffer S. J Phys Chem B. 2010; 114:6653. [PubMed: 20423074]
221. Marchetti L, Levine M. ACS Catalysis. 2011; 1:1090.
222. Rideout DC, Breslow R. J Am Chem Soc. 1980; 102:7816.
223. Schneider HJ, Sangwan NK. J Chem Soc, Chem Commun. 1986:1787.
224. Murase T, Horiuchi S, Fujita M. J Am Chem Soc. 2010; 132:2866. [PubMed: 20155904]
225. Liu L, Rozenman M, Breslow R. J Am Chem Soc. 2002; 124:12660. [PubMed: 12392403]
226. Zhou WJ, Liu L, Breslow R. Helv Chim Acta. 2003; 86:3560.
227. Sculimbrene BR, Miller SJ. J Am Chem Soc. 2001; 123:10125. [PubMed: 11592903]
228. Rosenholm JM, Duchanoy A, Linden M. Chem Mater. 2008; 20:1126.
229. Poe SL, Kobaslija M, McQuade DT. J Am Chem Soc. 2007; 129:9216. [PubMed: 17602626]
230. Land EJ, Porter G, Fang JY, Strachan E. Trans Faraday Soc. 1961; 57:1885.
231. Kuhne H, Brudvig GW. J Phys Chem B. 2002; 106:8189.
232. McEvoy JP, Brudvig GW. Chem Rev. 2006; 106:4455. [PubMed: 17091926]
233. Stubbe J, van der Donk WA. Chem Rev. 1998; 98:705. [PubMed: 11848913]
234. Pesavento RP, Van Der Donk WA. Adv Protein Chem. 2001; 58:317. [PubMed: 11665491]
235. Meyer TJ, Huynh MHV, Thorp HH. Angew Chem, Int Ed. 2007; 46:5284.
236. Umena Y, Kawakami K, Shen JR, Kamiya N. Nature. 2011; 473:55. [PubMed: 21499260]
237. Barry BA. J Photochem Photobiol, B. 2011; 104:60. [PubMed: 21419640]
238. Nordlund N, Reichard P. Annu Rev Biochem. 2006; 75:681. [PubMed: 16756507]
239. Minnihan EC, Nocera DG, Stubbe J. Acc Chem Res. 2013
240. Reece SY, Nocera DG. J Am Chem Soc. 2005; 127:9448. [PubMed: 15984872]
241. Irebo T, Reece SY, Sjödin M, Nocera DG, Hammarström L. J Am Chem Soc. 2007; 129:15462. [PubMed: 18027937]
242. Ishikita H, Soudackov AV, Hammes-Schiffer S. J Am Chem Soc. 2007; 129:11146. [PubMed: 17705482]
243. Rhile IJ, Mayer JM. J Am Chem Soc. 2004; 126:12718. [PubMed: 15469234]
244. Rhile IJ, Markle TF, Nagao H, DiPasquale AG, Lam OP, Lockwood MA, Rotter K, Mayer JM. J Am Chem Soc. 2006; 128:6075. [PubMed: 16669677]
245. Fecenko CJ, Thorp HH, Meyer TJ. J Am Chem Soc. 2007; 129:15098. [PubMed: 17999500]
246. Costentin C. Chem Rev. 2008; 108:2145. [PubMed: 18620365]
247. Costentin C, Robert M, Saveant JM. Chem Rev. 2010; 110:Pr1. [PubMed: 21192326]

248. Markle TF, Tronic TA, DiPasquale AG, Kaminsky W, Mayer JM. J Phys Chem A. 2012; 116:12249. [PubMed: 23176252]
249. Schrauben JN, Cattaneo M, Day TC, Tenderholt AL, Mayer JM. J Am Chem Soc. 2012; 134:16635. [PubMed: 22974135]
250. Saouma CT, Kaminsky W, Mayer JM. J Am Chem Soc. 2012; 134:7293. [PubMed: 22519585]
251. Carver CT, Matson BD, Mayer JM. J Am Chem Soc. 2012; 134:5444. [PubMed: 22394189]
252. Markle TF, Tenderholt AL, Mayer JM. J Phys Chem B. 2012; 116:571. [PubMed: 22148459]
253. Onuchic JN, Beratan DN, Winkler JR, Gray HB. Annu Rev Biophys Biomol Struct. 1992; 21:349. [PubMed: 1326356]
254. Peters JW. Curr Opin Struct Biol. 1999; 9:670. [PubMed: 10607666]
255. Frey M. ChemBioChem. 2002; 3:153. [PubMed: 11921392]
256. Fontecilla-Camps JC, Volbeda A, Cavazza C, Nicolet Y. Chem Rev. 2007; 107:5411.
257. Gloaguen F, Rauchfuss TB. Chem Soc Rev. 2009; 38:100. [PubMed: 19088969]
258. Gloaguen F, Lawrence JD, Rauchfuss TB. J Am Chem Soc. 2001; 123:9476. [PubMed: 11562244]
259. Gloaguen F, Lawrence JD, Rauchfuss TB, Benard M, Rohmer MM. Inorg Chem. 2002; 41:6573. [PubMed: 12470052]
260. Mejia-Rodriguez R, Chong DS, Reibenspies JH, Soriaga MP, Darensbourg MY. J Am Chem Soc. 2004; 126:12004. [PubMed: 15382935]
261. Liu TB, Darensbourg MY. J Am Chem Soc. 2007; 129:7008. [PubMed: 17497786]
262. Tard C, Pickett CJ. Chem Rev. 2009; 109:2245. [PubMed: 19438209]
263. Capon JF, Gloaguen F, Petillon FY, Schollhammer P, Talarmin J. Coord Chem Rev. 2009; 253:1476.
264. Tschierlei S, Ott S, Lomoth R. Energy Environ Sci. 2011; 4:2340.
265. Tye JW, Darensbourg MY, Hall MB. J Comput Chem. 2006; 27:1454. [PubMed: 16807976]
266. Liu CP, Peck JNT, Wright JA, Pickett CJ, Hall MB. Eur J Inorg Chem. 2011:1080.
267. Liu TB, Li B, Popescu CV, Bilko A, Perez LM, Hall MB, Darensbourg MY. Chem- Eur J. 2010; 16:3083. [PubMed: 20119989]
268. Keith JM, Hall MB. Inorg Chem. 2010; 49:6378. [PubMed: 20557131]
269. Yang XZ, Hall MB. J Am Chem Soc. 2009; 131:10901. [PubMed: 19722671]
270. Fraze K, Wilson AD, Appel AM, DuBois MR, DuBois DL. Organometallics. 2007; 26:3918.
271. Chen S, Raugei S, Rousseau R, Dupuis M, Bullock RM. J Phys Chem A. 2010; 114:12716. [PubMed: 21070021]
272. Chen S, Rousseau R, Raugei S, Dupuis M, DuBois DL, Bullock RM. Organometallics. 2011; 30:6108.
273. Wilson AD, Newell RH, McNevin MJ, Muckerman JT, DuBois MR, DuBois DL. J Am Chem Soc. 2006; 128:358. [PubMed: 16390166]
274. Wilson AD, Shoemaker RK, Miedaner A, Muckerman JT, DuBois DL, Rakowski DuBois M. Proc Natl Acad Sci U S A. 2007; 104:6951. [PubMed: 17360385]
275. Small YA, DuBois DL, Fujita E, Muckerman JT. Energy Environ Sci. 2011; 4:3008.
276. O'Hagan M, Shaw WJ, Raugei S, Chen ST, Yang JY, Kilgore UJ, DuBois DL, Bullock RM. J Am Chem Soc. 2011; 133:14301. [PubMed: 21595478]
277. Fernandez LE, Horvath S, Hammes-Schiffer S. J Phys Chem C. 2012; 116:3171.
278. Raugei S, Chen ST, Ho MH, Ginovska-Pangovska B, Rousseau RJ, Dupuis M, DuBois DL, Bullock RM. Chem- Eur J. 2012; 18:6493. [PubMed: 22532421]
279. O'Hagan M, Ho MH, Yang JY, Appel AM, DuBois MR, Raugei S, Shaw WJ, DuBois DL, Bullock RM. J Am Chem Soc. 2012; 134:19409. [PubMed: 23072436]
280. Horvath S, Fernandez LE, Appel AM, Hammes-Schiffer S. Inorg Chem. 2013; 52:3643. [PubMed: 23477912]
281. Venkataraman C, Soudackov AV, Hammes-Schiffer S. J Phys Chem C. 2008; 112:12386.

282. Navrotskaya I, Soudackov AV, Hammes-Schiffer S. J Chem Phys. 2008; 128:244712. [PubMed: 18601370]

283. Agarwal PK, Webb SP, Hammes-Schiffer S. J Am Chem Soc. 2000; 122:4803.

284. Waggoner NW, Spreer LS, Boro BJ, DuBois DL, Helm ML. Inorg Chim Acta. 2012; 380:14.

Biographies

Joshua Layfield completed his B.S. in chemistry at Davidson College in 2005 and Ph. D in 2011 at Virginia Tech. His graduate work focused on computational studies of gas-phase and gas/surfaces reactions working Dr. Diego Troya. He joined the Hammes-Schiffer lab in 2011 and currently studies non-natural amino acid probes that are sensitive to changes in local electric fields within enzymes.

Sharon Hammes-Schiffer received her B.A. in 1988 from Princeton University and her Ph.D. in Chemistry at Stanford University in 1993. She was a postdoc at AT&T Bell Laboratories and was appointed the Clare Boothe Luce Assistant Professor of Chemistry and Biochemistry at the University of Notre Dame in 1995. She moved to The Pennsylvania State University in 2000 and was appointed the Eberly Professor of Biotechnology in 2006. In 2012, she accepted a position as Swanlund Chair and Professor of Chemistry at the University of Illinois at Urbana-Champaign. In addition, she is the Deputy Editor of *The Journal of Physical Chemistry B*. Dr. Hammes-Schiffer's research centers on the investigation of proton, electron, and proton-coupled electron transfer reactions in chemical, biological, and interfacial processes. Her work encompasses the development of analytical theories and computational methods, as well as applications to a wide range of experimentally relevant systems. She is a Fellow of the American Physical Society, the American Chemical Society, and the American Association for the Advancement of Science, and she is a member of the American Academy of Arts and Sciences and the National Academy of Sciences.

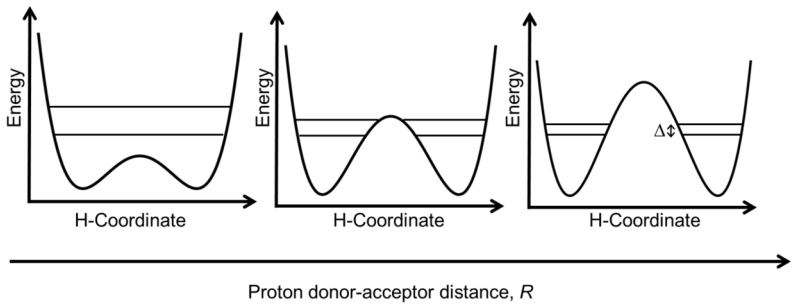

Figure 1.

Symmetric proton potential energy curves along the proton coordinate for three different proton donor-acceptor distances *R*. As the distance *R* increases from left to right, the width and height of the barrier increase. The ground and first excited proton vibrational states are depicted with solid black horizontal lines. At the smallest distance *R*, the proton vibrational ground state is above the barrier, representing the vibrationally adiabatic case. At the middle distance *R*, the ground and first excited proton vibrational states are slightly below the barrier with substantial splitting. At the largest distance *R*, the ground and first excited proton vibrational states are significantly below the barrier with relatively small splitting Δ, representing the vibrationally nonadiabatic case.

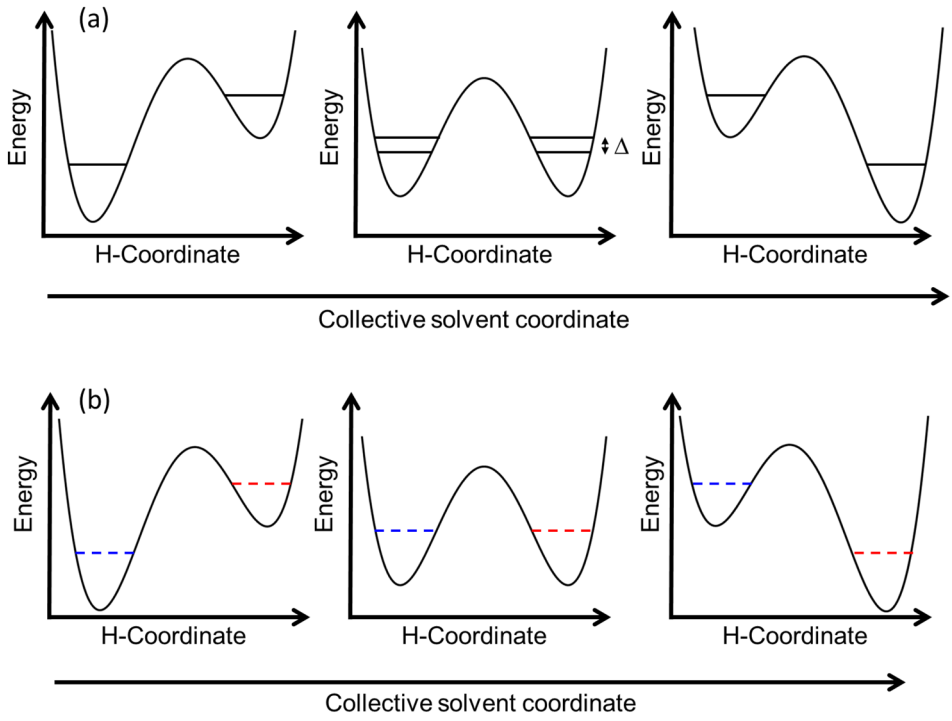

Figure 2.

Proton potential energy curves along the proton coordinate for three different solvent configurations. As the solvent configuration changes from left to right, the relative energies of the donor and acceptor wells change from the donor well lower in energy (left) to a symmetric potential (middle) to the acceptor well lower in energy (right). In part (a), the adiabatic proton vibrational states are depicted as solid black lines and are localized in the donor or acceptor well for the asymmetric proton potentials but are delocalized over both wells for the symmetric potential. In part (b), the diabatic proton vibrational states are depicted as dashed lines and remain localized in the donor well (blue dashed lines) or acceptor well (red dashed lines), even for the symmetric potential.

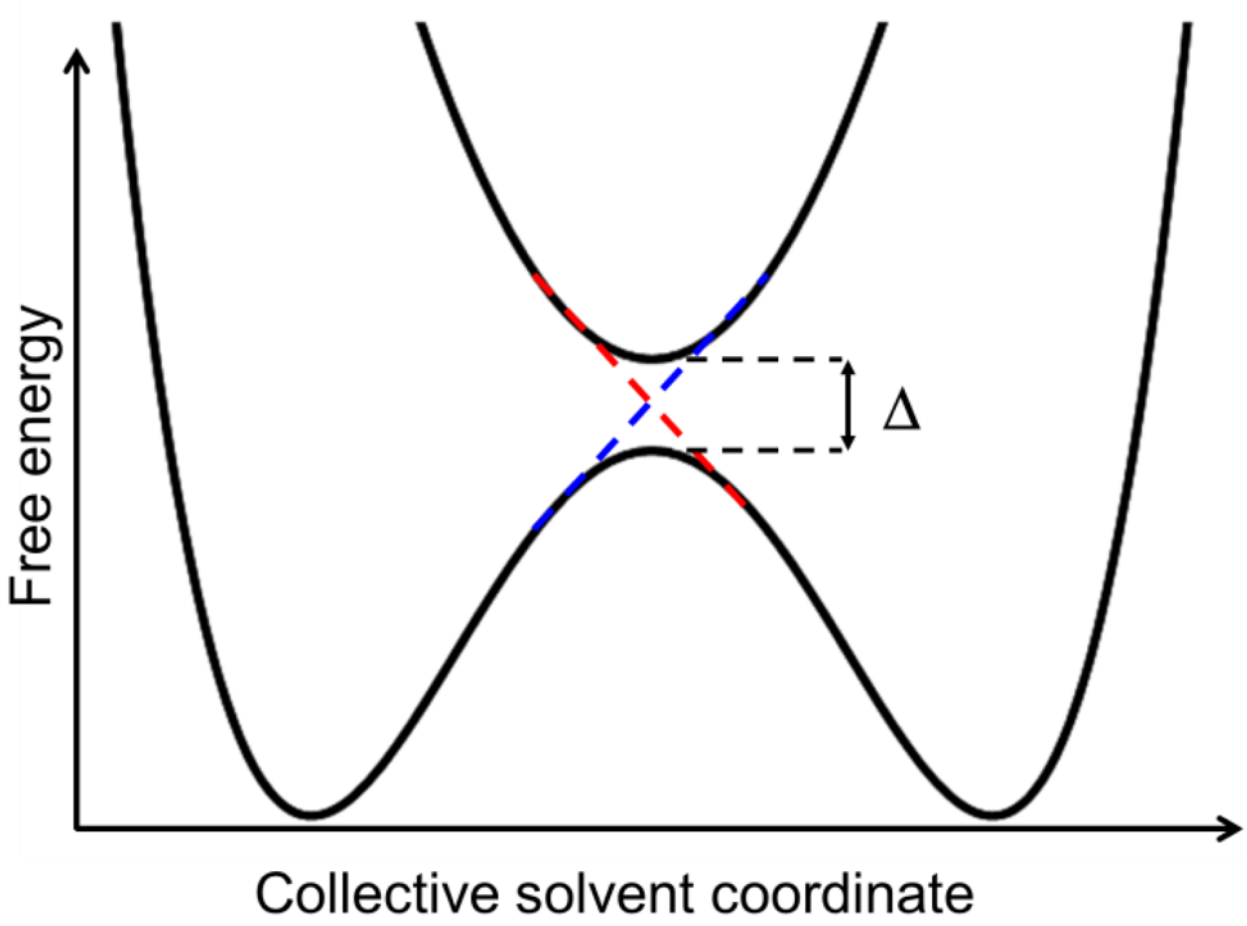

Figure 3.
Free energy curves associated with the adiabatic (solid black lines) and diabatic (blue and red dashed lines) proton vibrational states along the collective solvent coordinate for a symmetric proton transfer reaction. The adiabatic curves are associated with the energies of the adiabatic proton vibrational states depicted in Figure 2a. The minimum splitting between the adiabatic curves (solid black lines) corresponds to the tunneling splitting Δ indicated for the symmetric double well potential in the middle of Figure 2a. The diabatic curves are associated with the energies of the diabatic proton vibrational states depicted in Figure 2b with the same blue and red coloring scheme for the states localized in the donor and acceptor wells, respectively. For the symmetric double well potential shown in the middle of Figure 2b, the diabatic curves (dashed blue and red lines) are degenerate and therefore cross.

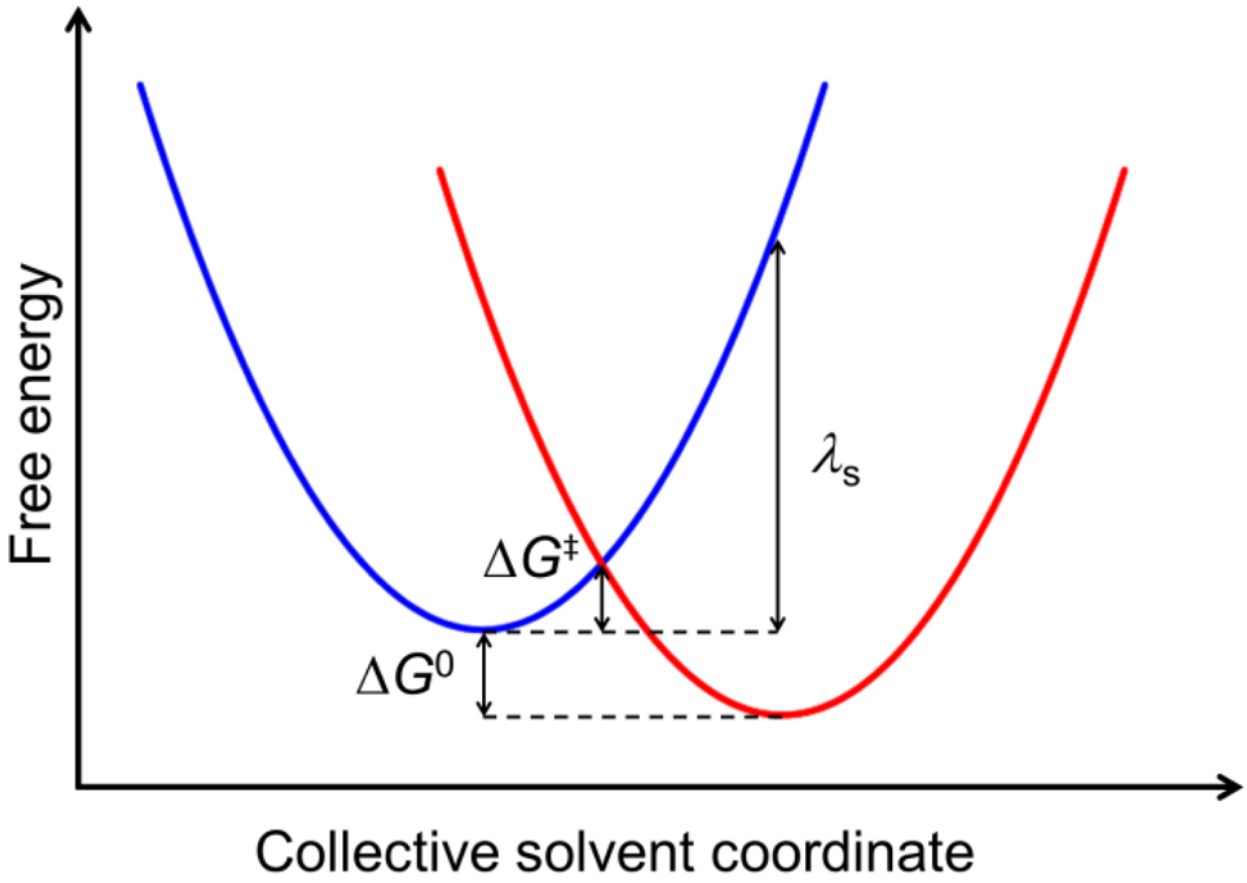

Figure 4.
Free energy curves associated with the diabatic proton vibrational states along the collective solvent coordinate for an asymmetric proton transfer reaction. The blue and red curves correspond to the diabatic states localized in the donor and acceptor wells, respectively. The solvent reorganization energy, λ_s, reaction free energy, ΔG^0, and free energy barrier, $\Delta G^{\ddagger}$, are indicated.

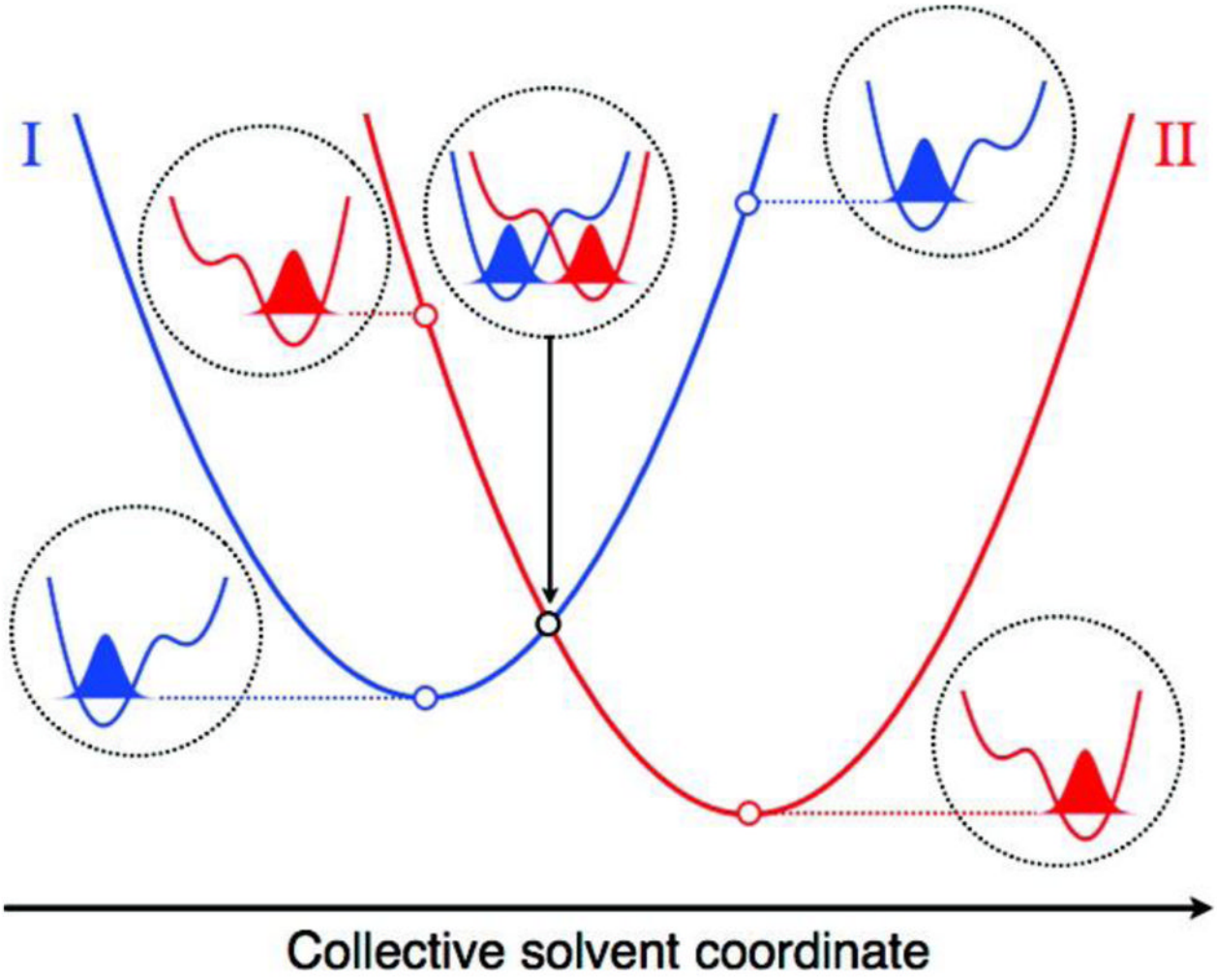

Figure 5.

Free energy curves for the ground reactant (I) and product (II) diabatic electron-proton vibronic states along the collective solvent coordinate for an EPT reaction. The reactant (blue) and product (red) diabatic states correspond to the electron localized on the donor and acceptor, respectively. The proton potential energy curves along the proton coordinate and the corresponding ground state proton vibrational wavefunctions are depicted for the reactant minimum, the crossing point, and the product minimum of the free energy curves. The energies of these proton vibrational states correspond to the open circles on the free energy curves. The proton potential energy curves associated with the crossing point are shifted higher in energy for clarity. The figure and caption reproduced with permission from Ref. 11. Copyright 2008 American Chemical Society.

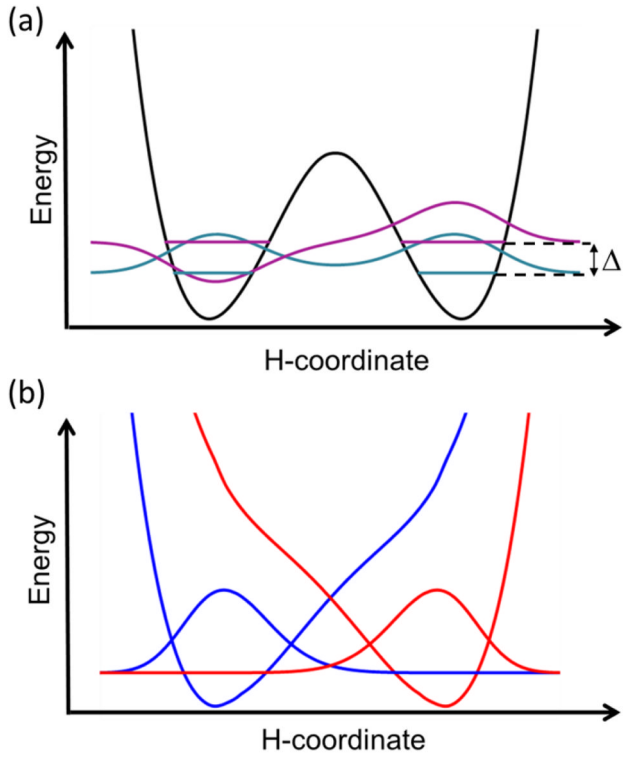

Figure 6.
(a) Electronically adiabatic ground state potential energy curve and the corresponding proton vibrational wavefunctions for the benzyl/toluene system. This reaction is electronically adiabatic, and the vibronic coupling is equal to half of the energy splitting Δ between the symmetric (cyan) and antisymmetric (magenta) proton vibrational states for the electronic ground state potential energy surface. For illustrative purposes, the splitting between the ground state and the excited state energy levels is increased significantly. (b) Diabatic potential energy curves corresponding to the two localized diabatic electronic states, I and II, and the corresponding proton vibrational wavefunctions in blue and red, respectively, for the phenoxyl/phenol system. This reaction is electronically nonadiabatic, and the vibronic coupling is the product of the electronic coupling V^{el} and the overlap of the reactant and product proton vibrational wavefunctions, $S_{\mu\nu}$.

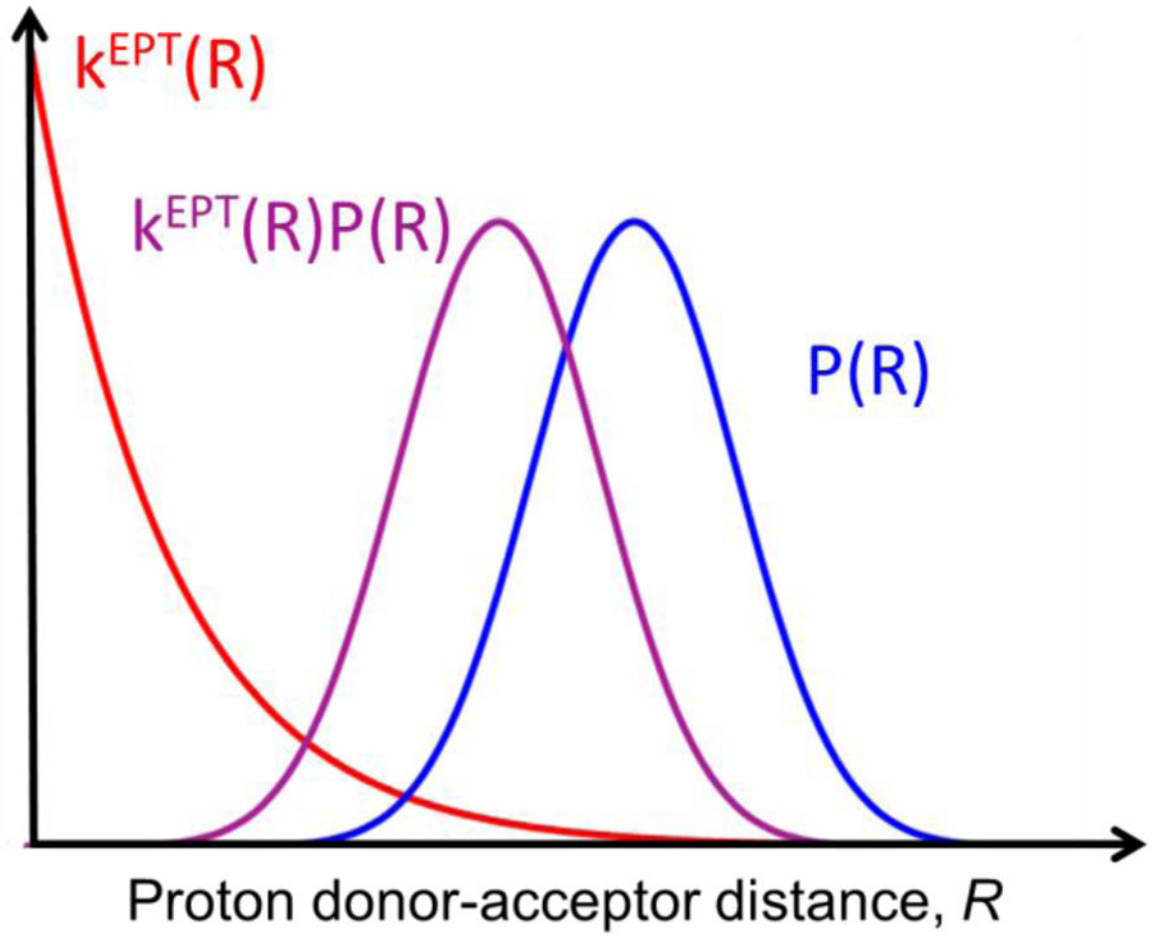

Figure 7.

Schematic depiction of the EPT rate constant $k^{EPT}(R)$ in red, the probability distribution function $P(R)$ in blue, and the product of these two factors in purple, as functions of the proton donor-acceptor distance R. The overall rate constant is the integral of the purple curve over R. The y-axis has no label because the quantities have different units and are scaled arbitrarily so they can be viewed on the same graph. The purple curve would be asymmetric but is depicted as a Gaussian and shifted slightly to the left for clarity. Figure modeled after Figure 2 in Ref. 62.

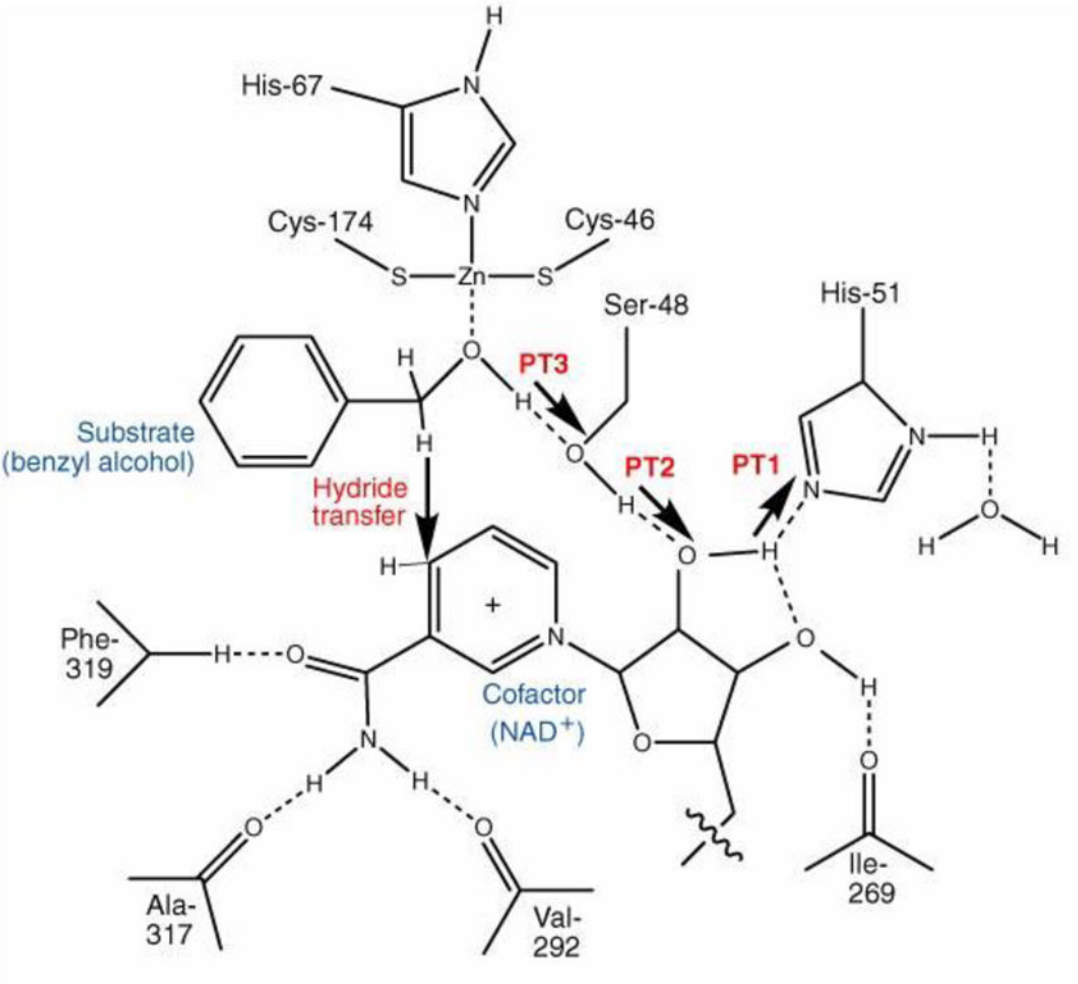

Figure 8.

Schematic representation of the mechanism of the oxidation of benzyl alcohol by the NAD^+ cofactor in the active site of LADH. The hydride transfer from the substrate to the NAD^+ is indicated by a labeled black arrow, and the proton transfer relay steps are indicated by black arrows labeled PT1, PT2, and PT3. Reproduced with permission from Ref. 283. Copyright 2000 American Chemical Society.

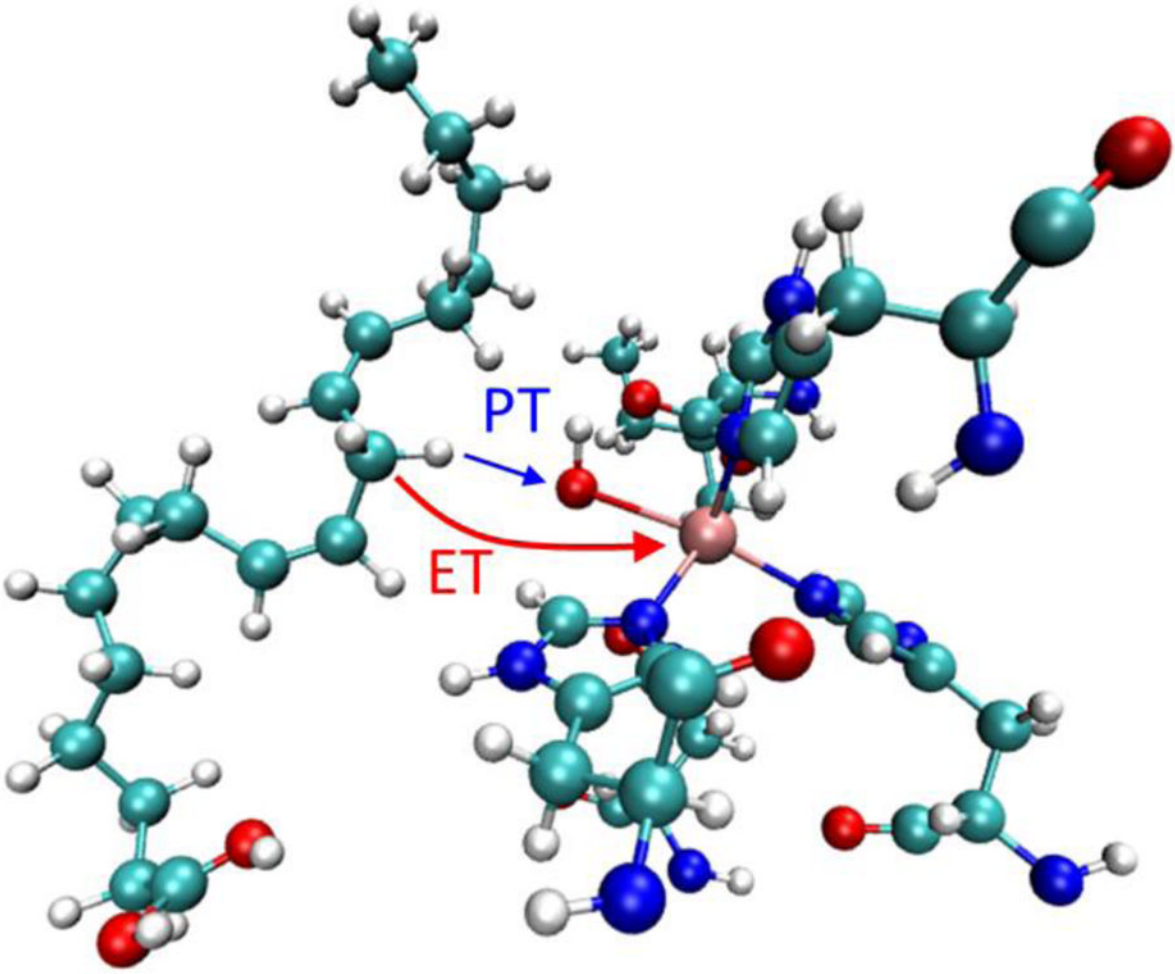

Figure 9.
Schematic representation of the net hydrogen atom transfer catalyzed by SLO with the linoleic acid substrate. This process is thought to occur via an EPT mechanism. The red arrow indicates the electron transfer from the π-backbone of the linoleic acid substrate to the iron of the cofactor, and the blue arrow indicates the proton transfer from C11 of the substrate to the iron-bound hydroxide to form water.

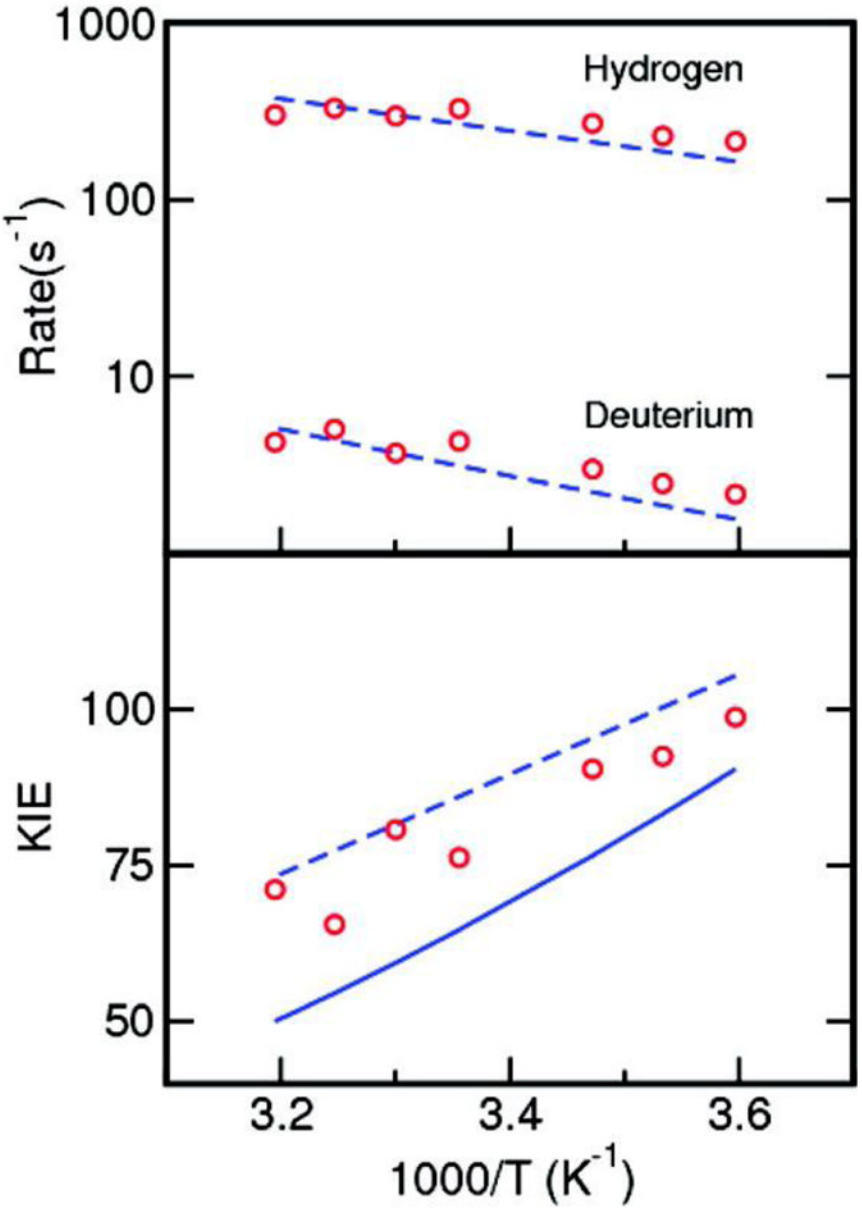

Figure 10.

Temperature dependence of the rate constants and KIE for the EPT reaction catalyzed by SLO with the linoleic acid substrate. The dashed lines depict the rate constants and KIE calculated with a variant of Eq. (22) in conjunction with a classical treatment of the proton donor-acceptor motion and multistate continuum theory. The solid line depicts the temperature dependence of the KIE obtained with a variant of Eq. (19) in conjunction with molecular dynamics simulations of the entire solvated enzyme, as well as quantum calculations on a model system to obtain the vibronic coupling parameters. The results obtained with the probability flux correlation function formalism are virtually indistinguishable from the solid blue line. The experimental data are depicted with circles.[213] The theoretical data were obtained from refs [43 and 44]. Reprinted with permission from Ref. 11. Copyright 2008 American Chemical Society.

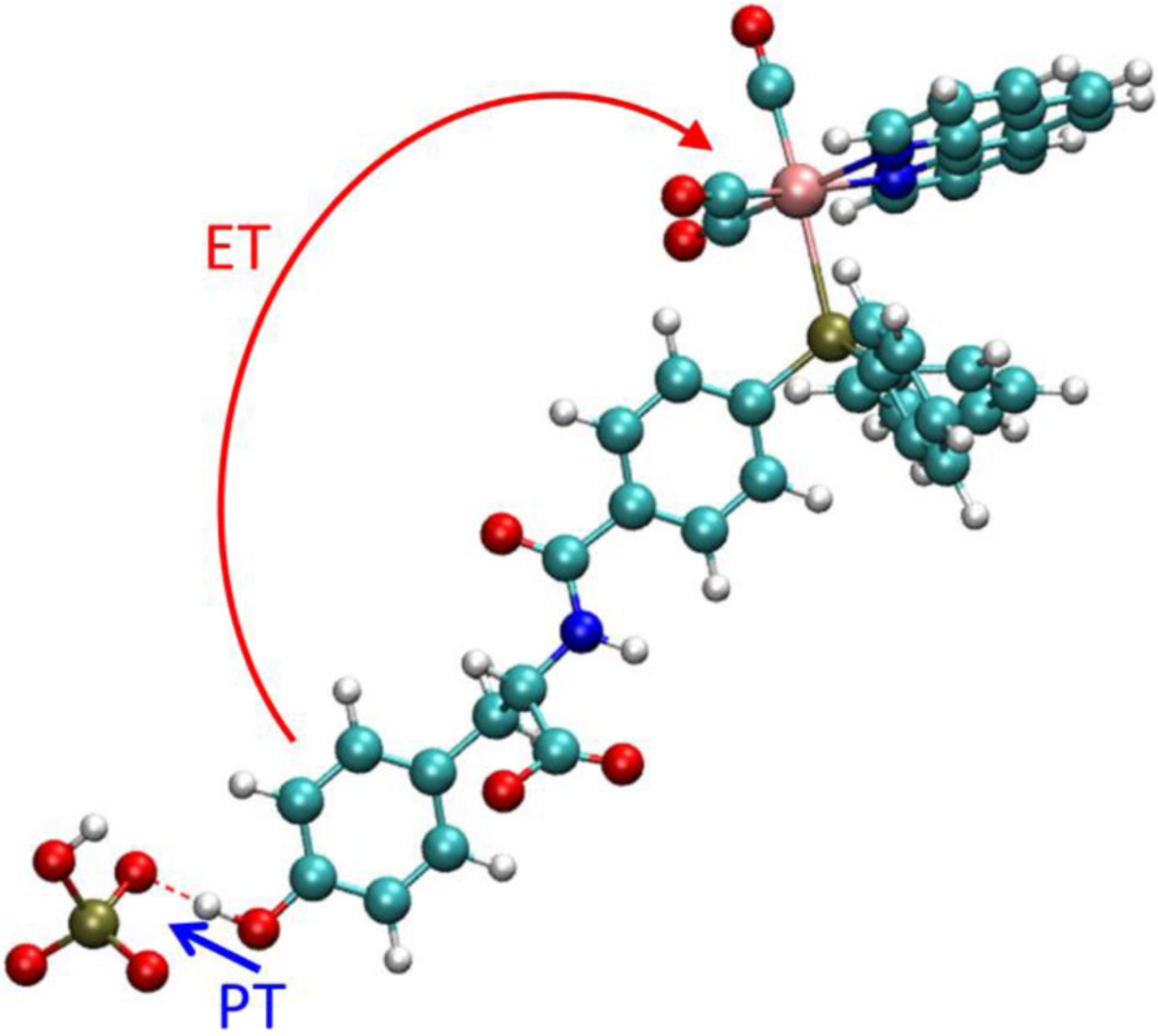

Figure 11.

Schematic depiction of the mechanism for electron transfer (red) and proton transfer (blue) in the $[Re(P–Y)(phen)(CO)_3]PF_6$ complex hydrogen bonded to a phosphate buffer molecule, HPO_4^{2-}. The electron is transferred from the tyrosine to the rhenium center, and the proton is transferred from the tyrosine hydroxyl group to the phosphate buffer molecule.

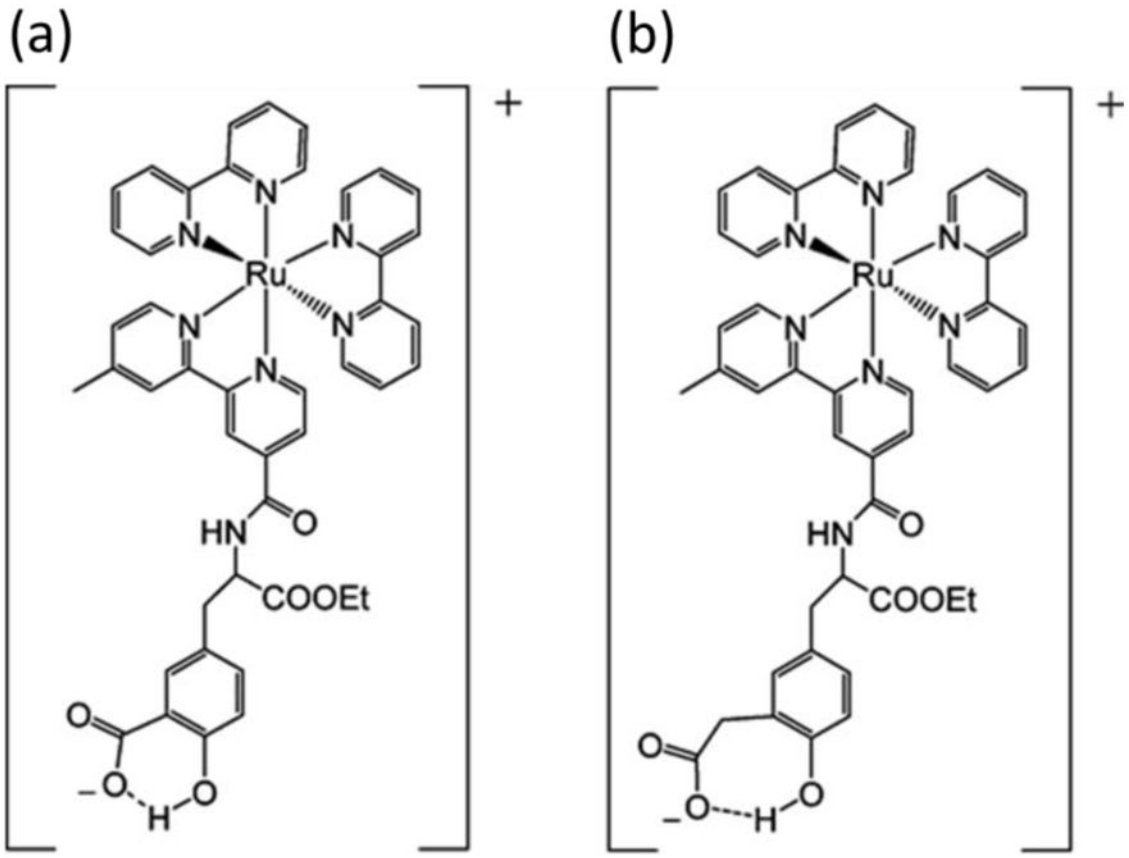

Figure 12.
Structures of the two ruthenium complexes studied as biomimetic models of redox-active tyrosine.[53] The phenolic group is (a) salicylic acid and (b) *o*-hydroxyphenyl-acetic acid.

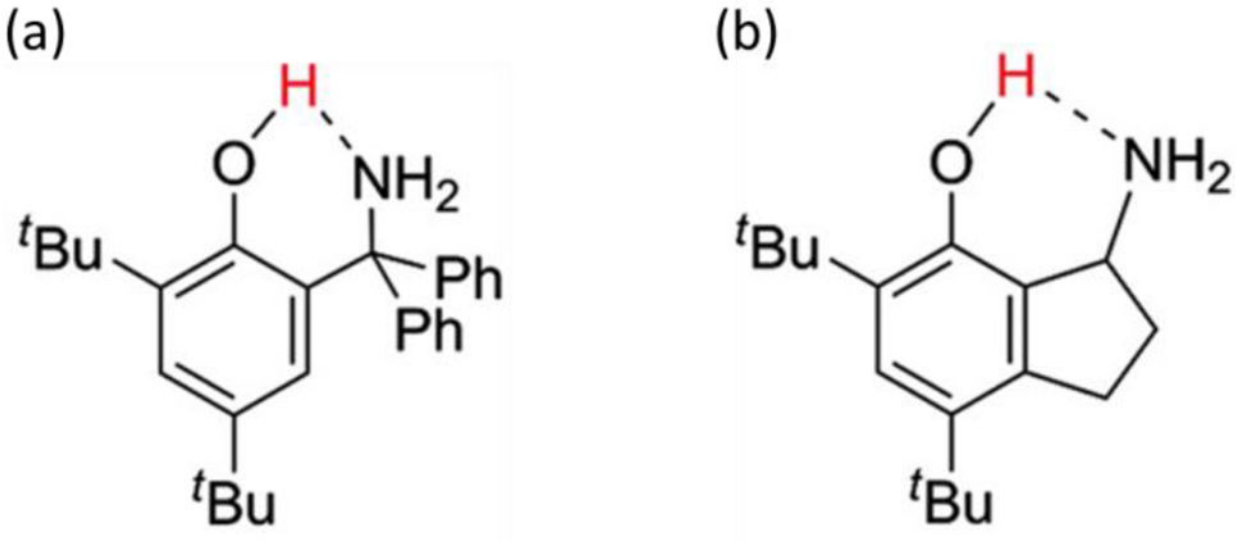

Figure 13.
Structures of two model phenol compounds studied as biomimetic models of redox-active tyrosine:[47] (a) 2,4-di-*tert*-butyl-6-(diphenylaminomethyl) phenol and (b) 1-amino-4,6-di-*tert*-butyl-7-hydroxyindan.

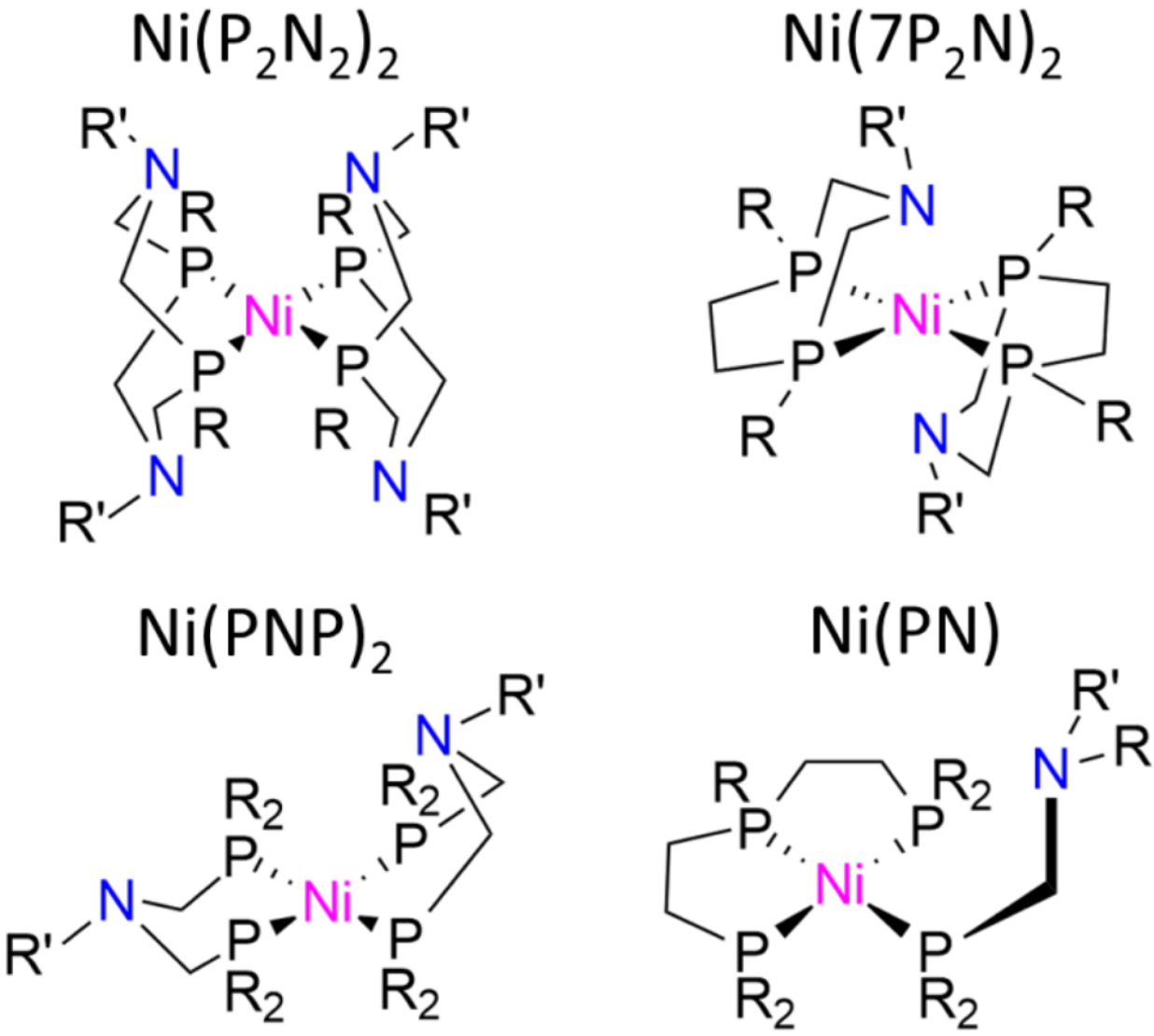

Figure 14.
Metal-based molecular electrocatalysts inspired by the active site of the hydrogenase enzyme and used for H_2 oxidation and production. The metal center is shown in magenta, and the pendant amine is shown in blue. These structures are depicted as unprotonated with +2 charge, although the charge is not given in the formulas. At least one pendant amine for each catalyst is in the active conformation. These catalysts have been studied experimentally[274,284] and theoretically.[62] Reprinted with permission from Ref. 62. Copyright 2013 American Chemical Society.

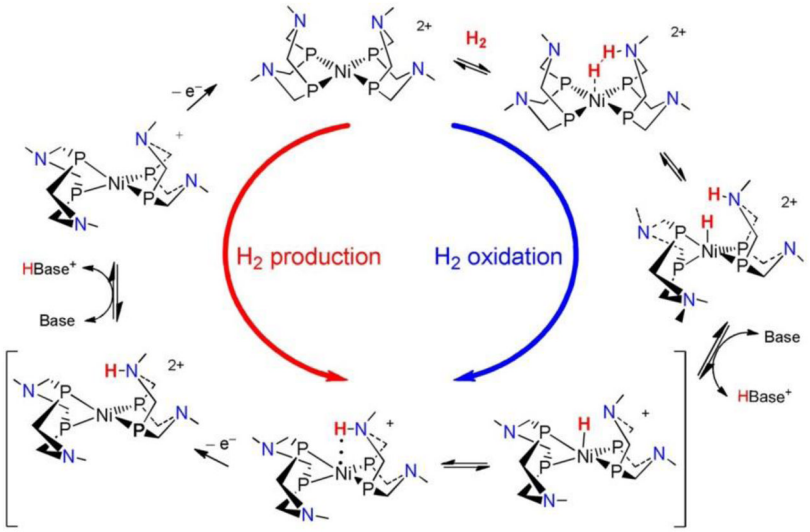

Figure 15.

Proposed mechanism of hydrogen oxidation (blue path) and hydrogen production (red path) for the $[Ni(P_2N_2)_2]^{2+}$ electrocatalyst. Ligands bound to P and N are omitted for clarity. The square brackets indicate the PCET reaction that has been studied with the nonadiabatic EPT theory. Reprinted with permission from Ref. 277, Copyright 2012 American Chemical Society.